# Implementacija i validacija elektrolitskog modela dva potencijala u numeričkom modelu gorivnog članka

**Bešenić, Tibor**




UNIVERSITY OF ZAGREB

Faculty of Mechanical Engineering and Naval Architecture

# MASTER'S THESIS

**Tibor Bešenić**

Zagreb, 2016

UNIVERSITY OF ZAGREB

Faculty of Mechanical Engineering and Naval Architecture

# IMPLEMENTATION AND VALIDATION OF THE TWO-POTENTIAL ELECTROLYTE ASSEMBLY EQUATIONS IN THE COMPUTATIONAL FUEL CELL MODEL

Supervisor:

Prof. Hrvoje Jasak, PhD

Student:

Tibor Bešenić

Zagreb, 2016

I hereby declare that this thesis is entirely the result of my own work except where otherwise indicated. I have fully cited all used sources and I have only used the ones given in the list of references.

I would like to express my gratitude to my supervisor Prof. Hrvoje Jasak for his guidance, patience and help provided when it was needed the most.

I am thankful to Prof. Steven Beale for his immeasurable patience and effort in helping me understand the physics of fuel cells.

Finally, I would like to thank everyone in the $8^{th}$ floor CFD group, especially Vuko Vukčević for crucial tweaks in the code.

SVEUČILIŠTE U ZAGREBU
**FAKULTET STROJARSTVA I BRODOGRADNJE**
Središnje povjerenstvo za završne i diplomske ispite
Povjerenstvo za diplomske ispite studija strojarstva za smjerove:
procesno-energetski, konstrukcijski, brodostrojarski i inženjersko modeliranje i računalne simulacije

| Sveučilište u Zagrebu<br>Fakultet strojarstva i brodogradnje | |
|---|---|
| Datum | Prilog |
| Klasa: | |
| Ur.broj: | |

# DIPLOMSKI ZADATAK

Student: **Tibor Bešenić** Mat. br.: 0035177873

Naslov rada na hrvatskom jeziku: **Implementacija i validacija elektrolitskog modela dva potencijala u numeričkom modelu gorivnog članka**

Naslov rada na engleskom jeziku: **Implementation and Validation of the Two-Potential Electrolyte Assembly Equations in the Computational Fuel Cell Model**

Opis zadatka:

Gorivni članci su elektrokemijski uređaji koji pretvaraju kemijsku energiju goriva direktno u električnu energiju, uz toplinu kao nusprodukt. Za razliku od izgaranja goriva (na primjer vodika) u njima je fizički razdvojena reakcija između vodika i kisika, tako da razlika između elektrokemijskih potencijala reaktanata uzrokuje postojani tok iona i elektrona umjesto burne reakcije. Izbjegavanje izgaranja pritom znači i izbjegavanje štetnih emisija.
U gorivnim člancima javlja se niz složenih pojava koje je potrebno opisati modelima, od mikroskopske razine do razine članka. Tok fluida i njihova difuzija kroz porozne materijale, toplinski fenomeni kondukcije i konvekcije te zračenja u kanalima, elektrokemijske reakcije u krutim i poroznim elektrodama i elektrolitu, te postojanje elektronskog i ionskog polja samo su neke od njih.
Kod jednostavnijih numeričkih modela moguće je pretpostaviti da je sklop elektroda i elektrolita dovoljno tanak da se pretpostavi dvodimenzionalnost gustoće električnog toka. U ovom radu izvršit će se izvod, validacija i implementacija više-zonskog modela transporta elektrona i iona u gorivnom članku s debelim elektrodama koji uzima u obzir prostornu varijaciju istog.
Kandidat će izvršiti sljedeće zadatke tokom izrade rada:

- opisati postojeći matematički model gorivnog članka i njegovu implementaciju u *open source* paketu OpenFuelCell. Posebnu pažnju potrebno je posvetiti elektrokemijskom modelu tankih elektroda (Faradayeva, Nernstova i Butler-Volmerova jednadžba);
- opisati predloženi pristup formulacije modela dva potencijala prikladnog za simulacije gorivnog članka s pretpostavkom debele elektrode;
- samostalno izvršiti implementaciju modela dva potencijala u više-zonskom pristupu u sklopu paketa OpenFuelCell;
- izvršiti verifikaciju i validaciju implementiranog modela;
- usporediti rezultate novog modela s rezultatima dobivenim s postojećim modelom aproksimacije tanke eletrode na odgovarajućim primjerima gorivnog članka.

U radu navesti korištenu literaturu i eventualno dobivenu pomoć.

| Zadatak zadan: | Rok predaje rada: | Predviđeni datumi obrane: |
|---|---|---|
| 5. svibnja 2016. | 7. srpnja 2016. | 13., 14. i 15. srpnja 2016. |

Zadatak zadao: Predsjednica Povjerenstva:

Izv. prof. dr. sc. Hrvoje Jasak

Prof. dr. sc. Tanja Jurčević Lulić

# Contents

# List of Figures

# List of Tables

# Nomenclature

| | | |
|---|---|---|
| $\alpha$ | Transfer coefficient | - |
| $\varepsilon$ | Efficiency | - |
| $\eta$ | Overpotential | V |
| $\mu$ | Chemical potential | J/mole |
| $\Phi$ | Electric potential | V |
| $\rho$ | Density | kg / $m^2$ |
| $\sigma$ | Electric conductivity | S / m |
| $\mathbf{u}$ | Velocity | m / s |
| $a$ | Activity | - |
| $F$ | Farraday's constant | V |
| $H$ | Enthalpy | J |
| $i$ | Current density | A / $m^2$ |
| $i_0$ | Exchange current density | K |
| $M$ | Molar mass | kg / mole |
| $m$ | Mass | kg |
| $n$ | Number of moles | - |
| $p$ | Pressure | Pa |

| | | |
|---|---|---|
| $Q$ | Heat | J |
| $R$ | Electric resistance | Ω |
| $S$ | Entropy | J / K |
| $T$ | Temperature | K |
| $U$ | Internal energy | J |
| $V$ | Voltage | V |
| $V$ | Volume | $m^3$ |
| $W$ | Work | J |
| $x$ | Molar fraction | - |
| $y$ | Mass fraction | - |

# Abstract

Fuel cells are devices for conversion of chemical into electric energy. Because of their high theoretical efficiency and low impact on environment, they are likely to have a major role during the current transition towards renewable energy sources. In order to design high-quality device that is reliable during its life-span, advances in fuel cell technology and materials are needed. Synergy of new numerical models and experimental data is therefore crucial.

Processes occurring in fuel cells are complex combination of fluid flow, heat transfer, species' transport and electrochemical reactions. Numerical models for fuel cells need to include all of these processes with a satisfactory precision on both the porous electrodes' micro-scale and the global scale of cell and complex geometry of supply channels.

Before model development, considerable understanding of physical processes is needed, especially for thermodynamics of electrochemical reactions for energy conversion.

`OpenFuelCell` is the open-source addition for OpenFOAM library that is developed for fuel cell modeling, focusing on solid oxide fuel cells (SOFC). Additional model for `OpenFuelCell` that includes more detailed potential field description is developed. For it, new mesh decomposition is needed, as well as significant modifications of source-code and governing equations.

Results of the new *two potential model* are given, although comparison with existing models is cumbersome due to underlying differences in model. Along with results, validity assessment of new model is also given.

Key words: *CFD*, *OpenFOAM*, *SOFC*, *fuel cell*, *openFuelCell*, *solid oxide*, *electrochemistry*, *potential field*.

# Sažetak

Gorivni članci su uređaji za pretvorbu kemijske energije goriva u električnu energiju. Zbog teoretski visoke efikasnosti i niskog štetnog utjecaja na okoliš, imaju priliku postati jedna od važnih tehnologija tijekom tranzicije prema obnovljivim energetskim izvorima. Kako bi gorivni članci bili kvalitetno konstruirani i pouzdani tijekom radnog vijeka, potreban je brži napredak tehnologije i materijala koji uključuje spoj novih računalnih modela i eksperimentalnih podataka.

Procesi koji se odvijaju u gorivnim članvima su kompleksan spoj toka fluida, provođenja topline, transporta specija i elektrokemijskih reakcija. Računalni modeli gorivnih članaka moraju sa zadovoljavajućom točnošću obuhvatiti ove procese na mikroskopskoj razini u poroznim elektrodama, kao i u složenim geometrijama dobavnih kanala.

Prije razvijanja računalnog modela za gorivne članke, potrebno je izuzetno razumijevanje fizikalnih procesa, posebice termodinamike elektrokemijskih reakcija koje su temelj pretvorbe kemijske u električnu energiju.

`OpenFuelCell` je nadogradnja na *open-source* softverski paket OpenFOAM i služi za modeliranje gorivnih članaka s naglaskom na gorivne članke s krutim oksidima. Razvija se nadogradnja postojećeg modela koja uključje detaljniji opis polja potencijala unutar aktivnih dijelova članka. Za novi *model dvaju potencijala* potrebna je značajnija prilagodba računalnog koda, dekompozicije proračunskih mreža i jednadžbi modela.

Zbog novog pristupa otežana je validacija s postojećim rezultatima i standardnim `OpenFuelCell` kodom. Daje se prikaz i analiza rezultata dobivenih novim modelom te ocjena primjenjivosti modela.

Ključne riječi: *CFD*, *OpenFOAM*, *SOFC*, *gorivni članci*, *openFuelCell*, *kruta elektroda*, *elektrokemija*, *polje potencijala*.

# Prošireni sažetak

## Gorivni članci

Napredak ljudskog društva i moderne civilizacije tijesno je bio vezan uz povećanje potrošnje energije. Velika većina potrebe za energijom tradicionalno je bila zadovoljena izgaranjem fosilnih goriva, a tradicionalne elektrane uzrokovale su zagađenje okoliša, ozbiljan utjecaj na klimu i ljudsku populaciju. Kako bi se razdvojilo ljudski napredak i povećanje energetskih potreba, kao rješenje su se pojavila dva smjera—smanjenje energetske intenzivnosti (energetska učinkovitost) i razvijanje novih tehnologija za pretvorbu energije. Tako su i gorivni članci jedna od rastućih tehnologija koja se pokušava nametnuti kao sve važnija opcija u trendu tranzicije s konvencionalnih na obnovljive energetske izvore.

Gorivni članci su elektrokemijski uređaji koji pretvaraju kemijsku energiju goriva direktno u električnu energiju, uz toplinu kao nusprodukt. Za razliku od izgaranja goriva u njima je fizički razdvojena reakcija između vodika i kisika, tako da razlika između elektrokemijskih potencijala reaktanata uzrokuje postojani tok iona i elektrona umjesto burne reakcije s naglim oslobađanjem topline. Izbjegavanje izgaranja pritom znači i izbjegavanje štetnih emisija. Jednadžba (1) prikazuje reakciju izgaranja s najjednostavnijim gorivom-vodikom rastavljenu na dvije *polureakcije* karakteristične za *SOFC* gorivne članke.

$$\begin{aligned} &H_2 + \tfrac{1}{2}O_2 \rightleftharpoons H_2O + \text{energy} \\ &H_2 + O^{2-} \longrightarrow H_2O^+ + 2e^- \\ &\tfrac{1}{2}O_2 + 2e^- \longrightarrow O^{2-} \end{aligned} \tag{1}$$

Svi gorivni članci sastoje se od elektroda—anode i katode koje su razdvojene elektrolitom. Na anodu se dovodi gorivo, najčešće vodik, a na katodu zrak, odnosno kisik. Na anodi se odvija oksidacija vodika, a na katodi redukcija kisika. Elektrolit koji sprečava dodir provodan je samo za ione a elektroni nastali oksidacijom putuju vanjskim električnim krugom od anode do katode, gdje ih je moguće iskoristiti za vršenje rada. Ove komponente i princip rada zajednički su svim gorivnim člancima, dok se tip elektrolita, geometrija i načini dobave plinova razlikuju između pojedinih vrsta. Slika 1 prikazuje shemu gorivnog članka (SOFC tip) s razdvojenim reakcijama i ucrtanim tokovima iona i elektrona.

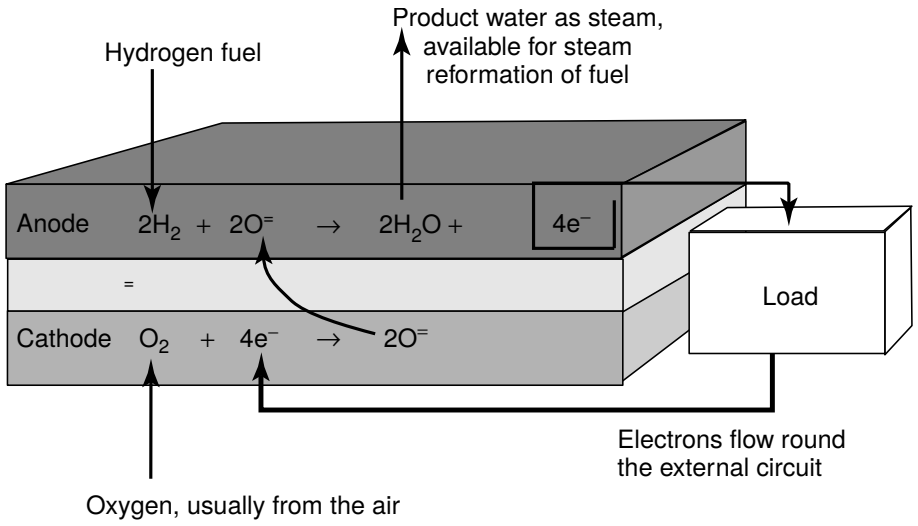


**Slika 1:** Shema reakcije u SOFC gorivnom članku.

Među gorivnim člancima najčešće se javljaju sljedeći tipovi: alkalni gorivni članak (*AFC-Alkaline fuel cell*), gorivni članak s protonski izmjenjivom membranom (*PEMFC–Polymer Exchange Membrane Fuel Cell*) i gorivni članak s krutim oksidima (SOFC – Solid Oxide Fuel Cell). U ovom radu fokus je bio usmjeren na SOFC tip.

Gorivni članak s krutim oksidima ističe se po tome što se kao elektrolit koristi kruta keramika—najčešće itrijem stabiliziran cirkonij (*Yttria-stabilized zirconia*), koja je provodna za ione kisika. SOFC gorivni članci rade na visokim temperaturama, 500 °C – 1000 °C, što sa sobom veže nedostatke kao što su potreba za kvalitetnijim materijalima otpornim na više temperature i toplinska naprezanja te duže vrijeme pokretanja. Dobre strane rada pri visokim temperaturama su mogućnost za dodatno povećanje energetske učinkovitosti u obliku kogeneracije, izbjegavanje potrebe za katalizatorima te mogućnost korištenja raznih vrsta goriva koja se mogu reformirati pri visokoj temperaturi. Ove gorivne članke također karakterizira visoka energetska učinkovitost (trenutno do 60 %), pouzdanost u radu (kao i kod ostalih, nema pokretnih dijelova osim opreme za dobavu reaktanata), fleksibilnost pogonskih uvjeta i mogućnost skaliranja od malih do velikih primjena (100 W - 2 MW).

## Termodinamika gorivnih članaka

U gorivnim člancima javlja se niz složenih pojava koje je potrebno opisati modelima, od mikroskopske razine do razine članka. Tok fluida i njihova difuzija kroz porozne materijale,

toplinski fenomeni kondukcije i konvekcije te zračenja u kanalima, elektrokemijske reakcije u krutim i poroznim elektrodama i elektrolitu te postojanje elektronskog i ionskog polja samo su neke od njih. U modelima je potrebno s odgovarajućom točnošću opisati ove pojave i procijeniti koje se od njih mogu zanemariti. Također, pojave svojstvene za gorivne članke u stvarnosti uzrokuju smanjenje efikasnosti i utječu na rad aparata. Tako je na primjer potrebno na odgovarajući način pristupiti difuziji reaktanata i njihovoj potrošnji duž dovodnih kanala, preklapanju ionskog i elektronskog polja, prenaponima—aktivacijskim, difuzijskim i otporničkim (omskim) nepovratnostima koje smanjuju učinkovitost.

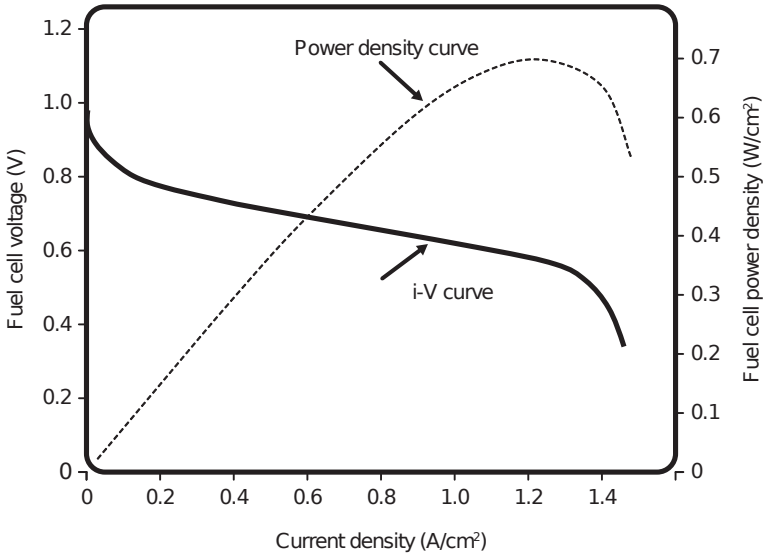


**Slika 2:** i-V krivulja za gorivne članke s dodanom krivuljom snage ($P = iV$).

Slika 2 prikazuje karakterističnu $i - V$ krivulju gorivnog članka. Razabrati se mogu tri regije: pri visokim naponima brzi pad performansi zbog **aktivacijskog prenapona**. To je gubitak u odnosu na idealni napon članka koji je "žrtvovan" kako bi se prešla *aktivacijska barijera* reakcije pokrenula ju u željenom smjeru. Linearna regija u sredinidio je gdje su najznačajniji **otpornički prenaponi**. Ovdje se gubitak povećava na račun povećane gustoće izlazne struje, a to izaziva veće otpore provođenja. Na kraju, **difuzijski prenapon** je gubitak pri izrazito aktivnim reakcijama i visokim gustoćama struje. U tom je režimu rada potrebna dobava velike količine reaktanata, koja zbog geometrije ili preslabe difuzije kroz porozni medij ne može biti osigurana.

U analizi termodinamike gorivnih članaka i kinetike reakcija na elektrodama, neizostavno

se uvodi pojam *Gibbsove slobodne energije*, koja je definirana prema jednadžbi (2):

$$dG = dH - T\,dS - S\,dT. \tag{2}$$

Gibbsova energija predstavlja maksimalni ne-ekspanzijski radni potencijal koji neki sustav posjeduje. Kad bi u idealnom slučaju sva ta energija bila iskorištena kao električna energija, dobio bi se reverzibilni potencijal članka $E^0$:

$$E^0 = -\frac{\Delta \hat{g}^0_{rxn}}{nF}. \tag{3}$$

Spomenuti prenaponi su gubici koji onemogućuju reverzibilni izlazni napon. Nernstova jednadžba (4) povezuje idealni napon pod standardnim uvjetima s radnim parametrima koje nalazimo u gorivnom članku:

$$E = E^0 - \frac{RT}{nF} \ln \frac{\prod p^{\nu_i}_{\text{products}}}{\prod p^{\nu_i}_{\text{reactants}}}. \tag{4}$$

Još jedna važna jednadžba za termodinamiku gorivnih članaka je Butler-Volmerova jednadžba, koja povezuje izlaznu gustoću struje i prenapon članka (na taj način sprežući napon i gustoću struje za numeričko modeliranje):

$$i = i_0 \left( e^{\alpha nF\eta/(RT)} - e^{(1-\alpha)nF\eta/(RT)} \right). \tag{5}$$

Aproksimacija koja vrijedi kod visokih prenapona i visokih gustoća struje te se često koristi opisana je Tafelovom jednadžbom (6), a vrijedi za eksponenecijalnu regiju na slici 3, koja prikazuje krivulju prema Butler-Volmerovoj jednadžbi.

$$i = i_0 e^{\alpha nF\eta_{act}/(RT)} \tag{6}$$

## `openFuelCell` model

`openFuelCell` je *open-source* računalni model namijenjen prvenstveno za simulaciju gorivnih članaka SOFC tipa. Obuhvaća široki raspon pojava u gorivnim člancima na mikroskopskim razinama i na razini cijelog članka. Izrazite razlike između dijelova gorivnog članka otežavaju dekompoziciju računalne mreže. Na primjer, provođenje topline odvija se u cijelom članku, tok fluida u kanalima i poroznim elektrodama, dok je usvojena pretpostavka da se

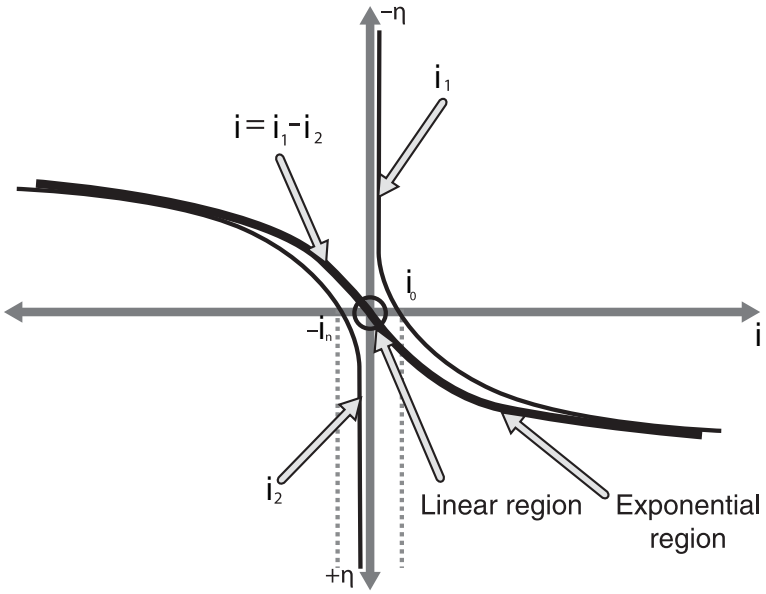


**Slika 3:** Butler-Volmerova krivulja. Prikazuje vezu između gustoće struje i prenapone$\eta$. Eksponencijalna regija na desnom rubu je dio gdje se može primijeniti Tafelova jednadžba

elektrokemijske pojave odvijaju samo u elektrolitu. Stoga se implementirana dekompozicija računalne mreže sastoji od globalne mreže ca cijeli članak te od regionalnih mreža koje obuhvaćaju zone u kojima se odvijaju slični procesi. Na slici 4 vidljivo je preklapanje korištenih regionalnih mreža s globalnom.

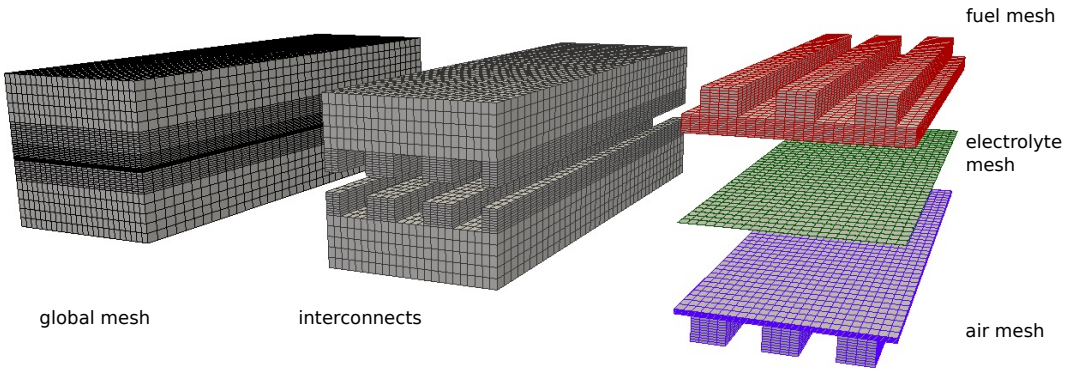


**Slika 4:** Dekompozicija računalne mreže u `openFuelCell` modelu

Jednadžbe za proračun elektrokemijskih procesa (za koje se pretpostavlja da su površinski fenomen na granici elektroda-elektrolit) već su predstavljene, a spregnute momentna i jednadžba kontinuiteta služe za proračun hidrodinamičkih pojava:

$$\operatorname{div}(\rho \mathbf{u}) = 0, \tag{7}$$

$$\operatorname{div}(\rho \mathbf{u}\mathbf{u}) = -\operatorname{grad} p + \operatorname{div}(\mu \operatorname{grad}\ \mathbf{u} - \frac{\mu \mathbf{u}}{\kappa_D}). \tag{8}$$

Transport specija modeliran je sljedećom jednadžbom:

$$\operatorname{div}(\rho \mathbf{u} y_i) = \operatorname{div}(\rho D_i^{eff} \operatorname{grad} y_i), \tag{9}$$

gdje su $y_i$ specije u fluidu, s time da je u svrhu očuvanja količine specija jedna postavljena kao pasivna i računa se oduzimanjem ostalih od 1.

Maseni izvori i ponori zbog reakcija na površini elektrolita modelirani su kao:

$$\dot{m}'' = \pm \frac{iM}{nF}. \tag{10}$$

Energetska jednadžba rješava se za čitavi volumen i uzima u obzir provođenje u krutini, kao i konvekciju u fluidima:

$$\rho c_p \mathbf{u} \cdot \operatorname{grad} T = \operatorname{div}(k \operatorname{grad} T) + \dot{q}'''. \tag{11}$$

Toplinski izvori zbog odvijanja egzotermne reakcije i zagrijavanje zbog Jouleove topline modeliraju se kao:

$$\dot{q}''' = \left( -\frac{1}{2F} \Delta H(T) - V \right) \frac{i}{\delta h_E}. \tag{12}$$

`openFuelCell` model je validiran u prijašnjim studijama i daje dobre rezultate za većinu radnih parametara SOFC gorivnih članaka. Međutim, uz ostala pojednostavljenje, zanemarena su polja potencijala u električno vodljivim elektrodama i potpornim elementima.

**Model dvaju potencijala**

Ovaj rad predstavlja nadogradnju na postojeći `openFuelCell` model koja je implementirana. Model dvaju potencijala implementira mogućnost odvojenog rješavanja električnih polja na odgovarajućim vodljivim krutinama. Stoga je implementirana nova dekompozicija mreže (prikazana na slici 5) koja uvodi dvije nove regije za proračun distibucije potencijala.

Umjesto dva električna i jednog ionskog polja, uvedeno je pojednostavljenje kojim je katoda ”pasivizirana”, tj. pretpostavilo se da se reakcija na njoj odvija, ali da nema utjecaj na

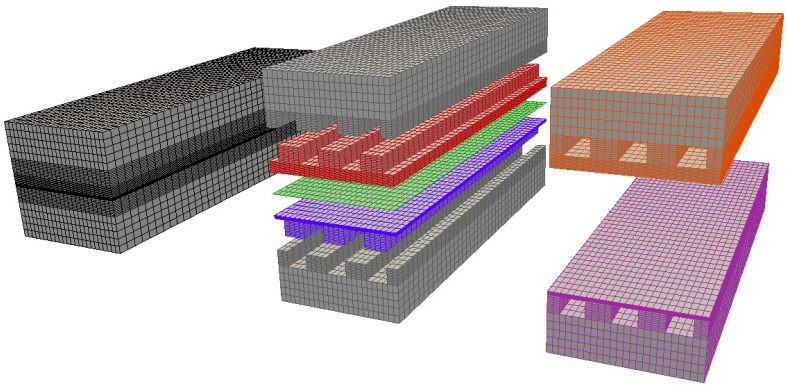

**Slika 5:** Nova dekompozicija računalne mreže za model dvaju potencijala

povećanje gubitaka. Ova pretpostavka dovodi do nove raspodjele potencijala u članku, s jednim skokom koji odvovara granici aktivne anode s elektrolitom (slika 6)

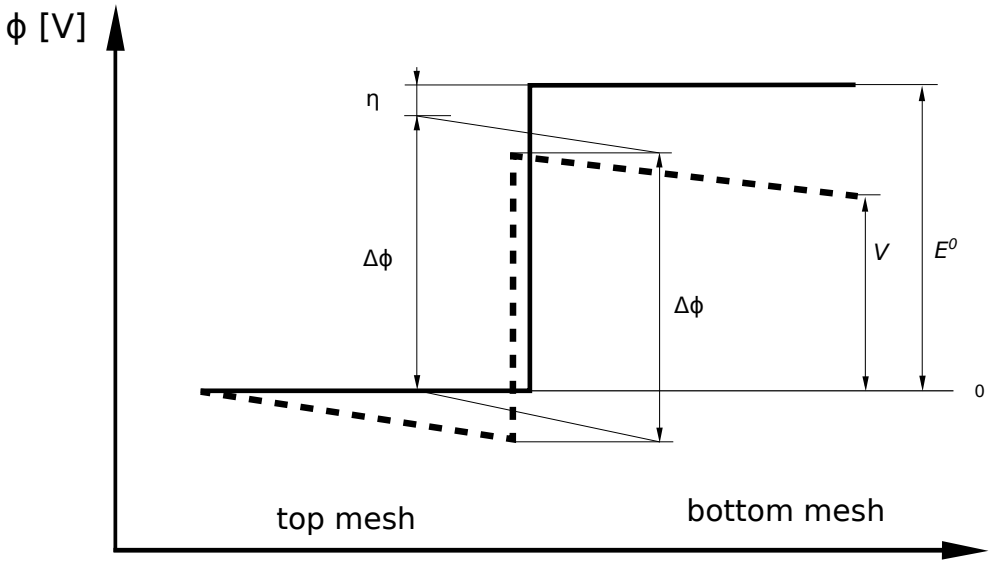


**Slika 6:** Distribucija potencijala u predstavljenom modelu. Puna linija označava potencijal u ravnotežnom stanju, a iscrtkana linija je potencijal kad je spojen krug i kad se crpi električna energija. Nagibi predstavljaju omske gubitke.

Razlika u odnosu na standardni `openFuelCell` model je i u tome što se koristi Tafelova umjesto Butler-Volmerove jednadžbe. "Skok potencijala" na granici računa se kao razlika

između ćelija susjednih mreža, a gustoća struje $i$ zadaje gradijent kao rubni uvjet za potencijal:

$$\frac{\partial \Phi}{\partial n} = -\frac{i}{\sigma}. \tag{13}$$

Nadalje, s definiranim rubnim uvjetima, distribucija potencijala $\Phi$ računa se pomoću Laplaceove jednadžbe, sa električnom provodnosti $\sigma$:

$$\nabla \cdot (\sigma \nabla \Phi) = 0. \tag{14}$$

**Rezultati**

Model dvaju potencijala pokazuje rezultate koji su djelomično usporedivi s postojećim modelima i rezultatima iz literature. Međutim, pokazalo se da je osjetljiv na promjene ulazne temperature i općenito daje rezultate gustoće struje koji nisu u potpunosti sukladni s prijašnjim rezultatima.

Slika 7 prikazuje orijentaciju kanala u simuliranim slučajevima—korištene konfiguracije su istosmjerno strujanje, protusmjerno te unakrsno.

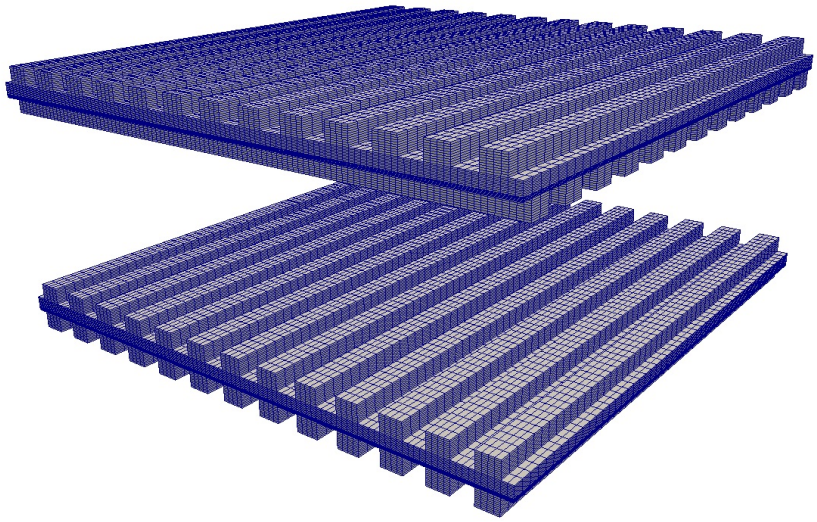

**Slika 7:** Orijentacija kanala u korištenim računalnim mrežama, prikladno za istosmjerni, protusmjerni te unakrsni slučaj.

Na slici 8 prikazani su ulazne temperature i naponi za simuliranu konfigurciju, kao i gustoće struje kao rezultat.

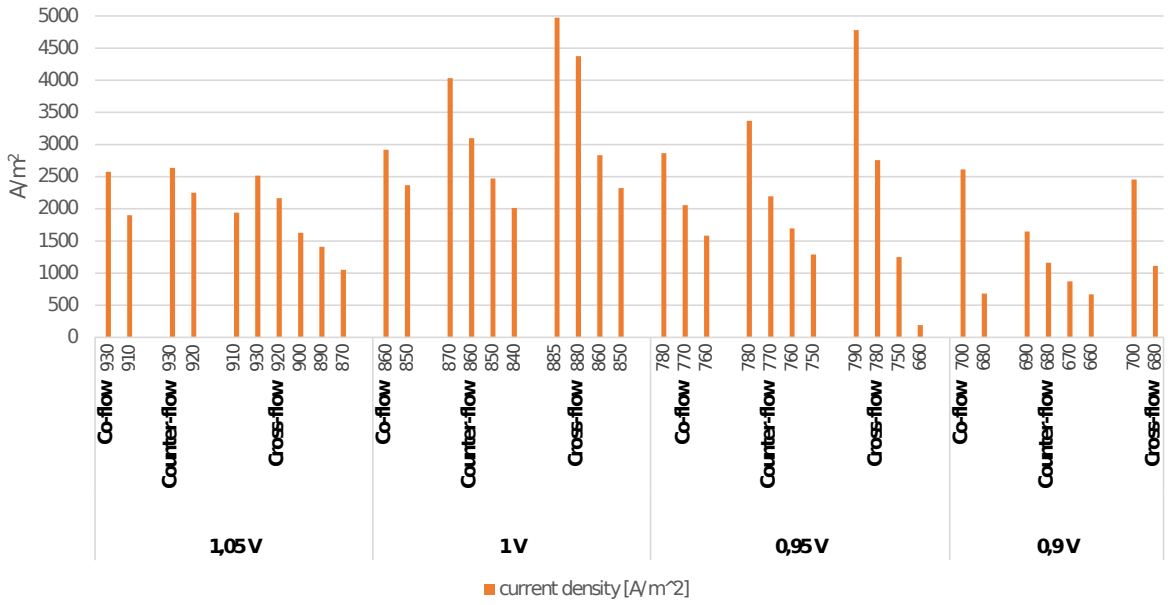


**Slika 8:** Varijacije ulaznih temperature i napona za rasličite konfiguracije.

Pokazano je da je model izuzetno osjetljiv na visoke ulazne temperature te dolazi do rušenja simulacije ukoliko je zadana temperatura previsoka za zadani napon. To se može uočiti na slici 9

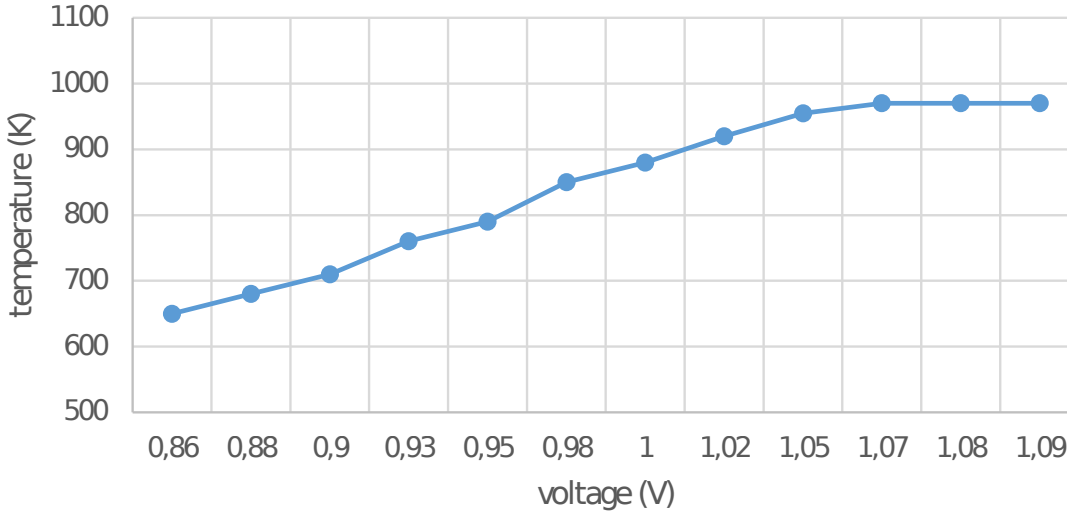


**Slika 9:** Granične temperature za napon iznad kojih dolazi do rušenja simulacije.

Slika 10 pokazuje rezultate simulacija za konstantnu temperaturu i raspon napona. Karakterističan oblik lijevog dijela $i - V$ krivulje je primjetan, što pokazuje u smjeru da model

dvaju potencijala dobro opisuje ovisnost gustoće struje i napona, barem pri radnim uvjetima s visokim naponom.

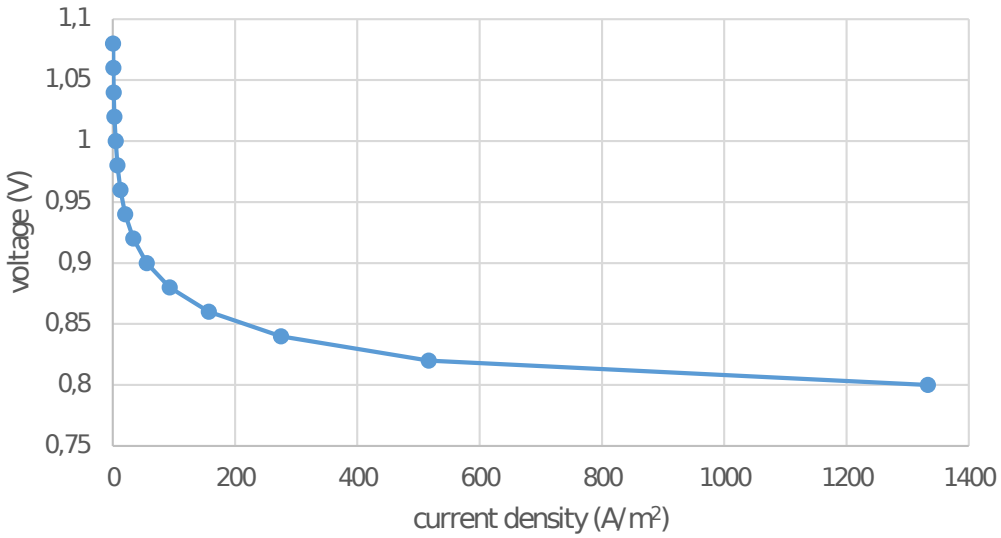


**Slika 10:** i-V krivulja za model dvaju potencijala.

Slijede prikazani rezultati za modelirani gorivni članak pri 860 K i 1.0Vi sve geometrijske konfiguracije. Slike pokazuju dobru podudardnost kvalitativnu podudarnost s rezultatima iz literature i postojećeg modela. Slika 11 prikazuje temperaturu na površini anode. Vidljivo je kako su temperature u kanalima više (zbog veće koncentracije reaktanata) te se također povećavaju duž smjer toka fluida. Poprečni presjek na slici 12 pokazuje najvišu i najravnomjerniju raspodjelu kod protusmjernog toka, dok je unaksni najlošiji što se tiče gradijenata temperature.

Drugi važni pokazatelj je koncentracija kisika i vodika, na slikama 13 i 14 primjećuje se potrošnja reaktanata duž kanale, a poprečno postoje znatne oscilacije koje su posljedica kanala, geometrije i otežane difuzije specija.

Koncentracije reaktanata direktno utječu na gustoću struje, koja je veća čim je više reaktivnih specija. Tako se na slici 15 primjećuje da je u protusmjernoj konfiguraciji i smjeru duž kanala gustoća struje izuzetno ovisna o koncentraciji vodika, dok u poprečnom smjeru koncentracija kisika ima znatno veći utjecaj.

Polja potencijala simulirana modelom dvaju potencijala vide se na slikama 16 i 17 u tlocrtu i presjeku. Uočljivo je da je gustoća znatno veća u predjelu kanala gdje su i reakcije burnije.

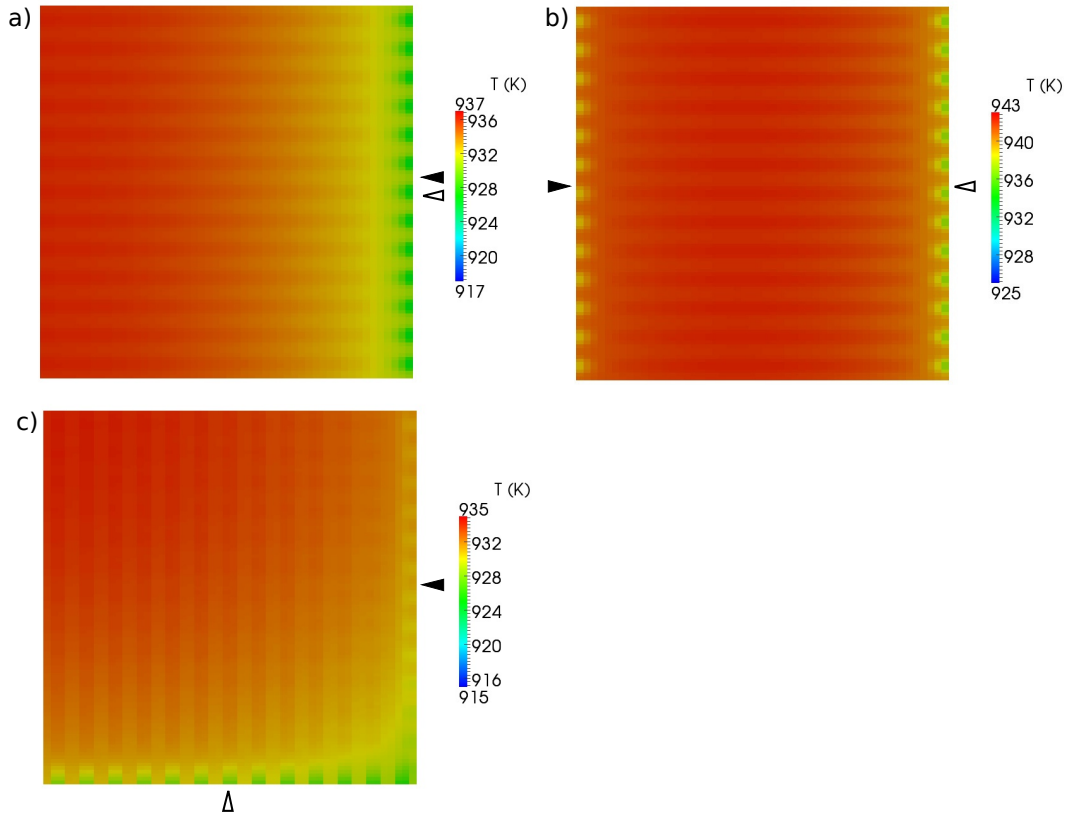


**Slika 11:** Raspodjela temperature na površini anode za a) istosmjerni, b) protusmjerni i c) unakrsni tok. Pune strelice pokazuju smjer strujanja goriva, prazne označavaju zrak.

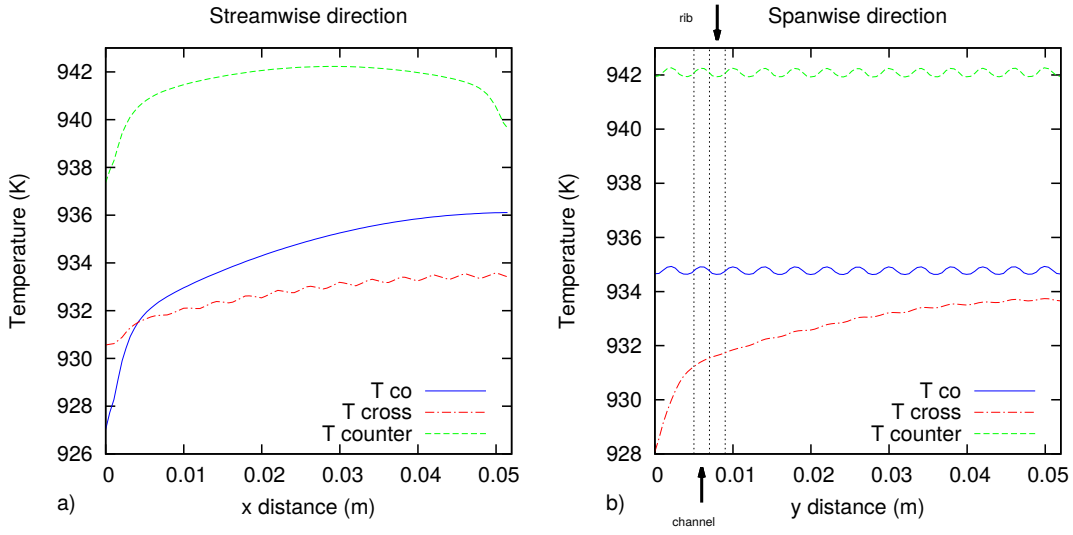


**Slika 12:** Temperaturna raspodjela u članku.

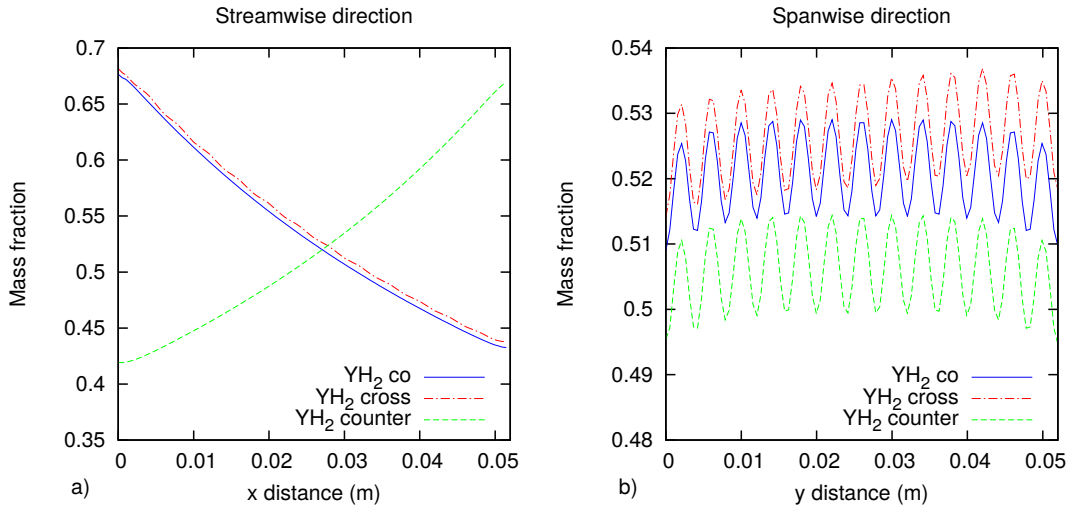


**Slika 13:** Maseni udjeli vodika u članku.

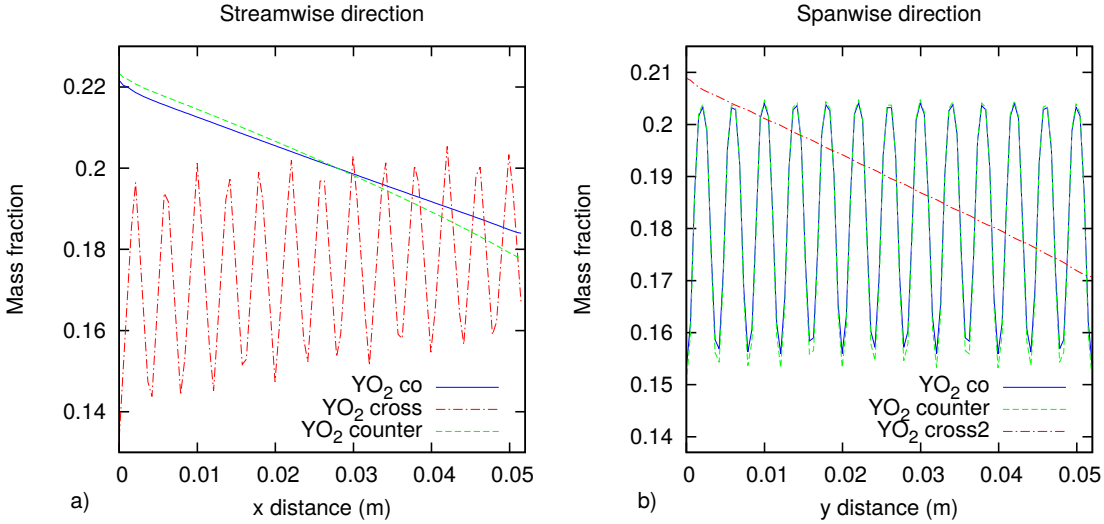


**Slika 14:** Maseni udjeli kisika u članku.

Difuzija potencijala kroz krutinu pokazuje eventualna mjesta koncentracije strujnica i ukazuje na lošu geometriju gorivnog članka.

Kranji cilj modeliranja gorivnih članaka je razvijanje pouzdanih i dobro konstruiranih uređaja za rastuće tržište tehnologija obnovljivih izvora energije, a za to su potrebni modeli koji variraju od detaljnih—koji u obzir uzimaju sve fizikalne pojave do jednostavnih koji služe za vođenje rada. Predviđanje životnog vijeka, pouzdanosti i iskoristivosti uređaja potrebni su kako bi se stvorili konkurentni i kvalitetni uređaji. Nadogradnja modela u obliku uvođenja mogućnosti za odabir pojednostavljenog rješavanja polja potencijala omogućuje korisniku

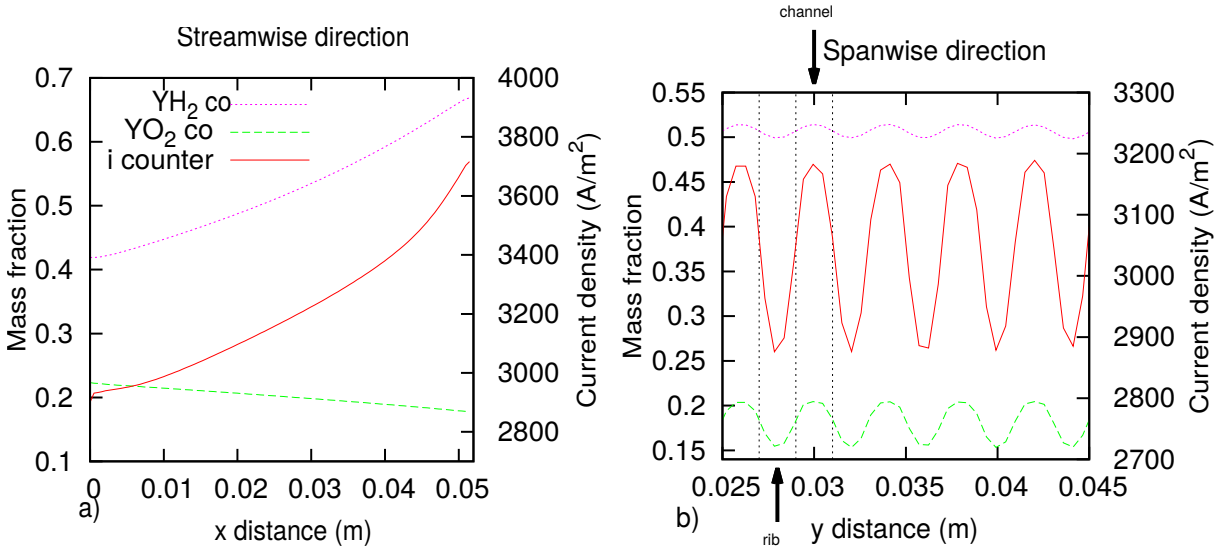


**Slika 15:** Prikaz gustoće struje i masenih koncentracija reaktanata u protusmjernoj konfiguraciji.

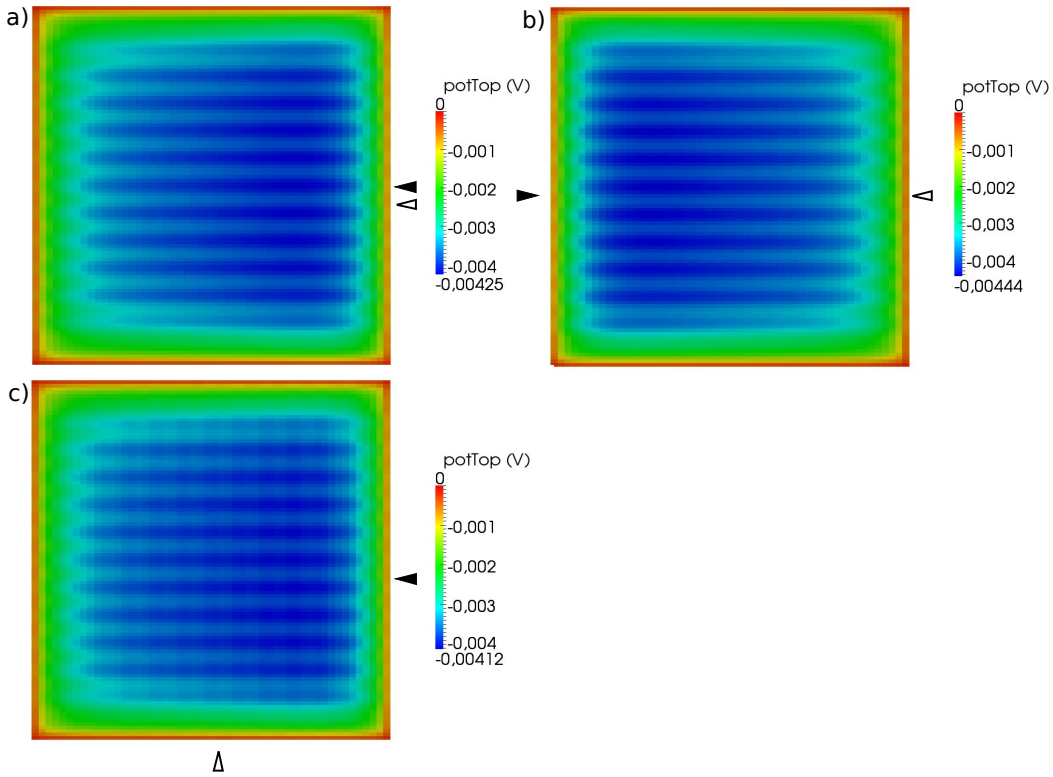


**Slika 16:** Distribucija polja potencijala za a) istosmjerni, b) protusmjerni i c) unakrsni tok. Pune strelice pokazuju smjer strujanja goriva, prazne označavaju zrak.

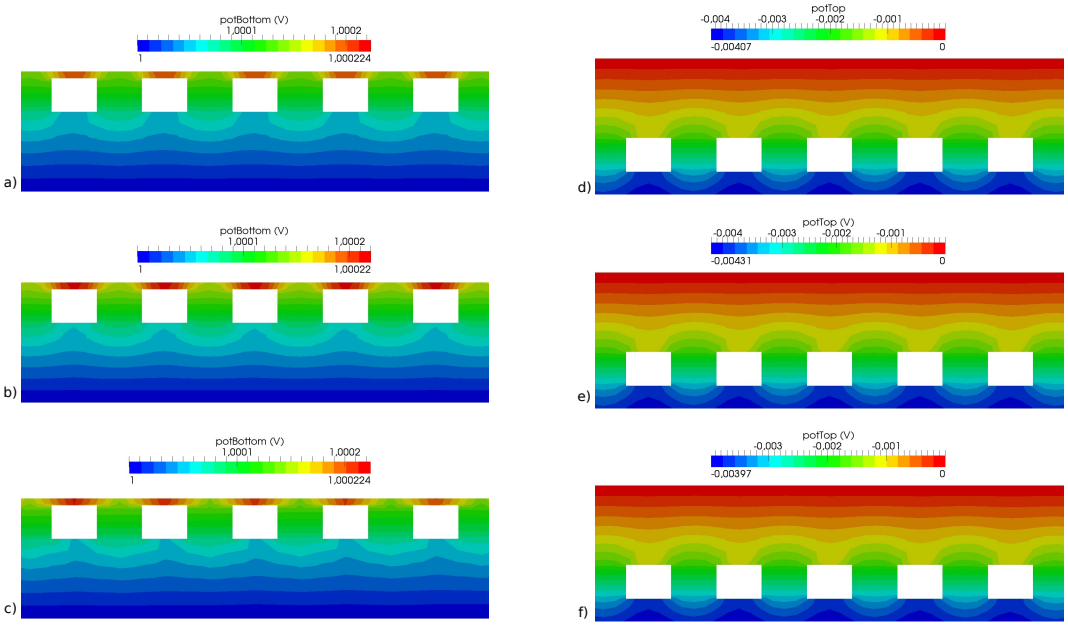


**Slika 17:** Potencijal u presjecima katodnog (lijevo) i anodnog (desno) dijela krutine. a), d) istosmjerni; b), d) protusmjerni; c), e) unakrsni tok.

željenu razinu detaljnosti simulacije modela. Model dvaju potencijala trenutno predstavlja jednostavnu bazu na koju je moguće nadograđivati kompleksnije i detaljnije modele za gorivne članke.

# Chapter 1

# Introduction

## 1.1 Thesis Outline

Present chapter provides introduction in fuel cell technology and types, gives fuel cell advantages and disadvantages, and explains the overall physical processes. Geometries are described, as well as fuel cell losses.

Chapter 2 provides a deeper inspection of electrochemical phenomena in fuel cell reactions. Electrode kinetics, mass and charge transfers are described, and thermodynamical foundations are derived. Connection between the chemistry of fuel reactions and the macroscopic phenomena is established. Crucial equations for modeling fuel cells are derived and detailed analysis of ireversibilities is given.

In Chapter 3 existing model for solid oxide fuel simulations is described, along with its assumptions, approach to mesh decomposition and governing equations.

Chapter 4 proposes new model for SOFC simulations. Two potential model focuses more on potential distribution in electrodes and electrolyte, and takes into account electric conductivity of solids. Mesh decomposition that is suitable for new approach is provided, along with new governing equations of the two potential model.

Finally, Chapter 5 provides result analysis, as well as the comparison with existing data.

## 1.2 Fuel Cells

Fuel cells are devices that convert chemical energy stored in fuel into useful electrical energy, with heat released as by-product. While there is a continuous supply of fuel, electricity will be produced. This is a key difference between fuel cells and batteries (which are energy storage devices and are consumed when discharged), and at the same time a similarity fuel cells share with combustion engines[1]. Both fuel cells and combustion engines are based on the chemical transformation during oxidation of fuel. Equation (1.2.1) represents the simplest example, combustion of hydrogen:

$$H_2 + \tfrac{1}{2}O_2 \rightleftharpoons H_2O + \text{energy}. \tag{1.2.1}$$

On the molecular level, in reactions between hydrogen and oxygen, hydrogen molecules are oxidized and produce water and release heat. In a time frame of picoseconds, molecular bonds are broken and new ones are formed by electron transfer. Produced water's bond energy is lower than the initial configuration, and the difference is released as heat[2]. Energy of the exothermic reaction of combustion can be utilized only as heat, because electron transfer is occurring at subatomic scales and in extremely short time spans.

Fuel cells employ another way of harnessing electron transfer from high-energy reactant bonds to low-energy product bonds: spatially separating oxygen and hydrogen reactions, thus forcing electrons to travel over a greater length scale. This way electrons can be directly used to do useful work while closing the circuit and completing reaction, which is more efficient than converting thermal to electric energy in case of combustion.

Equations (1.2.2) and (1.2.3) show the hydrogen combustion split into two *half reactions*:

$$H_2 \rightleftharpoons 2H^+ + 2e^-, \tag{1.2.2}$$

$$\tfrac{1}{2}O_2 + 2H^+ + 2e^- \rightleftharpoons H_2O. \tag{1.2.3}$$

These reactions occur at the electrodes which are spatially separated but connected by an external circuit for electron conduction. Oxidation of hydrogen is taking place at the anode, while reduction of oxygen is occurring at the cathode. Electrodes are separated by the electrolyte, which is impermeable for electrons, but allows transfer of ions. Figure 1.2.1 shows

schematics of a general fuel cell, with reactant, product, ion and electron flows. Just as electrons pass through external circuit, ions travel through the electrolyte from one electrode to the other to complete the reaction. Depending on the electrolyte used (i.e. type of fuel cell), ions can be positive or negative so the direction of travel can be different.

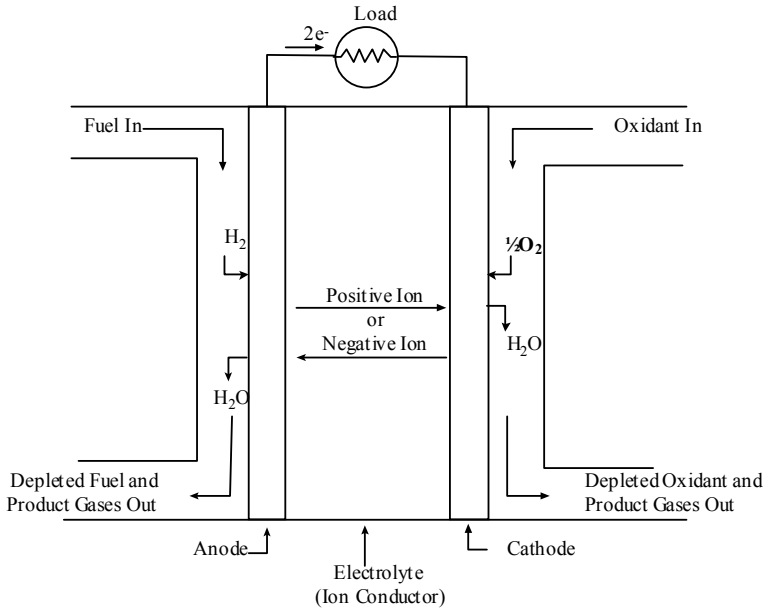


**Figure 1.2.1:** General scheme of single fuel cell.

Hydrogen is the most widely used fuel for powering fuel cells, although it is possible to use simple hydrocarbons as well. Using fuels that contain carbon can cause electrode *poisoning* due to carbon monoxide (CO) which is created during reactions, and which passivates the surface. Furthermore, more complex fuels lead to sluggish reactions. Both of the mentioned obstacles can be avoided in high-temperature fuel cells, where reaction kinetics are faster and internal reforming of the fuel can be utilized. Some types of fuel cells can even use CO as fuel and thus circumvent the problem with poisoning.

### 1.2.1 Advantages of Fuel Cell Technology

While currently not competitive with conventional technologies, different types of fuel cells have several advantages that position them as interesting and potentially important technology in future:

- **Efficiency**. Fuel cells' main advantage is the direct conversion of chemical into electri-

cal energy. When compared with combustion engines, fuel cells *generally* have higher efficiency because they do not subject to the Carnot efficiency limit[3]. Figure 1.2.2 compares maximum H2 fuel cell efficiency with the Carnot limit and it can be seen that efficiencies are temperature-dependent. It is important to notice that fuel cells do not *always* more efficient, and even though *ideal* efficiency is greater for lower temperatures, due to higher irreversibility and valuable high-temperature waste heat, fuel cells usually do have greater efficiency at higher temperatures[3].

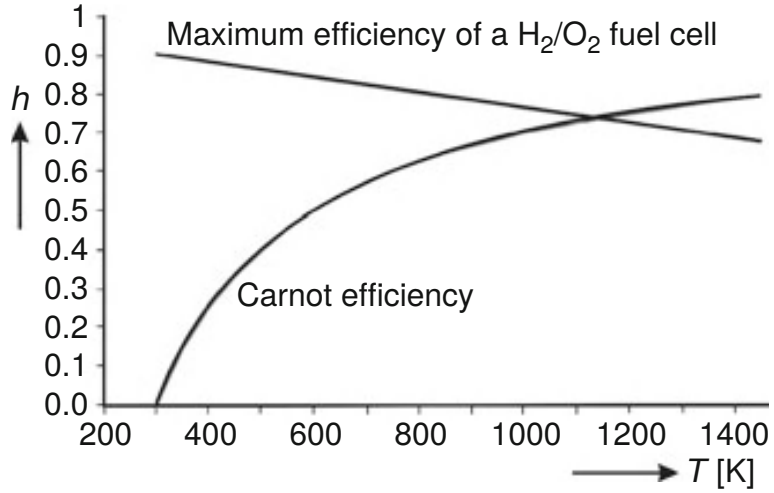


**Figure 1.2.2:** Comparison between maximum efficiency for fuel cell and Carnot cycle efficiency.

- **Scalability**. Unlike batteries, fuel cells are fully scalable between power and capacity. Batteries scale poorly at large sizes, have significantly shorter life span and need to be recharged, while fuel cells scale well from $1W$, small mobile applications to megawatt range for power plants.
- **Simplicity**. The core components of fuel cells have few (if any) moving parts and allow for the solid state device. This way systems are long-lasting and highly reliable. Another advantage of being stationary is silence, even for those fuel cells with equipment for fuel processing[3].
- **Low emissions**. When hydrogen is used as fuel, the only by-product of reaction is water. Thus fuel cells reduce pollutant emissions in both stationary and mobile applications. However, fuel production is currently still not fully pollutant-free.

### 1.2.2 Disadvantages of Fuel Cell Technology

Currently, the main disadvantage of fuel cells is their price. Because of their prohibitive costs, fuel cell technology is currently competitive only in niche applications, such as space exploration.

Using hydrogen as a preferred energy vector is problematic as well. Currently there is no developed infrastructure for its consumer-grade supply, and hydrogen storage has its own deficiencies. Using in-situ hydrogen production by solar powered water electrolyzer could prove as a completely clean energy cycle but at present such technology is not yet cost-effective.

Another major limit is the power density. It expresses how big is the energy output per unit volume or unit mass. When compared with combustion engines and batteries, on volumetric basis fuel cells are outperformed, and the situation is more favorable when seen on gravimetric terms, as seen in Figure 1.2.3.

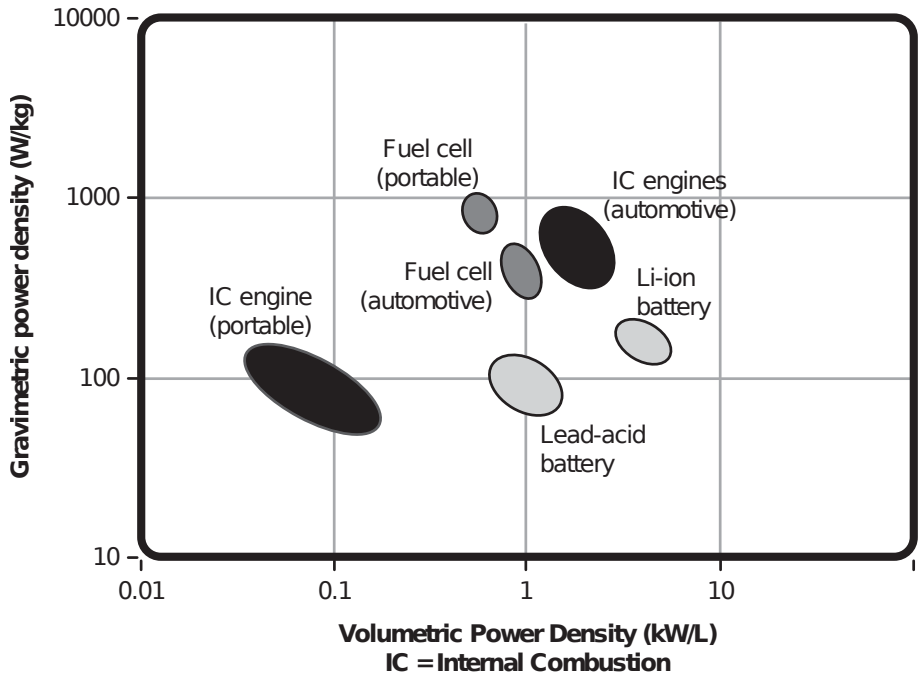


**Figure 1.2.3:** Power density comparison.

Additional limitations are temperature compatibility issues, liability to poisoning and fuel purity for some fuel cell types and durability under intermittent operation. These disadvantages pose a problem for wide adoption of fuel cells, and their technical solutions will decide the future of fuel cells.

**Table 1.3.1:** Fuel cell types.

| | PEMFC | AFC | PAFC | MCFC | SOFC |
|---|---|---|---|---|---|
| Electrolyte | Polymer Membrane | Immobilized Liquid KOH | Immobilized $H_3PO_4$ | Molten Carbonate | Perovskites (Ceramics) |
| Electrodes | Carbon | Carbon | Transition metals | Nickel Oxide | Perovskite |
| Catalyst | Platinum | Platinum | Platinum | Platinum | None (electrode material) |
| Temperature | $40\,°C - 80\,°C$ | $65\,°C - 220\,°C$ | $200\,°C$ | $650\,°C$ | $500\,°C - 1000\,°C$ |
| Charge carrier | $H^+$ | $OH^-$ | $H^+$ | $CO_3^{2-}$ | $O^{2-}$ |
| Fuel | $H_2$, methanol | $H_2$ | $H_2$ | $H_2$, $CH_4$ | $H_2$, $CH_4$, CO |

## 1.3 Fuel Cell Types

The main distinguishing feature between fuel cell types is the type of electrolyte. While all fuel cells rely on the same electrochemical principles, electrolyte dictates the operating temperature range, just as type of ions that pass through it. Further, the operating temperatures set requirements onto physiochemical and thermomechanical properties of materials. Temperatures also play an important role in deciding on suitable fuel: in low-temperature fuel cells fuel needs to be converted to hydrogen before entering and they are susceptible to CO poisoning. In high-temperature devices, CO and even $CH_4$ can be converted into hydrogen (internal reforming) or can be even directly oxidized in reaction.

The most common types of fuel cells are polymer electrolyte fuel cells (PEFC), alkaline fuel cells (AFC), phosphoric acid fuel cells (PAFC), molten carbonate fuel cells (MCFC), and solid oxide fuel cell (SOFC). Table 1.3.1 provides overview of the key features of the each type[1].

In this study, especially in later chapters, work is focused on solid oxide fuel cells, and their kinetics and particularities will be described in more detail. However, most of the underlying principles are valid for all fuel cell types. SOFCs are high-temperature devices that can use wider range of fuels, or even reform some of the more complex hydrocarbon fuels into $H_2$

and CO. They employ a thin solid ceramic layer as electrolyte that is conductible for oxygen anions ($O^{2-}$) and thus differ from proton conducting fuel cell types. Hence, equation (1.2.1) for hydrogen as fuel is rearranged to different half-reactions:

$$H_2 + O^{2-} \longrightarrow H_2O^+ + 2e^-, \tag{1.3.1}$$

$$\tfrac{1}{2}O_2 + 2e^- \longrightarrow O^{2-}. \tag{1.3.2}$$

The most common material for SOFC electrolyte is a oxide material called yttria-stabilized zirconia (YSZ)[4]. Solid oxide fuel cells operate at higher temperatures $> 600\,^{\circ}C$, which is advantageous in terms of higher efficiency, just as in ability to utilize waste heat via some of the available technologies (Organic Rankine cycle, combined heat and power technologies...).

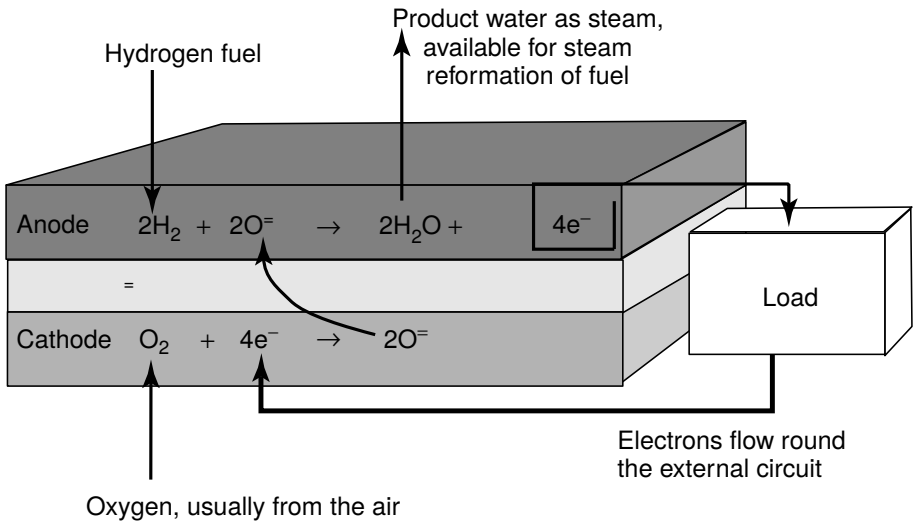


**Figure 1.3.1:** Separated reactions for SOFC with hydrogen as fuel.

## 1.4 Fuel Cell Operation

As mentioned in section 3.1, current is produced by forcing electron flow through the external circuit. One of the parameters electricity depends on is the reaction area of electrolyte and electrode where reactants meet. This is the reason why fuel cells are generally made in form of a thin, planar structures with high surface-to-volume ratio. Because it is critical to ensure

so called *triple phase boundary* between fuel (gas), electrode (solid) and electrolyte (solid or liquid), and also have high surface area, electrodes are made highly porous. This yields generally scalable power output to high levels - when more reactants can enter reaction on bigger area, larger is the current of electrons produced.

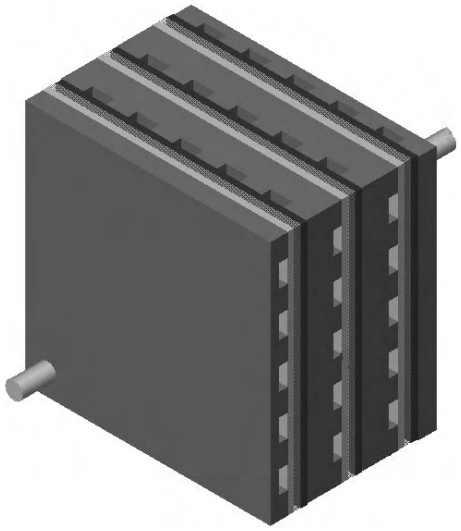

**Figure 1.4.1:** A three-cell stack showing geometry of fuel cells with channels, electrodes, electrolyte and bipolar plates.

Fuel cell operation depends on several major steps. First of them is equal distribution of reactant gases over the cell. To produce electricity, fuel and oxidant must be continually supplied. If that is not the case, the device can "starve", and that is problematic especially when we consider that demand for reactants can be extensive at high current densities. To uniformly deliver gases, combination of *flow field plates* and porous electrodes is used. When considering the more common, planar type of fuel cells, plates have many grooves or channels that distribute gases evenly to the surface, and their geometry greatly affect the performance. To further diminish the effect of the concentrated channels, electrodes are produced as porous structures, causing uniform fluid diffusion over electrolyte surface. Just as supplying the reactants to the reaction occurring spots, it is equally important to assure fast enough removal of reaction products to the bulk gas phase. Otherwise, products will build up and cause bottleneck, preventing more products to react and slowing the reaction. Managing reactants is usually a minor issue compared to the fuel distribution, and is dealt with in the same way as the supply. However, some fuel cell types are more susceptible to it, e.g. with PEMFC product

water can "flood" the cell and cause major efficiency downfall.

Generated current is in a direct relation with the speed of electrochemical reaction, thus, it is favorable to ensure energetic reaction rates. Catalysts are usually used to lower the reaction activation energy and increase its speed. Platinum is mostly used as catalyst for fuel cells and its cost was a big limiting factor during the development of fuel cells. Lately, however, quantity of platinum used was decreased significantly and led to further lowering of fuel cell prices. On the other hand, high-temperature fuel cells such as SOFC do not require catalyst because temperatures are high enough to ensure high reaction rates on their own.

As seen in equations (1.3.1) and (1.3.2), electrochemical reactions that occur in fuel cells produce or consume ions or electrons. To maintain charge balance, charged particles must be transported from the location they are produced to the location they are consumed. Managing electron flow is quite straightforward - electrodes are electrically conductive and they create a path via external circuit for electrons to travel through and do useful work. Ion conduction is a bigger issue since ions are bigger so their transport through defects in crystal structure is less efficient. Electrolyte must have high ion conductivity, but also prevent electrons to diffuse through it and "short-circuit" the electrodes. Since ion transfer is inefficient, it causes resistance loss and reduces cell performance. This is circumvented by using very thin ceramic electrodes to shorten the path ions need to travel.

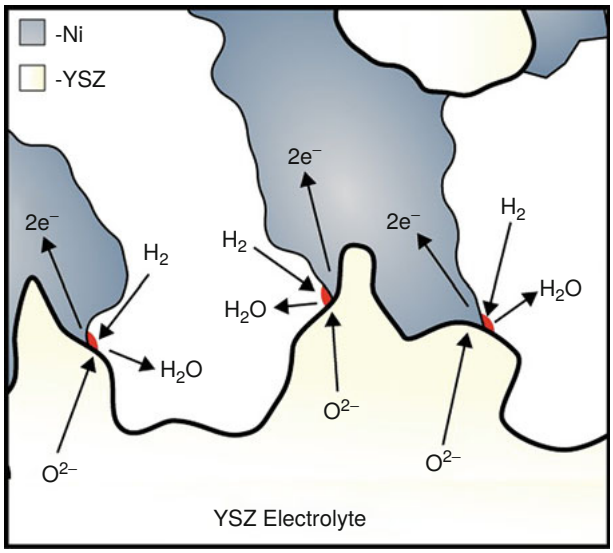


**Figure 1.4.2:** Schematics of a triple phase boundary of Ni-YSZ based anode operating with H2 fuel.

As mentioned earlier, electrode-electrolyte assembly is a three-phase system with porous materials: electrically conductive electrode and ionically conductive electrolyte and the pores themselves. On this triple phase boundary, where gases, ions and electrons meet is the location where reaction occurres. Figure 1.4.2 shows schematic of Ni-based anode operating with $H_2$ fuel.

## 1.5 Fuel Cell Performance

Since the basic overview of processes in a fuel cell has been presented, it is appropriate to explain fuel cell performance and introduce losses associated with steps involved in aforementioned fuel cell operation. The most useful graph when discussing fuel cell performance is the current-voltage ($i-V$) curve, showing voltage output for a given current. For easier comparison between differently sized cells, the current is normalized by area, yielding current density. Ideal fuel cell would produce any amount of current proportional to the fuel supplied and also maintain constant and maximum voltage output. However, due to real world irreversibilities this is not the case and the Figure 1.5.1 represent typical $i-V$ curve. Three separate regions can be distinguished. First is the rapid initial fall in voltage at low current density, followed by gradual and linear decline in the mid-high current densities. The last stage is again a steep fall of voltage at high currents. Another performance indicator is the power output of a cell, calculated as a product of current and voltage:

$$P = iV. \tag{1.5.1}$$

Since the current is proportional to the amount of the fuel provided, voltage corresponding to the current density can be viewed as a main measure of efficiency. It is critical to achieve high voltages, especially under high current densities. However, because of the irreversibilities it is impossible to maintain ideal, thermodynamically calculated voltage levels and because of that power density curve rises due to increased current, peaks, and then plummets at the far end of graph, just as the $i-V$ curve does (Figure 1.5.1).

Since fuel cells are an interdisciplinary technology, various fields of studies have used different names for losses causing voltage drops. Most common term is *overpotential*, but polarization, losses, voltage drop and irreversibility are used as well[3].

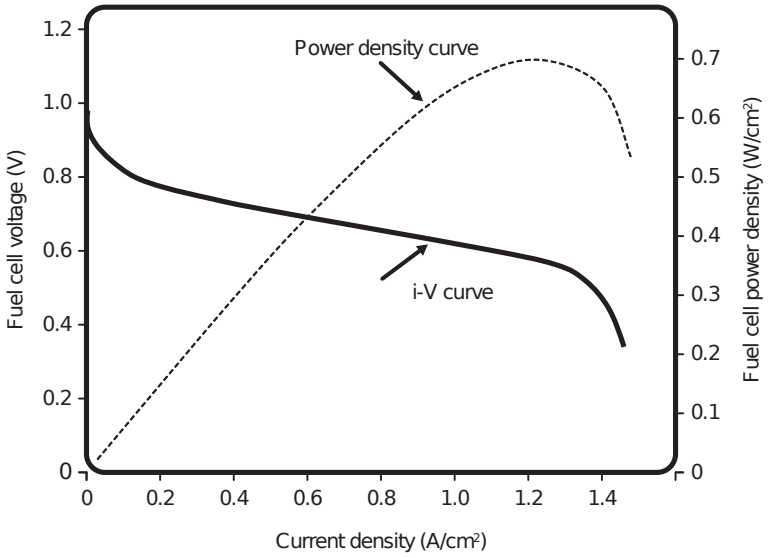


**Figure 1.5.1:** i-V curve for fuel cell combined with power density curve.

Losses below correspond to steps mentioned in section 1.4 in fuel cell operation and can be correlated to characteristic regions of the $i-V$ diagram.

- **Activation losses** are caused by slow reaction speed on the electrode surface. A highly non-linear fragment of voltage is lost in driving the electrochemical reaction and overcoming the activation energy. They are dominant in the low current density region, especially with low temperatures and are the main reason why catalysts are used.

- **Ohmic losses** are linear irreversibilities due to resistance to electron and (to a lesser extent) ion conduction through electrodes, electrolyte and interconnections. These losses are directly proportional to current density.

- **Mass transport losses** (concentration overpotential) result from the changes in concentration of reactants on the electrodes, their distribution and poor removal of the reaction products.

- Additional losses are **fuel crossover** and **internal currents**. Because electrolytes are not ideal, fuel can diffuse through it and pass to the other side without participating in reaction. Furthermore, since electrolytes are not ideal electrical insulators, small amount of electron conduction will happen. Effects of these losses are negligible compared to the previous three.

In fuel cell terminology overpotentials are usually denoted by Greek letter $\eta$. If losses mentioned above cause difference from ideal case, cell voltage output can be written as:

$$V = V_{ideal} - \eta_{act} - \eta_{ohmic} - \eta_{conc}, \tag{1.5.2}$$

where subscripts denote corresponding overpotentials to their physical causes.

Basics of fuel cell technology presented in this chapter, their types, performance and overview of the phenomena occurring during operation serve as introduction to more detailed thermodynamic description of fuel cell background in following chapter.

# Chapter 2

# Thermodynamics and Fuel Cell Kinetics

## 2.1 Introduction

Previous chapter gave the introduction into physical processes occurring in fuel cell operation, and identified main causes of discrepancies between ideal case and real world application. In this chapter thermodynamics of reactions in fuel cells will be given, as well as more detailed analysis of reaction kinetics and charge and mass transfer[5].

## 2.2 Thermodynamic Fundamentals and Gibbs energy

Fuel cells are devices that *convert* chemical energy of the fuel into electricity for doing work. However, implication of term 'chemical energy' and what portion of energy is converted is not quite obvious. Therefore, to explain and derive important terms for considering fuel cell thermodynamics, we start with a well known expression for internal energy:

$$dU = dQ - dW. \tag{2.2.1}$$

If we for now assume that only mechanical work $p\,dV$ is being done, and if we combine the $2^{nd}$ law of thermodynamics (entropy production), we get another familiar equation for internal energy, which is based on independent variables.

$$dU = T\,dS - p\,dV \tag{2.2.2}$$

Enthalpy is a system state function that includes its internal energy and the amount of energy required to make room for it by displacing its environment and establishing its volume and pressure:

$$H = U + pV. \tag{2.2.3}$$

Just as enthalpy is conveniently defined variable, such is the *Gibbs energy* (Gibbs free energy) regularly introduced for describing electrochemical systems. Compared to enthalpy, it is the energy needed to create a system (its internal energy), displace environment to make room for it, while neglecting energy that can be exchanged with system due to heat transfer.

$$G = U + pV - TS \tag{2.2.4}$$

Now, when we substitute in the expression for enthalpy, we get the usual equation for Gibbs energy:

$$G = H - TS. \tag{2.2.5}$$

Similarly as with enthalpy and entropy, we are actually interested in change of Gibbs energy, $\Delta G$, which then represents maximum non-expansion work that may be performed by a thermodynamic system at a constant temperature and pressure. One of the motivations behind Gibbs energy formulation is the need to define system with variables that are easily measured, unlike $S$ and $V$ in equation (2.2.2). If we differentiate equation (2.2.4), we obtain:

$$dG = dU + p\,dV + V\,dp - T\,dS - S\,dT, \tag{2.2.6}$$

and bearing in mind that $dU = T\,dS - p\,dV$, the variation of $G$ equals

$$dG = V\,dp - S\,dT. \tag{2.2.7}$$

This shows that Gibbs energy is nothing more than a thermodynamic description of a system that depends on $T$ and $p$ instead of $S$ and $V$.

Usually, it is more useful to calculate energy changes on a per-mole basis, so we have $\Delta\hat{g}$, $\Delta\hat{s}$ and $\Delta\hat{h}$. Furthermore, just as with defining entropy and enthalpy, it is convenient to reference all values to a set of standard-state conditions, which are labeled by superscript zero.

As the change during thermodynamical reaction is of interest, e.g. if we consider a standard $H_2 - O_2$ reaction in fuel cell, for one mole of $H_2$

$$H_2 + \tfrac{1}{2}O_2 \longrightarrow H_2O, \tag{2.2.8}$$

we obtain

$$\Delta\hat{g} = \hat{g}_{products} - \hat{g}_{reactants}, \tag{2.2.9}$$

and specifically,

$$\Delta\hat{g}_{rxn} = \hat{g}_{H_2O} - \hat{g}_{H_2} - \hat{g}_{H_2} = -237.2\,\text{kJ/mol}\,H_2. \tag{2.2.10}$$

This is the value for the reaction at 25 °C, read from available tables. Just as molar enthalpies and entropies, Gibbs energies are not constant and are temperature-dependent. It is important to note that the value of Gibbs energy for hydrogen reaction is negative. That means that the energy is released, and if process could be reversible, all of the Gibbs energy would be available to harness. Equations where reversibility is presumed apply to equilibrium conditions, where there is no net current flow in the fuel cell. As soon as the current is drawn, equilibrium is lost. In order to distinguish between reversible and non-reversible voltages, symbols $E$ and $V$ are used, respectively.

Another connection that is useful to make is a relation between Gibbs energy and spontaneity of a reaction. If $\Delta G$ of reaction is zero, then no work can be extracted from it. $\Delta G < 0$ means that reaction is favorable (spontaneous) and that energy can be gained. On the other hand, if $\Delta G > 0$ then reaction can not occur by itself in that direction, and for it to proceed, work has to be input into the system.

## 2.3 Gibbs Energy and Work

Gibbs free energy represents maximum work potential of the system, so it is our goal to be able to calculate its value. If we look at equation (2.2.5) and differentiate it, we obtain

$$dG = dH - T\,dS - S\,dT. \tag{2.3.1}$$

If we assume isothermal process and setting the constant temperature, $dT = 0$, we can still calculate $dG$ for other temperatures and the only limitation is that temperature does not vary during the process. When we write the equation in molar terms, we have

$$\Delta\hat{g} = \Delta\hat{h} - T\,\Delta\hat{g}. \tag{2.3.2}$$

Here, we must also take into account standard-state values as references, check for tabular values of enthalpies and entropies for both products and reactants in considered reaction, and calculate the result.

Since electrical work is of interest, its relation with Gibbs energy is derived. First, we expand equation (2.2.2) to include electrical work as well:

$$dU = T\,dS - (p\,dV + dW_{elec}). \tag{2.3.3}$$

Then, equation (2.2.6) is included in equation (2.3.3) and we obtain

$$dG = T\,dS - (p\,dV + dW_{elec}) + p\,dV + V\,dp - T\,dS - S\,dT, \tag{2.3.4}$$

when canceled out, with constant pressure and temperature applied ($dT = 0$, $dp = 0$), equation (2.3.4) reduces to

$$dG = -dW_{elec}, \tag{2.3.5}$$

and for molar values we write

$$W_{elec} = -\Delta g_{rxn}. \tag{2.3.6}$$

For a reaction under constant pressure and temperature, the maximum amount of electrical work is given by a negative value of Gibbs energy.

## 2.4 Reversible Voltage

Measure of the system's ability to do work is the voltage (electrical potential). That work is done by moving charge $Q$ through the electrical potential field $E$:

$$W_{elec} = EQ. \tag{2.4.1}$$

In our case charge carriers are electrons, while the charge is defined as

$$Q = nF, \tag{2.4.2}$$

where $n$ is the number of moles of electrons that travel through the external circuit, and $F$ is Faraday's constant, $F = 96\,485\,\mathrm{C/mol}$. In case of hydrogen reaction it can be seen from equations (1.3.1) and (1.3.2) that for every molecule of $H_2$, two electrons are transferred, therefore $n = 2$. When equation (2.3.6), equation (2.4.1) and equation (2.4.2) yields:

$$\Delta\hat{g} = -nFE, \tag{2.4.3}$$

or, in a more common form for $E$:

$$E = -\frac{\Delta\hat{g}}{nFE}. \tag{2.4.4}$$

We can see that Gibbs' energy magnitude determines reversible voltage $E$ for the cell. Again, when we consider hydrogen reacting in fuel cell, with $\Delta g^0_{rxn}$ previously calculated as $-237.2\,\mathrm{kJ/mol}$, we get:

$$E^0 = -\frac{\Delta\hat{g}^0_{rxn}}{nF} \tag{2.4.5}$$

$$= -\frac{-237.2\,\mathrm{kJ/mol}}{(2\,\mathrm{mol}\,e)(96\,485\,\mathrm{C/mol})} = 1.23\,\mathrm{V}. \tag{2.4.6}$$

In equation (2.4.6) $E^0$ represents standard-state reversible voltage, which is the highest reversibly and thermodynamically achievable voltage for this chemical reaction. For real world applications, 1.23 V is too low a value. Choosing different reaction instead of hydrogen would change reversible cell voltage, but voltages for feasible cell reactions range about 0.8–1.5 V. To obtain desired voltage outputs, fuel cells are usually stacked and combined into serial and parallel circuits.

The transition from thermodynamic to electrochemistry by using the quantity $nF$ is the very cornerstone of electrochemistry, and combines the idea of moles of reacting species with

quantized electron transfer. As mentioned above, value of $n$ depends on the reaction (in case of hydrogen reaction it is 2). Feasibility of fuel cells lies here as well: because Faraday's constant is a high number ($F = 96\,485\,\mathrm{C/mol}$), it means that charge produced per mole is very high (equation (2.4.2)) and this way a small amount of electrochemical reaction results in a significant amount of transferred charge.

## 2.5 Thermodynamic Efficiency

Efficiency of a fuel cell was briefly considered in Section 1.2.1, but now that the thermodynamic background is laid out, it can be quantified more formally. In a reversible process, all of the Gibbs free energy is converted into electricity, and efficiency is 100 %. Thus, it is not really practical to define efficiency this way because its theoretical limit would always be 100 % (it is worth remembering that Gibbs energy is temperature-dependent and can change). A more useful way is to compare electrical energy to heat that would be produced by burning the fuel, since it usually is used for burning in order to release the energy. This way, enthalpy-based efficiency also serves as comparison parameter between fuel cells and combustion engines.

Usually when discussing fuel cells $\eta$ is reserved for overpotentials, so some textbooks[2] use $\varepsilon$ instead:

$$\varepsilon = \frac{\Delta\hat{g}}{\Delta\hat{h}}. \tag{2.5.1}$$

For equation with hydrogen, as used in the example above, where at standard state conditions $\Delta\hat{g}^0 = -273.17\,\mathrm{kJ/mol}$ and $\Delta\hat{h}^0_{HHV} = -285.83\,\mathrm{kJ/mol}$ (for exothermic reaction like this one change of enthalpy is negative), our reversible efficiency is $\varepsilon = 83\,\%$. As an example, a Carnot cycle that operates between 400 °C and 50 °C (that corresponds to steam turbine with the water exhaust through condenser), has the reversible efficiency of 52 %.

Another way of looking at efficiency is to consider how much fuel is actually consumed in the reaction. Some of the fuel that enters the fuel cell might flow through it without reacting at all or participate in reaction that does not produce wanted electric current. Thus, *fuel utilization efficiency* is the ratio of fuel used to generate electric energy versus total fuel supplied to the cell.

$$\varepsilon = \frac{\text{fuel reacted}}{\text{fuel supplied}}. \tag{2.5.2}$$

## 2.6 Nernst Equation

When deriving Gibbs energy, a system that is a function of $p$ and $T$ was described: $G = G(p,T)$. However, temperature and pressure are not the only variables that Gibbs energy depend on and effects of concentration need to be taken into account. This will lead to one of the main electrochemistry equations, the *Nernst equation*. Concept of *chemical potential* is therefore introduced. Chemical potential $\mu$ is somewhat vaguely described as measure of change of the system's Gibbs energy when chemistry of system changes[1]. If a system is in a thermal equilibrium, there is no exchange of energy; if pressure is constant, there is no net change of volume. Similarly, in a chemical equilibrium there is no flow of particles. This physical concept plays an important role in chemistry, especially when some kind of phase change is occurring.[1] If system is more accurately defined as $G = G(p,T,\mu_i)$, with $\mu_i$ being chemical potential of species $i$, then partial derivative with respect to chemical potential, with temperature and pressure constant is

$$\mu_i = \left(\frac{\partial G}{\partial n_i}\right)_{T,p,n_{j\neq i}} \tag{2.6.1}$$

This formulation represents chemical potential of a species in a mixture as the slope of the free energy with respect to a change in the number of moles of only that species. Therefore, the amount of species is linked to the Gibbs free energy. Finally, the concentration is linked to the chemical potential via another chemical concept - *activity a*. Activity is a measure of the effective concentration of species under non-ideal (concentrated) conditions and it determines the real chemical potential for a real solution rather than an ideal one:

$$\mu_i = \mu_i^0 + RT\ \ln a_i. \tag{2.6.2}$$

The activity of a species depends on its chemical nature and phase and it differs for ideal or non-ideal gases, diluted solution, electrons in metals etc. For ideal gases, which fuels in

[1] Water has lower chemical potential in ice phase below 0 °C, but above lower potential in liquid phase, thus phase transition).

fuel cells at temperatures up to 1000 °C can be considered as, activity is defined as $a_i = p_i/p^0$, with $p_i$ being partial pressure of species in the mixture, and $p^0$ is the standard pressure at 1 atm.

Equations equations (2.6.1) and (2.6.2) are now combined and changes in the Gibbs energy for a system of $i$ chemical species are:

$$dG = \sum_i \mu_i dn_i = \sum_i (\mu_i^0 + RT \ln a_i) dn_i. \tag{2.6.3}$$

For a hypothetical equation $a\,\mathrm{A} + b\,\mathrm{B} \longrightarrow c\,\mathrm{C} + d\,\mathrm{D}$, molar difference in Gibbs energy can be written with consideration for products and reactants

$$\Delta\hat{g} = (m\mu_M^0 + n\mu_N^0) - (a\mu_A^0 + b\mu_B^0) + RT \ln \frac{a_M^m a_N^n}{a_A^a a_B^b}. \tag{2.6.4}$$

First two terms in Equation (2.6.4) above are equal to $\Delta\hat{g}^0$, and from equation (2.4.3) we have $\Delta\hat{g} = -nFE$. Combining them we obtain:

$$-nFE = \Delta\hat{g} + RT \ln \frac{a_M^m a_N^n}{a_A^a a_B^b}. \tag{2.6.5}$$

After rearranging and using equation (2.4.5):

$$E = E^0 - \frac{RT}{nF} \ln \frac{a_M^m a_N^n}{a_A^a a_B^b}. \tag{2.6.6}$$

Finally, when fraction is written as a product of equation products and reactants, with $\nu_i$ as stoichiometric coefficient, we obtain Nernst equation, which shows how reversible voltage of a fuel cell vary with species parameters.

$$E = E^0 - \frac{RT}{nF} \ln \frac{\prod a_{\text{products}}^{\nu_i}}{\prod a_{\text{reactants}}^{\nu_i}}. \tag{2.6.7}$$

Additionally, if activity is written for ideal gas, a most common form of equation is obtained:

$$E = E^0 - \frac{RT}{nF} \ln \frac{\prod p_{\text{products}}^{\nu_i}}{\prod p_{\text{reactants}}^{\nu_i}}. \tag{2.6.8}$$

When calculated for ranges of temperatures and pressures, it looks like increase of variables does not contribute significantly to raise of voltage[1]. So it would seem that operating

at higher parameters is simply not worth the effort. However, it will be shown that higher temperature and pressure are more important due to reaction kinetics and mass transfer.

## 2.7 Reaction Kinetics

So far fuel cell thermodynamics were considered as a reversible process. Now the details behind some of the processes occurring will be explained and their connection to efficiency will be presented.

### 2.7.1 Activation Overpotential

Reaction kinetics describe how the reaction practically occurres, contrary to ideal reversible scenario. Basically, kinetics refer to electrochemical reaction, thermodynamically favorable ($\Delta\hat{g} < 0$) electron transfer. For example, *hydrogen oxidation reaction* (HOR), characteristic for PEM fuel cells:

$$H_2 \rightleftharpoons 2H^+ + 2e^-, \tag{2.7.1}$$

is a reaction that takes place at the interface between anode and electrolyte. Just as every reaction, it actually consists of a series of steps that, when taken together make overall reaction. Basic steps for HOR might be transport of $H_2$ to the electrode, its absorption to surface, separation of $H_2$ into two hydrogen atoms bound to the surface, transfer of electrons from bound atoms to anode while releasing $H^+$ to bulk electrolyte and so on. Every reaction is limited by its slowest step, called *rate limiting step*, and since it is of interest to accelerate the overall reaction, the slowest step needs to be stimulated. If we take the last step as an example—even if it is energetically favorable, atoms need to have certain amount of chemical free energy to overcome the initial barrier. That barrier is called the *activation potential*. As can be seen in Figure 2.7.1.a, transition from one state to the another is more likely to happen, since the energy barrier is lower. That does not mean that reverse reaction is not occurring, just that its rate is less probable and that its rate is lower. This is the case until reaction balance shifts and new equilibrium is found. In the aforementioned case that would mean that concentration buildup of $e^-$ electrons in metal and $H^+$ ions in electrolyte would shift the reaction into

balance.

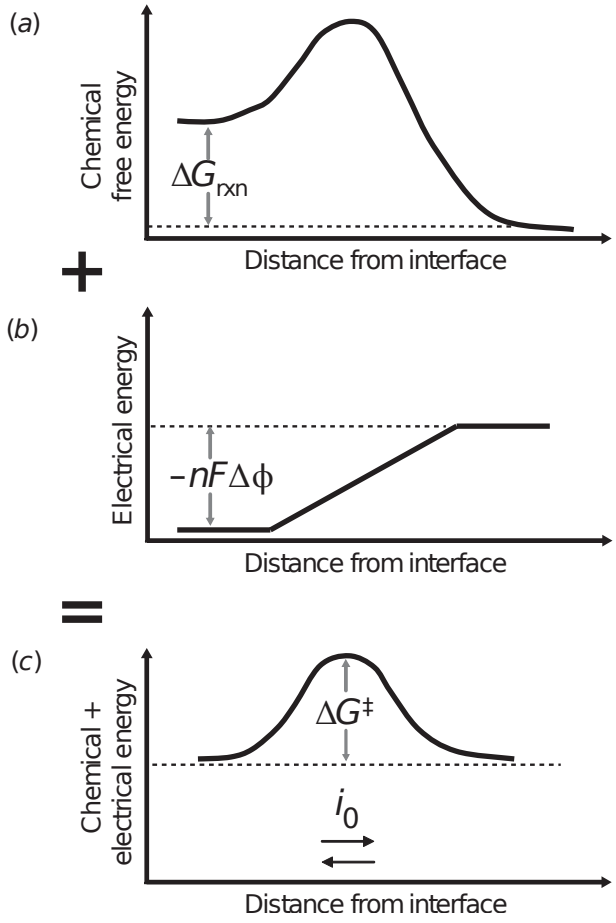


**Figure 2.7.1:** Equilibrium for a step of HOR reaction. *a)* Chemical free energy distribution across a single electrode interface. It is balanced by electrical potential difference due to electron buildup *b)*. These potentials combined result in a zero net reaction rate *c)*.

Reaction rates are here in direct relation to currents, which are of interest when studying fuel cells. Usually, for comparison between differently sized electrodes, area-normalized *current densities i* are used instead of currents. So in the electrode there are continuous forward and backward reactions which result in forward and backward current densities. When the system is in equilibrium, these are equal:

$$i_1 = i_2 = i_0 \tag{2.7.2}$$

and the $i_0$ is called the *exchange current density*. Although net reaction is zero, both forward and reverse reactions exist. In Figure 2.7.1.b it can be seen that the force keeping balance is the

electrical potential difference across interface. When both chemical free energy and electrical potential are super-imposed, result is overall zero current density (Figure 2.7.1.c).

The free energy is dependent on voltage. By changing the cell voltage the free energy of the charged species taking part in a reaction changes, and therefore lowers the activation barrier. By sacrificing fraction of a reversible voltage, potentials at the anode and cathode are lowered, and net current can be produced. Figure 2.7.2.b the dotted line represents voltage lowered by an amount $\eta$. This overpotential is called *activation overpotential* $\eta_{act}$. Further, by decreasing the the potential for $\eta$, Figure 2.7.2.c shows how the activation energy for forward reaction ($\Delta G^{\ddagger}$) is lowered, but asymmetrically due to the asymmetrical factor $\alpha$ (see below). This way, the activation energy for backward reaction is increased and reaction proceeds in the forward direction.

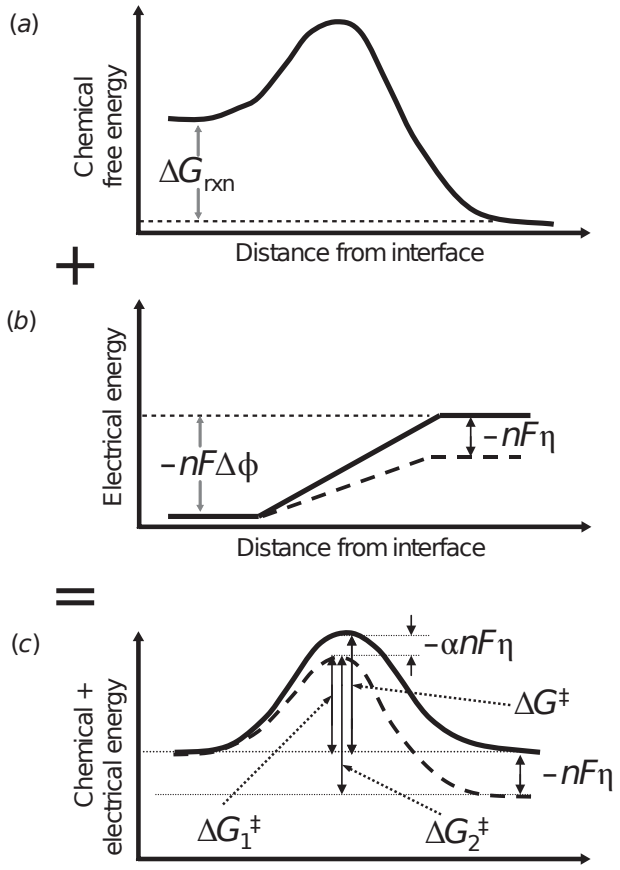


**Figure 2.7.2:** Electric potential $\Delta\Phi$ is lowered by a factor $nF\eta$ due to sacrificed voltage $\eta_{act}$. Balance is upset and the result is the lowered forward activation barrier $\Delta G_1^{\ddagger} < \Delta G^{\ddagger}$, and increased backward activation barrier $\Delta G_2^{\ddagger} < \Delta G^{\ddagger}$ compared to the equilibrium state.

Finally, *Butler-Volmer* equation is introduced to quantify the terms. It combines current densities away from equilibrium (when net current exists) with activation overpotential—part of reversible voltage sacrificed to lower the energy barrier for forward reaction to take place. It is a difference between forward and backward current densities:

$$i_1 = i_0 e^{\alpha nF\eta/(RT)}, \tag{2.7.3}$$

$$i_2 = i_0 e^{(1-\alpha)nF\eta/(RT)}, \tag{2.7.4}$$

where $\alpha$ is the *transfer coefficient* and shows how asymmetric is the change in electric potential across the interface. Value of $\alpha$ depends on the reaction and the electrode material, but is always in range between 0-1. Usually, its value for the cathode is about 0.5, and ranges a bit more for anode, but as will be seen, neither $\alpha$ nor temperature are the most significant terms[3]. Subtracted, these equations form the Butler-Volmer equation for net current, with the first term in bracket representing forward reaction, and second accounting for backward reaction:

$$i = i_0 \left( e^{\alpha nF\eta/(RT)} - e^{(1-\alpha)nF\eta/(RT)} \right) \tag{2.7.5}$$

Butler-Volmer equation, although derived for simple, single-electron transfer reactions with one rate-determining step, is used as good approximation for complex multi-step reactions, such as ones in fuel cells. Figure 2.7.3 shows plot of a relation between $\eta$ and $i$, with contributions of forward and backward reactions. There are the two regions in the plot, one linear at current densities around zero and the second, exponential, at higher current densities. In these regions simplifications for Butler-Volmer equation can be made.

$\eta_{act}$ is the sacrificed voltage used to shift reaction out of balance and provide useful current density. Thus, graph in Figure 2.7.4 represents thermodynamical voltage with $\eta_{act}$ subtracted from it. Hence, activation overpotential is a necessary loss that lowers fuel cell voltage output. Overpotential depends on reaction kinetics, but the most important parameter in the Butler-Volmer equation is the exchange current density, as can be seen in Figure 2.7.4. It is then crucial to keep $i_0$ as high as possible, in order to have high current density output.

Exchange current density can vary by orders of magnitude, suggesting a strong catalytic effect, which can be seen in table 2.7.1 for several electrodes. Furthermore, in case of a hydro-

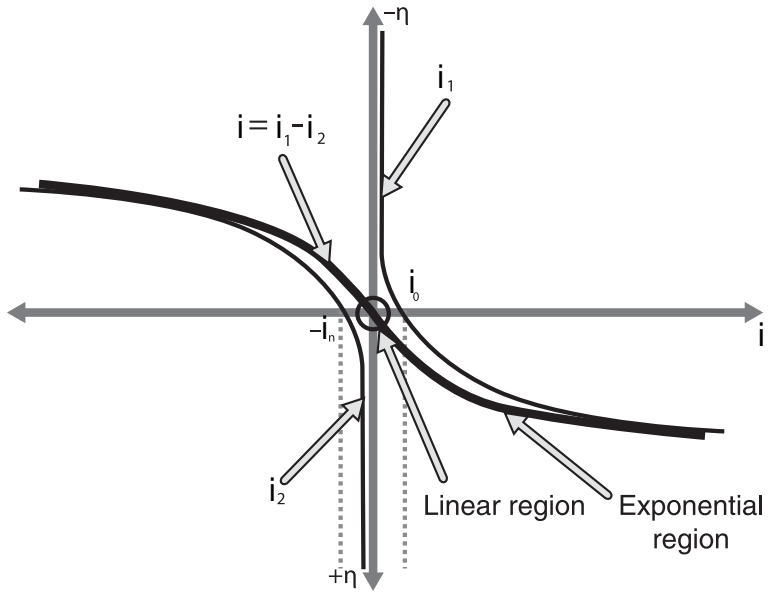


**Figure 2.7.3:** Plot of forward and backward current densities with the Butler-Volmer curve as their sum. Linear region in the middle and exponential regions at the ends can be clearly distinguished.

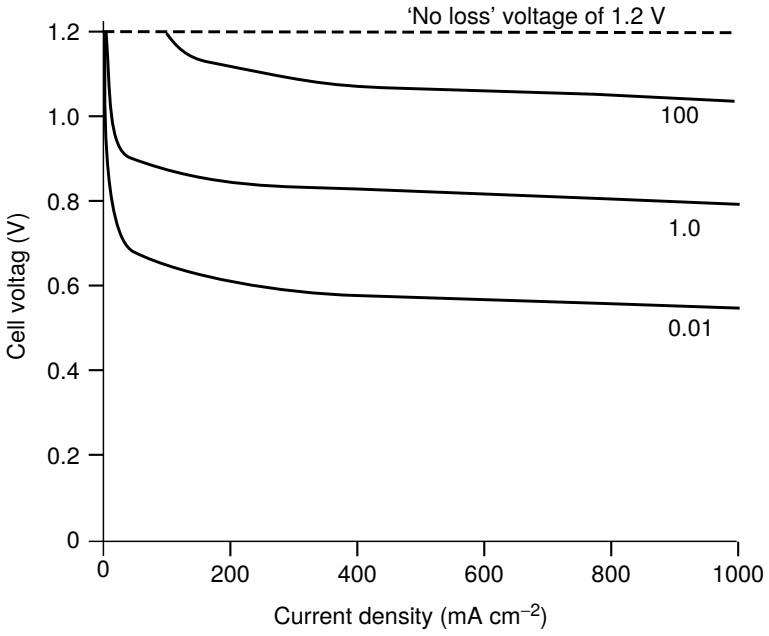


**Figure 2.7.4:** Range of current densities and activation overpotentials they cause. Benefits of high exchange current density is crucial and evident.

**Table 2.7.1:** $i_0$ for the hydrogen electrode for various metals[3].

| Metal | $i_0(A\,cm^{-2})$ |
|---|---|
| Pb | 2.5e−13 |
| Zn | 3e−11 |
| Ag | 4e−7 |
| Ni | 6e−6 |
| Pt | 5e−4 |
| Pd | 4e−3 |

gen fuel cell, oxygen electrode (cathode) has much smaller $i_0$ than the one for anode, so much so that it is negligible when relatively compared. Exchange current density, a crucial factor in improving performance can be increased in several ways:

- By increasing the **temperature**, the initial drop in cell voltage at low current density is significantly reduced (Figure 2.7.5).
- Increasing the the **roughness** of electrode creates much more potential reaction spots, and increases area of electrode.
- Benefits of using **catalysts** are shown in Table 2.7.1. Exchange current density varies by orders of magnitude just by using different material for catalyst layer.
- Increasing **concentration** and **pressure**. Although in section 2.6 it was stated that rise of gas pressure and species concentration has minimal effect on rise of ideal, Nernst potential, it is highly beneficial for increase of exchange current density. This way reaction sites are more likely to be occupied by reactants

### 2.7.2 Tafel Equation

Two characteristic regions in $i_0$-$\eta$ plot can be used for simplifying Butler-Volmer equation, which can sometimes be unwieldy (due to two exponential terms with $\eta$, especially for numerical calculations). These approximations are valid only if activation overpotential is either small or large:

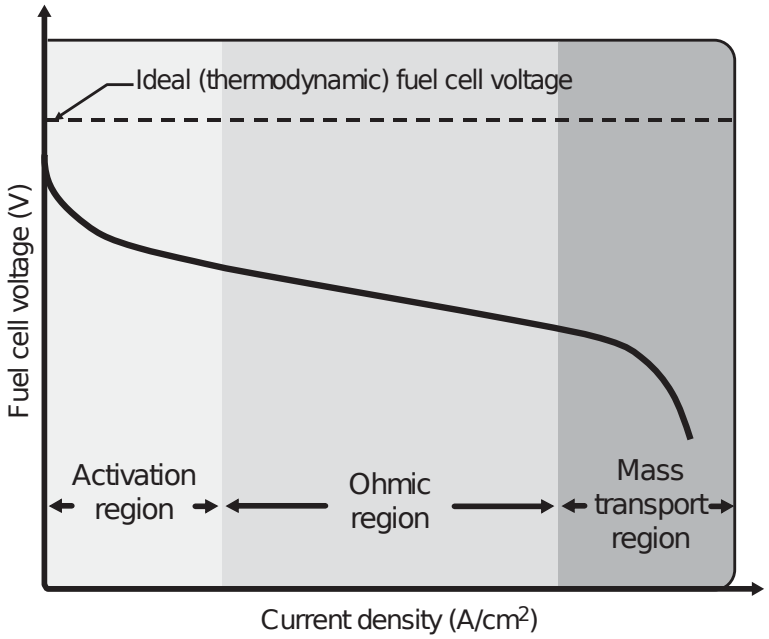


**Figure 2.7.5:** i-V curve of fuel cell; regions represent three major losses, their influence on the curve and diffenrence from ideal voltage.

- When $\eta_{act}$ is very small, or when $i << i_0$ exponential terms can be expanded via Taylor series, and linear relation of current and overpotential can be obtained. This is valid for small deviations from equilibrium and is not dependent on the transfer coefficient $\alpha$.

$$i = i_0 \frac{nF\eta_{act}}{RT} \tag{2.7.6}$$

- When $\eta_{act}$ is very large, or when $i >> i_0$ the second exponential term in Butler-Volmer equation (one relating to backward reaction) becomes small enough that its influence is negligible. In Figure 2.7.3 it can be seen that this is the exponential region where forward reaction is dominant and signifies completely irreversible process. This is known as *Tafel equation*, and it can be used to simplification when said conditions are met.

$$i = i_0 e^{\alpha nF\eta_{act}/(RT)} \tag{2.7.7}$$

## 2.8 Ohmic and Concentration Overpotential

Apart from the activation overpotential, there are two other main losses related to reaction in fuel cells. The first of them are losses related to transfer of charges through solids, and the second cover transport of gaseous species to the reaction sites on electrolyte.

### 2.8.1 Charge Transfer

There are two types of charged particles that move in response to forces in fuel cells. On the cathode of SOFCs (equations (1.3.1) and (1.3.2)) oxygen reduction is occurring, and it consumes electrons. This creates a voltage gradient, a driving force for electrons to travel through the external circuit from anode to cathode. On the other hand, oxygen $O^{2-}$ anions are driven through the electrolyte by both concentration and electric potential gradient, with latter being predominant. This process of charge transport is much simpler for electrons, which are smaller and in free-electron model can freely travel through metal. On the other hand, ions are larger and jump from one crystal defect to the other, which makes their transfer more challenging. Because of these physical constraints, charge conductivity is not ideal and the macroscopic property describing it is *conductivity*, separate for ionic and electric particles.

Usually, it is more common to talk in terms or *resistance R* of a conductor. This way losses due to charge transfer can be related to voltage via Ohm's law:

$$V = iR. \tag{2.8.1}$$

Because voltage is in it linearly dependent on current density, its profile is linear. Again, speaking in terms of losses in fuel cells, term *ohmic overpotential* combines electric and ionic contributions to resistance, and since overpotential is voltage drop, they can be lumped together as:

$$\eta_{ohm} = iR_{ohm} = i(R_{elec} + R_{ionic}). \tag{2.8.2}$$

In the curve that depicts overpotential-current density dependence, Figure 2.7.5, $\eta_{ohm}$ is the cause of the linear region in the middle, and its magnitude rises with the increase of current density. Ohmic overpotential can be thought of as a loss, sacrifice of voltage that ensures flow of charged particles.

Electron transfer in the external circuit is effortless compared to ion transfer across the electrolyte. This is why electrolytes are made as thin as possible, while external circuit length does not matter as much. Thinner electrolyte means less distance for ions to travel, and lower ionic losses, but raises the possibility of electrons passing through it, causing "shorting" and internal currents, as well as fuel crossover without participating in reaction.

In solid oxide fuel cells, which are of particular interest in this thesis, electrolyte materials are solid crystalline oxide materials that can conduct ions. Most often used material is yttria-stabilized zirconia (YTS), which is compound made out of zirconium oxide ($ZrO_2$) and yttria is oxide of yttrium ($Y_2O_3$). This mixture has cubic crystal structure and has high concentration of vacancies in it that are favorable for oxygen ions. Doping the zirconia with yttrium increases vacancy concentration, but only to around 8 % of yttrium, after which ion conductivity starts to decline.

### 2.8.2 Mass Transfer

Mass transfer in fuel cells relates to the delivery of reactants to the location of reaction they participate in, just as removal of products out of fuel cell. Both of them are divided in two major parts, distinguished by their characteristic length scale. First one is transfer of gases in fuel cell flow structures, which are generally on millimeter to centimeter length scale. These geometrically well-defined structures are formed to direct and evenly distribute gas flow to or from electrodes, and transport is dominated by convection. The second one is diffusive flow on micrometer and nanometer scale within highly porous electrodes whose internal geometry is not well defined.

Reactions taking place on electrodes consume and produce species, whose concentrations thus rise or decline. This concentration gradient creates driving force for mass transfer. As was mentioned in section 1.4, electrodes are three-phase systems, with triple-phase boundary where electrode, electrolyte and gas meet. Concentration on electrode interstitial surface where reaction occurres is crucial, and rises or falls (depending which electrode and which specie) through porous electrode to equalize with bulk concentration values.

Since electrochemical reaction leads to reactant depletion and product accumulation near electrode surfaces, intent is to design fuel cell as to have maximal supply and removal of

species. However, if due to vigorous reaction reactant concentration in electrode drops to zero, the reaction stops - there is a current density limit above which fuel cell cannot sustain a chemical reaction. Current density that limits reaction by depleting reactants is called the *limiting current density*, $i_L$. It can be calculated with the equation below, where $D^{eff}$ is effective diffusivity, $c_R^0$ is bulk reactant concentration (in channel), and $\delta$ is electrode (diffusion layer) thickness.

$$i_L = nFD^{eff}\frac{c_R^0}{\delta} \tag{2.8.3}$$

It is clear that optimizing electrode structure and operating parameters (high concentration $c_R^0$ in channels, large diffusivity $D^{eff}$ and low electrode thickness) leads to rising restrictions of limiting current density.

Therefore, concentration has an impact on current density as seen above and, if we recall the discussion of Nernst equation, concentration levels also affects reversible voltage of fuel cell.

Providing accurate analytic equation that accounts for mass transfer losses is hard, since geometries differ significantly. However, speaking in terms of voltage overpotentials, concentration losses can be approximated as $\eta_{conc}$:

$$\eta_{conc} = c\,ln\frac{i_L}{i_l - i}, \tag{2.8.4}$$

with $c$ being a constant dependent on the geometry and mass transport properties of the fuel cell and is sometimes obtained empirically, although some approximations exist.

However, due to the inconsistency with experimental data, different equation for determining concentration overpotential has been proposed, with $B$ being the driving force for mass transfer[1]

$$\eta_{conc} = \frac{RT}{\alpha nF}ln\left(\frac{1+rB}{1+B}\right). \tag{2.8.5}$$

Concentration losses are most important in high current density regime, fig. 2.7.5 because at lower densities enough fuel can be supplied to the electrodes. In SOFC fuel cells, this is the most important loss type, since they operate at high temperature, which lowers activation overpotential, and ohmic losses are relatively small due to good conduction in solid electrolyte.

From the steep drop on the right side of the Figure 2.7.5 it can be seen that limiting current decreases current rapidly, when critical species supply is reached. Thus, a good mass transfer design is imperative for high efficiencies and high current outputs.

Unlike the complex microscopic geometry of diffuse layers, channels that supply gases from the outside of cell are well defined and larger, so the main mass transfer process in them is convection. Design of these channels vary significantly, but the main task is to evenly distribute gases to electrode diffuse layers and provide more contact points across the surface of the electrode. Interactions with walls, and to some extent internal viscosity of fuel are the main causes of pressure drop along the channels. Fluid flow is usually laminar and due to variety of geometries and dimensions, generally numerical simulations are used to determine validity of channel design. Channel design can vary, but most common patterns are spirals and snake-like shapes that convey fuel across flow field plate. Some of them are depicted in Figure 2.8.1.

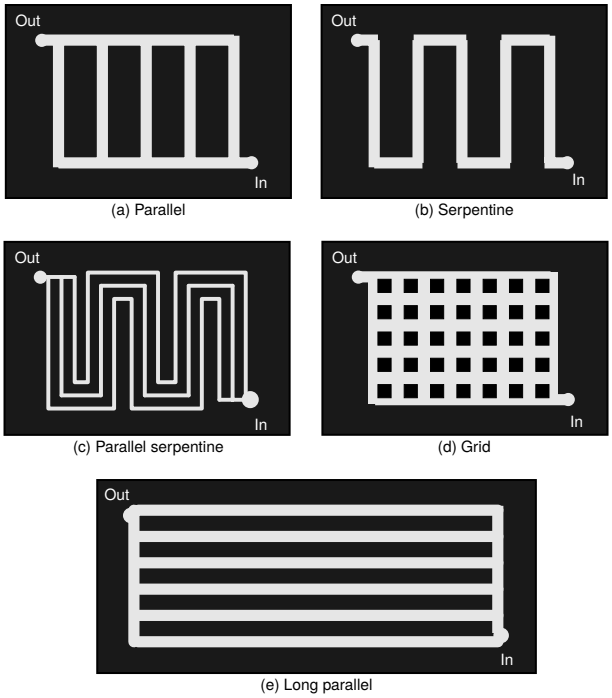


**Figure 2.8.1:** i-V curve for fuel cell combined with power density curve.

Another thing to consider is the fact that fuel cells, if used for commercial purposes, come in stacks for achieving higher voltages. Thus, fuel flow must be equally distributed among cells.

## 2.9 Closure

In this chapter basics of fuel cell thermodynamics and kinetics were presented, as well as efficiency and operational losses. Insight in complex physics behind reactions and transfer of charges and mass was presented, along with derivation of Nernst, Butler-Volmer and Tafel equations, while focusing mainly on solid oxide fuel cells. In next chapter numerical modeling of fuel cells will be discussed, and *openFuelCell* package for simulating fuel cells will be presented.

# Chapter 3

# openFuelCell model

## 3.1 Background

Previous chapters gave an insight into physical processes, electrochemistry and some of the most important equations for dealing with fuel cells. Fuel cells are not a new technology - since their first demonstration by William Grove in 1839,[3] throughout the $20^{th}$ century and first commercial applications, electrochemical fundamentals and underlying physics were very well studied. However, technology was not perfected enough and made available to that extent to achieve wide adoption. To compete in today's market and gain bigger share among renewable technologies, fuel cells need to be exceptionally well designed, with performance, working conditions and life cycle optimized to be presentable as efficient and reliable technology of the future. Numerical simulations can accelerate design and development, especially since experimental prototypes and data for high-temperature cells are scarce and offer limited measurements on detailed performance parameters such as temperature and mass fraction distributions, current density and similar[6].

Numerical simulations of fuel cells began as in-house codes made by researchers and continued through commercial software packages such as PHOENICS, Fluent, Star-CD, COMSOL and others[6]. In recent years, a program to develop fuel cells and stacks models in open-source enviroment OpenFOAM has begun and is ongoing. Limitations of proprietary software are users' inability to significantly alter the source code and its "black-box" nature[7]. When developing new technologies that rely on significant code modification, it is beneficial to have full access to all of the program's features. Furthermore, OpenFOAM's open-source

environment provides wider framework for scientists and users to research and develop fuel cell technology, which is harder to achieve with licensed software[7].

Result of this program is `openFuelCell`, object-oriented open-source C++ library that integrates in OpenFOAM. Class hierarchy and run-time selection mechanism of OpenFOAM allow for high modularity when implementing new or selectable model features. `openFuelCell` is a multi-physics and multi-scale calculation tool developed for modeling of SOFC, but can be applied to the PEMFC type as well. It is a 3D model that describes complex micro-scale electrochemistry and mass and charge transfer outlined in previous chapters, just as conjugated heat transfer and flow through geometry on a cell or a cell stack-scale.

## 3.2 Model overview

### 3.2.1 Mesh

Physical phenomena in fuel cells occur throughout the whole cell body and are not restricted to single region: fuel flows through channels and enters the micro-porous electrode while opposite stands for reactants; heat is released by electrochemical reaction in electrode-electrolyte assembly, but is transfered to channels and supporting structures; potential fields are present in solids, but not in insulating channels, etc. Choice of regions included in model depends on the idea behind it, as well as on what phenomena wants to be simulated or ignored, but generally includes air and channels, anode and cathode, electrolyte and some kind of support structure which serves for electricity conduction and heat dissipation. This problem with region decomposition in numerical modeling of fuel cells, which are multi-physics, multi-scale devices, can be approached in several ways[7]:

- **Single global mesh** can be made for whole fuel cell, with solving governing equations for whole domain and disabling appropriate fields in parts where needed. This approach is perhaps simpler because of only one mesh, but is rather computationally inefficient due to all equations being unnecessarily solved on the whole mesh. Furthermore, OpenFOAM code does not permit internal boundary conditions on single mesh, which creates problem with this approach.
- **Coupled meshes** can be tessellated individually and correlate to appropriate fuel cell

region. Equations are solved on each mesh separately, with coupled boundaries when needed. So, for example, boundary between air channels and cathode would be coupled for mass transport because air flows into it, but not the boundary between channels and solid support because there is no flow between them. Similarly, for heat transfer all boundaries would be coupled to provide global temperature solution. This approach is not well suitable for parallelization and when coupling dominates.

- **Integrated cell concept** is approach where single global mesh is created and then separated in several "child" meshes. Energy equation is solved for on the global mesh, while the rest of fields are enabled on child meshes as needed. Mapping from global to component meshes and vice versa is possible, and boundaries are incorporated as internal surfaces between meshes.

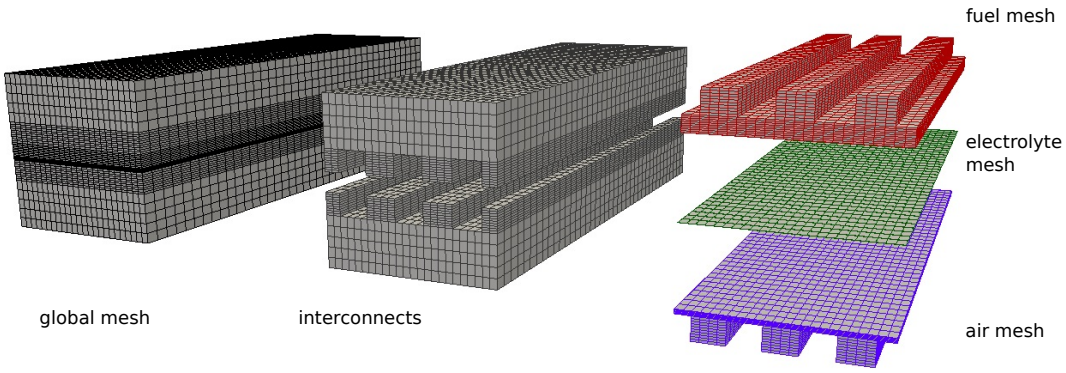


**Figure 3.2.1:** `openFuelCell` mesh for *co-flow* case decomposed in region meshes. Bottom to top: interconnect, air, electrolyte, fuel, interconnect.

The third solution is applied in `openFuelCell` code, although the coupled mesh has been considered as well[7]. Its main drawbacks were being unsuitable with overlapping subregions and inefficiency when dealing with large stacks due to increased data transfer for many coupled regions. This way fuel cell model in `openFuelCell` consists out of global mesh for entire fuel cell with subregions for air, fuel, electrolyte and interconnects. Fuel and air meshes are further divided into zones to enable distinction between, e.g. air channels and porous cathode inside air mesh. This is used only for defining properties such as diffusivity, but the equations are solved over the whole child mesh. So, computational approach was to have a multiple-region model that solves for region-specific fields for every distinct region.

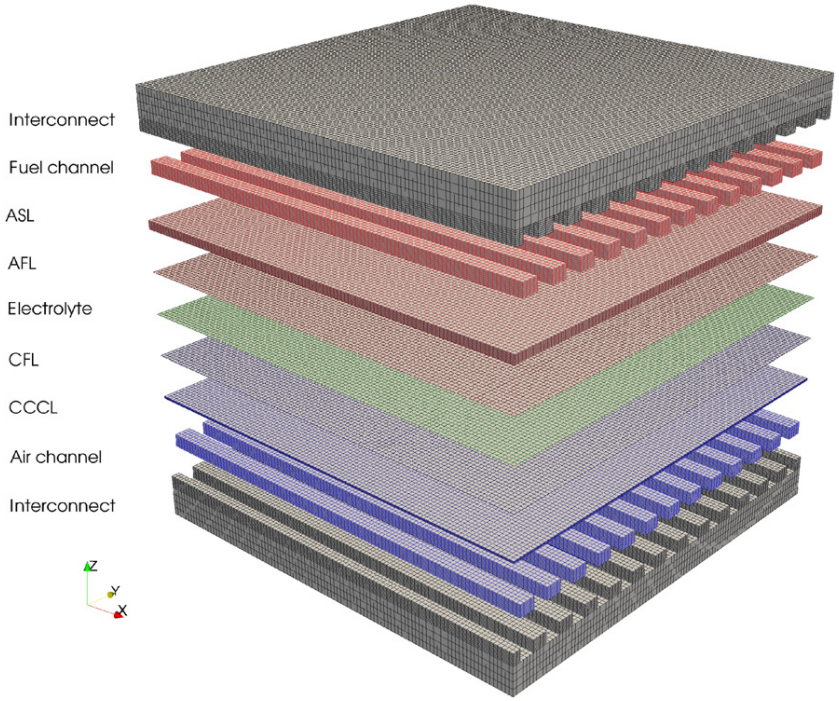


**Figure 3.2.2:** Regional and zonal decomposition of a mesh. It can be seen that regions (child meshes) from Figure 3.2.1 are further divided into zones of uniform physical properties. However, equations are solved on the mesh levels.

OpenFOAM provides modern automatic meshing techniques with unstructured polyhedral mesh support for capturing the complex geometry of SOFC. Depending on the model and the phenomena wanted to be captured, computational grid can be finer or coarser, as well as structured or unstructured. Mesh can be concentrated in the near of boundary regions of fluid channels to capture details of diffusion terms, as shown in Figure 4.2.1.a. On the other hand, *rate-equations* can be used, and with it coarser body-fitted mesh in Figure 4.2.1.b or locally volume-averaged mesh in Figure 4.2.1.c. When having more complex geometries with a lot of channels, the first approach can be unfeasible, and with volume averaging storage must be allocated for more than one phase of a computetional cell, and there is no distinction between different materials in fuel cell. Disadvantage of the second approach, which is used in the `openFuelCell` model, is that material properties and inter-phase coefficients must me stored. When boundary-fitted rate-based formulation (Figure 4.2.1.b) is used, mesh is not tessellated finely enough to capture diffusive components, and rate-equations are used. They replace the local gradient of some field $\Phi$ with its bulk-to-wall difference, $\Delta\Phi$, with $g$ denoting

general conductance[8]:

$$-\Gamma \left.\frac{\partial \Phi}{\partial y}\right|_w = g\Delta\Phi \tag{3.2.1}$$

.

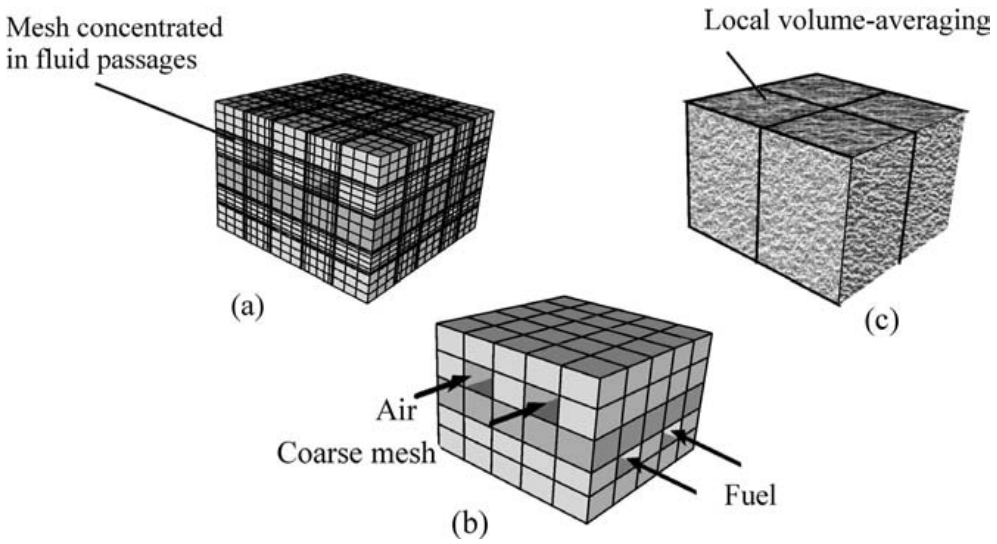


**Figure 3.2.3:** Computational grid approaches used to discretize planar SOFC. a) Detailed boundary-fitted, b) boundary-fitted rate-based approach, c) volume-averaged.[8]

### 3.2.2 Governing Equations

The set of governing equations is solved for on volumetric fields using second order accurate finite-volume methods which are included in OpenFOAM. The approach is highly modular, with ability to replace or implement new parts of the cell model (e.g. electrochemistry or thermodynamics) without violating overall structure of the solver. As mentioned earlier, physics behind fuel cells is rather complex and includes transport phenomena, fluid flow in both channels and porous media, multi-species transport, multi-region thermal analysis and electrochemical effects. These are modeled by by sets of equations presented below.

#### Continuity and Momentum

Hydrodynamic phenomena are governed by the coupled continuity and momentum equations with presumed steady-state conditions:

$$\operatorname{div}(\rho \mathbf{u}) = 0, \tag{3.2.2}$$

$$\operatorname{div}(\rho \mathbf{u}\mathbf{u}) = -\operatorname{grad} p + \operatorname{div}(\mu \operatorname{grad}\ \mathbf{u} - \frac{\mu \mathbf{u}}{\kappa_D}), \tag{3.2.3}$$

where $\mathbf{u}$ is the local velocity, $p$ is the pressure, $\kappa_D$ is the permeability for zones inside air and fuel regions that act as distributed resistance and pressure loss. $\mu$ is the mixture viscosity and $\rho$ is the mixture density:

$$\rho = \frac{p}{RT}\sum x_i M_i = \frac{p}{RT}/\sum \frac{y_i}{M_j}. \tag{3.2.4}$$

$M_i$ is the molecular weight of a species $i$, while molar and mass fractions are denoted by $x_i$ and $y_i$, respectively. Working with both mass and molar fractions is unfortunate but usual with fuel cell modeling, since there is a transition from molar-based electrochemistry domain to mass-based units for fuels[8].

$$\operatorname{div}(\rho \mathbf{u} y_i) = \operatorname{div}(\rho D_i^{eff} \operatorname{grad} y_i) \tag{3.2.5}$$

Species are solved for by partial differential equation for all of them except for the inert one (nitrogen), which is obtained by subtracting the sum of other species' mass from unity to ensure conservation, $y_n = 1 - \sum_{i-1}^{n-1} y_i$. For effective diffusivity calculation, $D_i^{eff}$, there are several of run-time selectable options. Just one of them is the approach by Wilke[7], where for multi-component mixture, species' diffusivity can be estimated from individual diffusivities of one species in all others (binary coefficient of diffusivity):

$$D_i = (1 - x_i)\left(\sum_{j \neq i} \frac{x_j}{D_{ij}^{eff}}\right)^{-1}. \tag{3.2.6}$$

At the boundaries of sub-regions, namely between electrolyte and electrodes, mass flux rate-equations are prescribed as a result of reactants or products of reaction moving (resulting in positive or negative flux). These boundaries are treated as flat surfaces and the mass flux is just the sum of individual species' fluxes:

$$\dot{m}'' = \sum_i \dot{m}_i'', \tag{3.2.7}$$

where species' fluxes are computed by Faraday's law of electrolysis, which is a modified version of equation (2.4.2), with $n$ being the charge number and $i$ representing current density, and serves as connection between current density (rate of reaction) and mass flux of consumed and produced species:

$$\dot{m}'' = \pm \frac{iM}{nF}. \tag{3.2.8}$$

For individual species diffusion equations boundary values following relation connects normal mass flux and species mass fraction:

$$\dot{m}'' - \frac{\partial}{\partial n}(\rho D_i^{eff} y_i) = \dot{m}_i''. \tag{3.2.9}$$

**Electrochemistry**

In reality, as presented in previous chapters, electrochemical reactions take place at triple phase boundary, the interface between electrolyte and electrodes which is three-dimensional and extends over porous zones in electrodes. However, to simplify the model, in the `openFuelCell` code electrochemical reactions are treated as surface phenomena and are presumed to occur on boundaries between electrolyte and electrodes[6]. Reversible or *open circuit voltage* is given by the Nernst equation (equation (2.6.8)), which for the generic reaction $\sum a_i R_i \longrightarrow \sum b_j P_j$ becomes:

$$E = E^0 - \frac{RT}{nF} \ln Q, \tag{3.2.10}$$

while

$$Q = \frac{\sum P_j^b}{\sum R_i^a} \tag{3.2.11}$$

and $P$ and $R$ are molar concentrations of reactants and products. Only active species are included in this equation, while others, such as nitrogen, are marked as inert.

Ideal open circuit voltage is reduced by anode and cathode overpotentials as well as by voltage loss due to the local ohmic loss:

$$V = E - \eta_a - \eta_c - iR. \tag{3.2.12}$$

This equation is obtained by combining the Kirchoff's second law with Ohm's law, and is called "Kirchoff-Ohm relationship"[7], and relates fuel cell voltage with current density. Overpotentials $\eta_a$ and $\eta_c$ are caclulated from a Butler-Volmer equation, which is explained in section 2.7. For temperature-dependant ohmic resistance $R$ there are several run-time selectable models available.

Overpotentials for equation (3.2.12) are obtained out of Butler-Volmer equation equation (3.2.13) for each of the electrodes. Since overpotential terms are in the exponent, Ridder's method of root finding is used. Another simplification that can be implemented in code is to use Tafel equation instead, which has an analytical solution and the need for root-finding methods is avoided.

$$i = i_0 \left( e^{\alpha n F \eta / (RT)} - e^{(1-\alpha) n F \eta / (RT)} \right) \tag{3.2.13}$$

This is the Butler-Volmer equation that is solved for both anode and cathode overpotentials, $\eta_a$ and $\eta_c$ on the surfaces of the electrodes.

As shown during derivation of Nernst equation in section 2.2, electrochemical reaction in fuel cell releases heat. In ell releases heat that heat is modeled as volumetric heat source in the whole electrolyte:

$$\dot{q}''' = \left( -\frac{1}{2F} \Delta H\left(T\right) - V \right) \frac{i}{\delta h_E}. \tag{3.2.14}$$

$\Delta H$ is the enthalpy of formation, and it is calculated (as well as enthalpies and entropies for Nernst equation) with polynomial functions of temperature. There is as well the voltage $V$ term that takes into account heat source due to the Joule heating, and since source is presumed to be volumetric, it is multiplied by current density ($\mathrm{A/m^2}$) and divded by electrolyte density $\delta$.

Assuming surface occurring electrochemistry seems to be popular choice for simplifying fuel cell model, since it provides satisfactory results while avoiding volume-occurring reactions. This way, potential, current density and overpotentials are calculated locally on the boundary of electrolyte and are "smeared" over the volume.

**Heat Transfer**

Heat transfer is being solved for on the whole mesh, with equation written for temperature and not for enthalpy or internal energy. Gases flow into channels with set boundary temperature, and heat sources due to electrochemical and Joule heating from electrolyte are mapped to cell level mesh. With $\dot{q}'''$ being aforementioned source, $k$ being thermal conductivity, and $c_p$ standing for specific heat, temperature equation for solids and fluids becomes:

$$\rho c_p \mathbf{u} \cdot \operatorname{grad} T = \operatorname{div}(k \operatorname{grad} T) + \dot{q}'''. \tag{3.2.15}$$

Radiation heat transfer present in fuel and air channels was not yet implemented in ell releases heat model[7].

### 3.2.3 Boundary Conditions and Numerical Implementation

Fuel cells are devices that are usually run under higher-than-ambient pressure because of the efficiency benefits discussed in section 2.6. In order to keep pressurized conditions, complex sealing system are often used. In the `openFuelCell` model all pressure boundary conditions are set to zero gradient, except for outlets. Similarly for temperature field, external walls were presumed adiabatic, except for the fuel and air inlets.

In addition to the mass transfer equation in previous section, due to low Reynolds number in channels, turbulence models were not invoked[9] and flow was assumed to be laminar, with gases behaving like ideal mixtures. Furthermore, channel walls have no-slip boundary conditions applied to them, with prescribed inlet velocity of fuel and air. For air, a binary mixture of oxygen and nitrogen was presumed on the cathode side, while fuel consists out of hydrogen and water vapor, which is in accordance with real hydrogen fuel. Boundary conditions for velocity and species' mass fractions on internal boundaries between electrodes and electrolyte are given by the rate-equations and rate of electrochemical reaction. Species' boundary conditions are governed by equation (3.2.9), but is written in code as a Neumann condition, so algebraic equation system introduces some additional stiffness into model when compared to linear formulation[6][10]. PISO algorithm is used to solve pressure and momentum equations in fuel and air regions, with porous zones acting as distributed resistivity as a volumetric source term. For more entails, reader is reffered to[11].

Simulation can be run in galvanostatic or in potentiostatic mode. When in potentiostatic mode, voltage $V$ is prescribed and kept constant, while when galvanostatic mode is chosen, overall current density is constant, which is more appropriate when simulating stacks to ensure charge conservation from cell-to-cell within it. Voltage values are then adjusted until correct values are achieved.

An iterative procedure was employed for solving a system of matrix equations: symmetric linear equations were solved using an incomplete Cholesky pre-conditioning scheme (ICCG), while asymmetric systems were solved with a bi-conjugate gradient solver Bi-CGStab[12].

### 3.2.4 Solution Algorithm

With the governing equations, mesh decomposition and boundary conditions described, computational algorithm is presented below. Depending on the choice of simulation mode (galvanostatic or potentiostatic), solution algorithm differs slightly, but not in a momentous way.

1. Initialize global and region meshes, constants and model parameters. Set the initial fields and boundary conditions, physical properties, cell voltage or average current density (depending on a mode). Create methods for inter-mesh mapping.

2. Map the temperature field from global to region meshes.

3. Compute temperature-dependent properties: air and fuel density, viscosity and conductivity. Solve equations (3.2.2) and (3.2.3) for pressure and momentum according to the PISO algorithm.

4. Calculate mass diffusivity according to selected model and solve equation (3.2.5) for species mass fraction in fuel and air regions.

5. Calculate Nernst potential, equation (3.2.10), calculate local current density on anode-electrolyte interface from equation (3.2.12). From equation (3.2.13) get $\eta_a$ and $\eta_c$ for both electrodes with iterative root-finding method.

6. Smear surface values across the electrolyte volume. Calculate heat sources within the electrolyte volume according to equation (3.2.14).

7. Calculate electrochemical mass fluxes due to reaction on boundaries adjacent to electrolyte and set the boundary conditions for species' mass fractions and momentum.

8. Map region fields to global mesh.

9. Solve global temperature equation equation (3.2.15)

10. Loop from step 2. until convergence is obtained. For potentiostatic mode voltage is fixed, while for galvanostatic it needs to be corrected with relaxation constant until current density $i$ is identical to the set value.

## 3.3 Summary

`openFuelCell` model was developed to enable advances in fuel cell design that are needed for creating durable, high quality devices. It can be used for simulation of fuel cell working conditions and studying parameters such as efficiency, current output, temperature distribution, pressure drop, etc. all of which are crucial for optimizing geometry and optimal operation points. When compared to the previous models and data, `openFuelCell` model provides results that are overall in good agreement, with some differences due to discrepancies in input parameters[12][7][11].

This model is believed to be the first fully comprehensive code developed for solid oxide fuel cells[7], and the authors' wish is to develop it further and create a wider base of users, both within the scientific community and industry, that would contribute to it. Code is open-source and can be downloaded from `openfuelcell.sourceforge.net`. Development of `openFuelCell` model will go in direction of minimizing the assumptions included, as well as in adding new model options and features. For example, radiation phenomena in channels is neglected or, as was discussed in section 2.8.1, across the electrode-electrolyte assembly there are two fields that take place—ionic and electric. In current model that fact is not taken into consideration, and voltage is solved for just in the electrolyte. In the next chapter modifications to code will be presented, that expand model to account for potential distribution across the fuel cell.

# Chapter 4

# Two Potential Model

## 4.1 Introduction

In the previous chapter it was mentioned that the `openFuelCell` model, although quite comprehensive and suitable for simulating solid oxide fuel cells with a satisfying level of accuracy, does not take into account all of the physical phenomena occurring in fuel cells, and also introduces approximations that are unavoidable when developing consumer-grade models for simulations with limited time or computational resources. Moreover, `openFuelCell` code is made publicly available and modifications to it are welcomed and encouraged.

In this chapter a new approach for solving electrochemistry in solid oxide fuel cells is presented, with detailed description of equations, meshes, algorithm and assumptions used.

## 4.2 Potentials in Fuel Cells

As was described in chapter 2 and especially in section 2.8.1, fuel cells are electrochemical devices in which internal energy of fuel is converted into electricity. In reactions between the fuel and the air electrons are released and form a useful current that can be used for doing work via external circuit. On the opposite side, inside the electron-insulating electrolyte, ion transfer is taking place. In case of SOFC type, ions are negatively charged $O^{2-}$ anions.

Due to electrochemical reactions, electrons released on the anode have a tendency to flow to the cathode, and means of collecting and delivering the current from and to the electrodes must be used. Planar fuel cells usually have current collection plates which have several

purposes: they keep the structural integrity of a fuel cell and serve as a frame for electrode-electrolyte assembly; they are used to spread the energy released during fuel conversion away from electrolyte and anodes; they collect electrical current from the anode and the cathode. These current collection plates (interconnects in `openFuelCell` model, Figure 3.2.2) are usually made out of metal, to distribute heat by conduction more uniformly than ceramic ones, and to be able to conduct electricity.

It can be noted that across the single cell there is an alternation of electric and ionic fields: electricity flows through the interconnects and the electrodes, while ions are present in electrolyte and in the parts of electrode volumes where reactions occur—the triple phase boundary. This creates three potential fields in the cell that are partially overlapping, as in Figure 4.2.1.

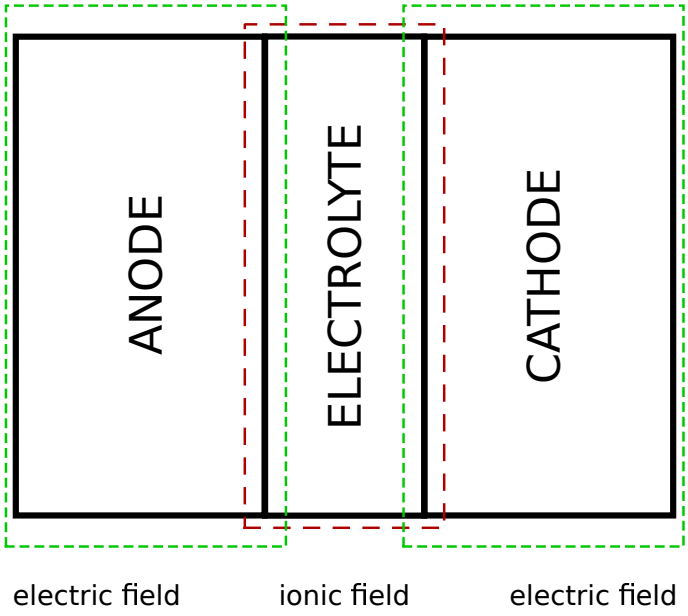


**Figure 4.2.1:** Schematics of the overlapping potential fields over electrode-electrolyte assembly.

Handling the potentials in the `openFuelCell` model was limited to the calculation of output voltage on boundary between electrolyte and fuel regions, and then smearing it over the electrolyte volume. This is valid if the only information of interest is the value of voltage, however, knowledge of detailed potential distribution can be of great importance when designing the fuel cell geometry.

When discussion about electrode reaction kinetics (Section 2.7) is applied to whole assembly, potential distribution over it can be drawn. In section 2.7, potential distribution on electrode—electrolyte interface has been described. It is worth mentioning that Figure 4.2.2a. shows potential distribution and activation energy on a very small, molecular scale, and that when our scope is widened from microscopic phenomena to cell level, that curve is translated into a one-dimensional jump that takes place on the interface, Figure 4.2.2a.

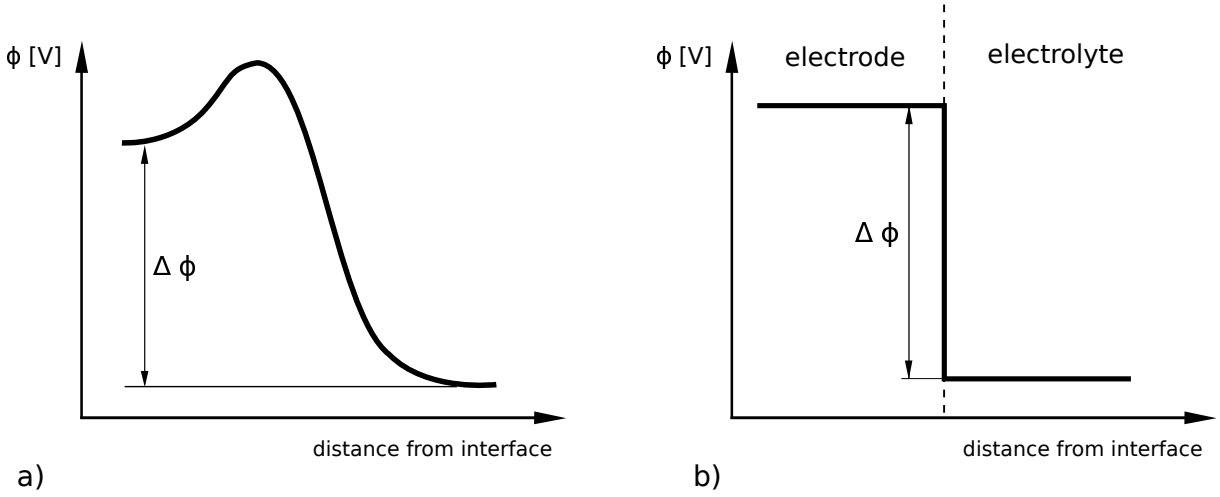


**Figure 4.2.2:** Potential distribution across electrode-electrolyte interface. a) Capturing atomic level distribution and activation energy. b) Macro-level distibution.

Furthermore, such curve exists for both electrodes adjacent to electrolyte. When they are drawn on the scheme of electrode-electrolyte assembly, hypothetical[1] distribution such as Figure 4.2.3 is obtained. Potential distribution here represents combined ionic and electric potentials, which can be superimposed. It can be seen that the cathode potential is higher and it decreases towards anode by jumps on the interfaces of electrolyte. Conveniently, anode potential is set to be zero, since only the relative difference is of interest.

Instead of analyzing reaction steps on each electrode, as was done in section 2.7 for PEMFC anode, more practical way to understand charge transfer is to consider motion of particles in presence of potential fields. Electrons are negatively charged particles, and as such they have a tendency to move *opposite* of a electric field in e.g. copper wire that forms external circuit.

[1]Distribution is hypothetical because the potential difference (Galvani potential $\Delta\Phi$) between two phases, cannot be directly measured. What can be measured is the overall potential difference between two electrodes[13].

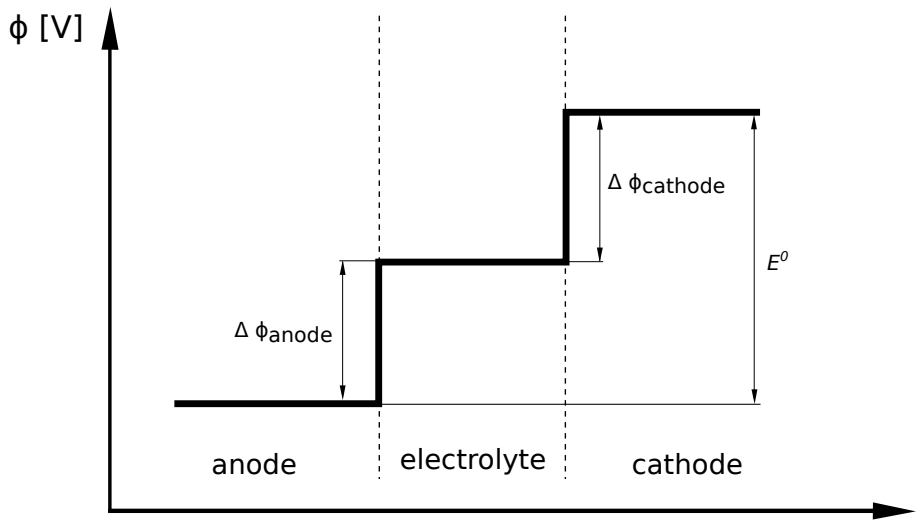


**Figure 4.2.3:** Potential distribution over electrode-electrolyte assembly of a fuel cell for equilibrium conditions (no current drawn).

They move from the anode with lower potential to the cathode with higher potential[2], and have the ability to perform work. This is the driving force behind electrons in their completion of the electrochemical half-reactions. Different situation is with anions—they should also have a tendency to move from anode to cathode, but work is being done on them, on account of decrease of Gibbs free energy, and so they can move from high potential to a lower one. So, unlike PEMFC type, SOFC's charge circulation consists entirely out of transfer of negatively charged particles, with reaction reactants converted into products with lower chemical potentials. Figure 4.2.4 shows these transfers schematically.

## 4.3 Two Potential Model Overview

An addition to the `openFuelCell` model presented in this thesis tackles the issue of modeling potential fields in solid oxide fuel cells. To account for potentials present in a fuel cell, electrochemical model had to be adjusted, just as additional mesh decomposition had to be added.

[2]Test charge (or a positive charged particle) would have a tendency to move from higher to lower potential, thus being in accordance with more intuitive behavior of mass in gravitational potential difference. Also, conventional electrical current is described this way, although the electron is physical charge carrier.

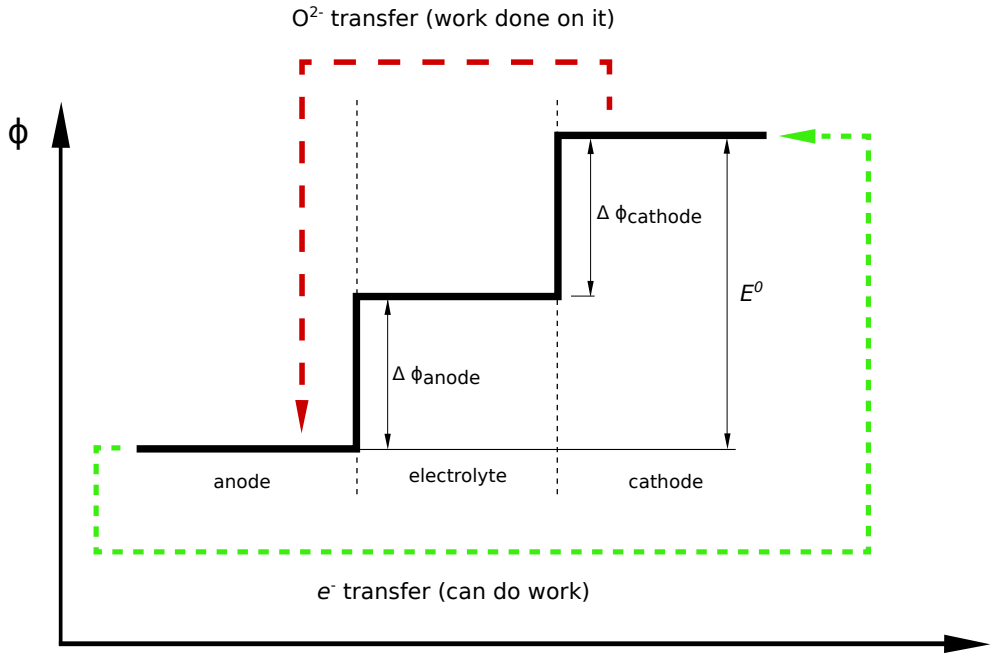


**Figure 4.2.4:** Charge transfer in electrode-electrolyte assembly of a SOFC.

### 4.3.1 Model Assumptions

An assumption that is used in stock `openFuelCell` code, as well as in other models[9][14], is to presume *thin electrodes*. This is valid for the model presented here as well. Basically, electrochemistry is treated as a surface phenomena, and triple phase boundary is reduced to planar geometry. This is beneficial since there is no need to have allocated memory for both ionic and electric potential fields in the overlapping volume. Furthermore, this kind of setting circumvents the need to implement volumetric current sources, characteristic for *thick electrode formulation* with overlapping potential fields, and instead prescribes sources as boundary conditions.

The next simplification is presuming only one electrode is "active". This is a major simplification that leads to a model being the *two potential model*. Making one of the electrodes "passive" does not eliminate the idea of reactions occurring on it, nor does it turn off one of the half-reactions and stop ion or electron creation and transport. This simply means that the losses associated with this electrode will be neglected, and the overpotential for this electrode will be disregarded. Choice of electrode that should be passive is different for fuel cell types. For PEMFCs, activation losses associated with anode are smaller when compared to cathode

losses. This was partially discussed in Section 2.7, and it happens because oxygen reduction on cathode is the most sluggish process, which cannot be ignored. So if anode is made passive, model will be appropriate for PEM-fuel cells. On the other hand, in the SOFCs anode loss is more significant than the cathode one, due to mass transport constraints for hydrogen in anode-supported SOFC[1]. In this model, where solid oxide fuel cells are simulated, the cathode is "turned off" and anode losses impact potential distribution across the cell. This way model includes two potential fields with one jump between them: one that covers interconnect and the anode, and the other one which spreads over electrolyte, cathode and adjacent interconnect, Figure 4.3.1.

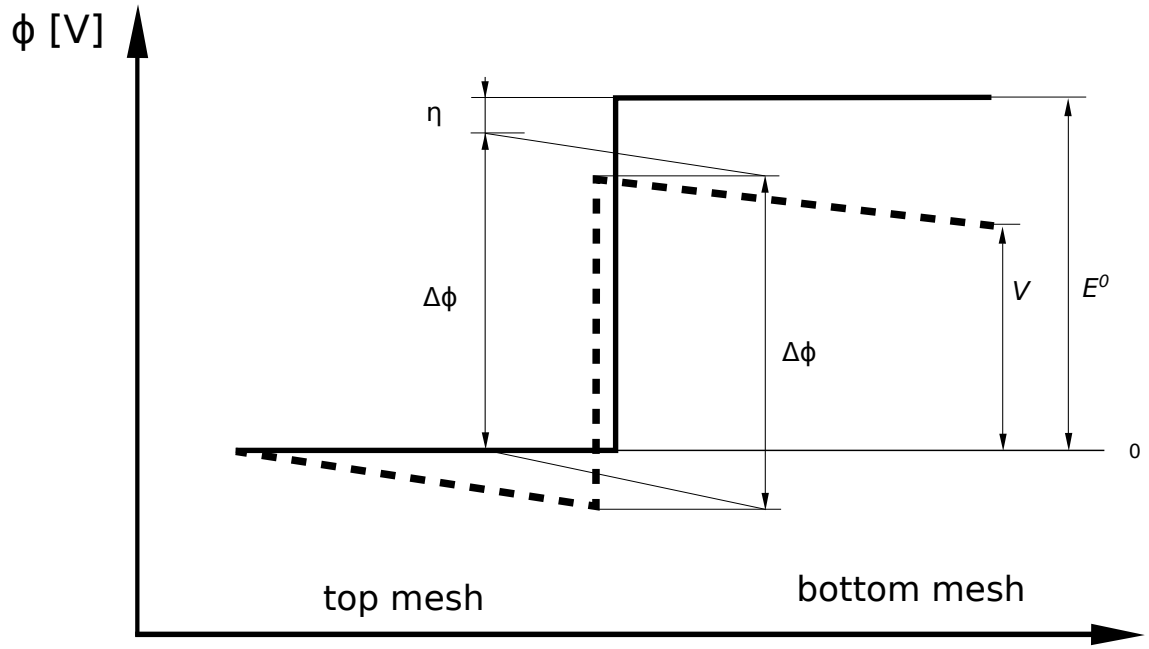


**Figure 4.3.1:** Potential distribution in *two potential model.* Solid line represents equilibrium state when voltage equals to reversible potential $E^0$. Dotted line shows operating condition, with drop representing loss at the electrode, and slopes representing ohmic losses in conducting solids.

Another model simplification is the usage of a more convenient version of Butler-Volmer equation, the Tafel equation. It serves as a connection between anode overpotential and current density, but as was stated in section 2.7.2, it is only valid at high overpotentials and high current densities, where backward current density is negligible. For SOFCs operating at high temperature this was presumed to be valid as well.

With these simplifications taken into consideration, new mesh and equations are presented below.

### 4.3.2 Two Potential Model Mesh Decomposition

New fields for potentials in fuel cell need to be solved on appropriate regions, when choice of active electrode is taken into account. There are two potential fields but they span over multiple sub-regions each. In section Section 3.2.1 several approaches for mesh decomposition were presented, and reasons for choice of integrated cell concept were stated. Following this approach, the potential field that covers two or more regions cannot be solved on those separated and uncoupled meshes. Thus, new regional meshes are introduced (**top** and **bottom**), one for each potential field to be calculated. Unlike other regions in the `openFuelCell` model, these new meshes overlap with existing regions. The ability to compute with overlapping regions is the advantage of the chosen integrated cell concept, and because of the OpenFOAM's modifiable mapping features, fields can be transferred between meshes and used in new electrochemical model. Figure 4.3.3 shows the schematics of new mesh decomposition in two potential model and it can be noted that top and bottom mesh together cover the whole volume of fuel cell, except for the air and fuel channels, since they are insulators and potential fields do not exist in them.

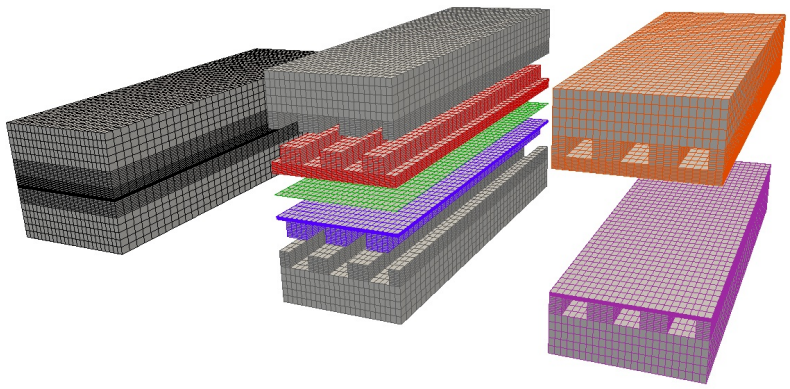

**Figure 4.3.2:** New mesh decomposition for two potential model.

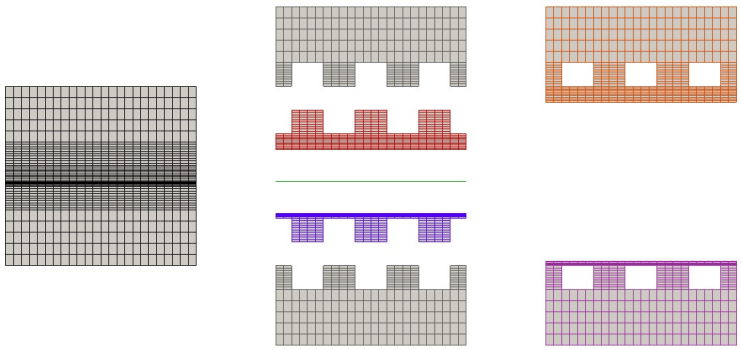

**Figure 4.3.3:** Front view of the mesh decomposition

### 4.3.3 Electrochemistry Calculation for the Two Potential Model

Electrochemistry model and equations are changed compared to `openFuelCell`, in order to take into account potential distributions. Since only anode is the active electrode, there is a discontinuity in the potential field on its surface. As stated, this jump coincides with the boundary between two new region meshes. Two potential model is posed as potentiostatic problem, with potential on the anode side (top) set to zero, while on the bottom a prescribed voltage $V$ is aplied. Hence, voltage drop on the anode boundary can be calculated as a difference between surfaces of electrolyte and anode. Or, if described in terms of two potential model decomposition—voltage drop is the difference between adjacent cell faces on top and bottom mesh. This way the equation for potential jump $\Delta\Phi$ simply becomes:

$$\Delta\Phi = \Phi_{bottom} - \Phi_{top}. \tag{4.3.1}$$

Ideal potential is obtained from the same equation as in the regular `openFuelCell`, equation (3.2.10), and the anode overpotential is calculated as folllows[15]:

$$\eta = E - \Delta\Phi. \tag{4.3.2}$$

Since thin electrode assumption was used, these parameters are defined as localized, surface values on the interface between top and bottom region mesh.

The equation above is valid for a case with only one jump across the fuel cell. It is a mod-

ified version of a Kirchoff-Ohm relation and when rearranged shows that ideal cell voltage is equal to all potential differences in the cell: $E = \Delta\Phi + \eta$. This can be seen in Figure 4.3.1 where the solid line represents *open circuit voltage* with no current drawn and no overpotential. When the circuit is closed, current is drawn and losses in solids become present (they cause slopes in the graph—they are ohmic losses due to conducting charge, see section 4.3.4 below), just as overpotential $\eta$ further reduces output voltage when compared to the ideal case.

Another simplification, the use of the Tafel equation (equation (2.7.7)), provides current density values that are function of exchange current density and overpotential. This equation is valid for high current densities and high overpotential values, which has been taken as an acceptable assumption[16] for SOFCs:

$$i = i_0 e^{\alpha n F \eta_a / (RT)}. \tag{4.3.3}$$

This equation calculates current density on the boundary between anode and electrolyte, and is a simplification when compared to the `openFuelCell` model. These boundary values are used in the same way as was before to set the mass and species boundary conditions. The difference is that in this model mapping from bottom/top region to the air/fuel is needed. Furthermore, current density is used for setting boundary conditions on top and bottom region potential fields. Neumann boundary conditions (fixed gradient) are defined on the boundary corresponding to the anode-electrolyte interface as:

$$\frac{\partial \Phi}{\partial n} = -\frac{i}{\sigma}. \tag{4.3.4}$$

In this equation $\sigma$ is the region's electrical conductivity. It is calculated for both regions as function of temperature according to[17] :

$$\begin{aligned} &\text{Anode} && \sigma = (2.98\text{e}{-5}\ \exp^{-1392/T})^{-1} \\ &\text{Cathode} && \sigma = (8.11\text{e}{-5}\ \exp^{600/T})^{-1} \end{aligned} \tag{4.3.5}$$

Region that contains electrolyte within it (in present case that is the bottom) causes another discrepancy with reality because equations for $\sigma$ used for conductivity calculation are obtained for anode and cathode materials. They do not represent conductivity in electrolyte

accurately (Figure 4.3.4). However, due to the thinness of electrolyte when compared to electrode sizes, this was presumed to be a valid assumption. This is also true for metallic interconnects.

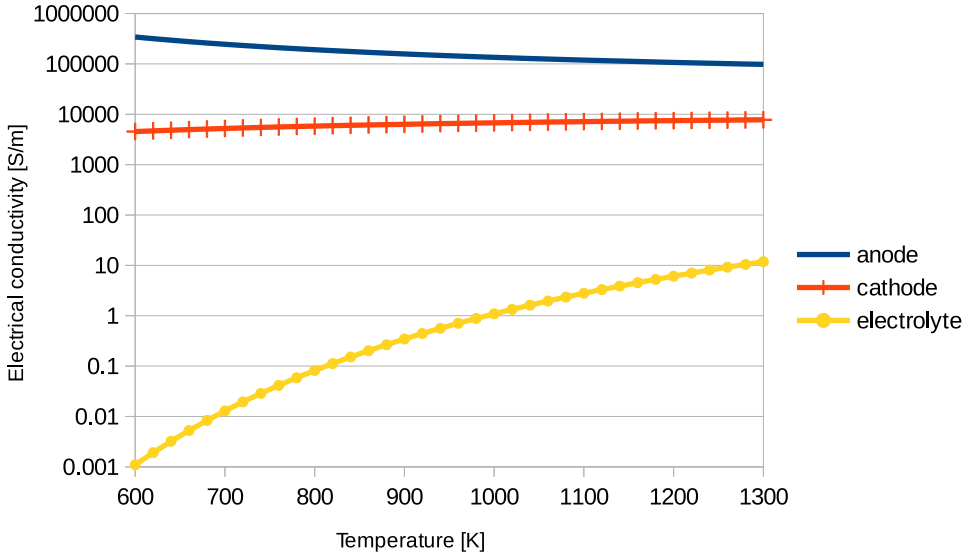


**Figure 4.3.4:** Electrical conductivity for SOFC anode, cathode and electrolyte ($\sigma = (2.94\text{e}{-5}\ \exp^{10350/T})^{-1}$). Although the difference is substantial, electrolyte thickness is significantly smaller than one of the electrodes.

Finally, with top and bottom mesh having fixed values prescribed on one side (set at the beginning of a calculation) and having prescribed gradient (function of current density) on the side corresponding to anode-electrolyte interface, potential fields can be solved for. Since there are no volumetric source terms for potential fields in top and bottom region, just as there are no potential jumps or discontinuities, distribution can be calculated by solving Laplace equations for each field.

$$\nabla \cdot (\sigma \nabla \Phi) = 0. \tag{4.3.6}$$

Laplace equation solutions for potential fields provide the distributions across two new meshes, and calculate values on boundaries that are needed for determining jump values on the interface. Conductivity $\sigma$ shows how well does the material conduct charged particles (it is the inverse of resistivity, $\Omega$). When potential distribution is calculated this way, it substitutes the ohmic overpotential $\eta_{ohm}$ or the usage of term $Ri$ in the Kirchoff-Ohm relation, equation (3.2.12).

### 4.3.4 Solution Algorithm

Algorithm for solving equations is mostly the same as in the `openFuelCell` model, except for the electrochemistry solution. Creating meshes, reading properties and initialization is identical, with the addition of two new meshes. Differences for electrochemistry calculations are listed below.

1. Temperature is mapped from global level to top and bottom mesh is used for conductivity calculation.
2. Potential jump $\Delta\Phi$, equation (4.3.1) is calculated on zhe boundary between two meshes. Overpotential $\eta_a$ is obtained with equation (4.3.2).
3. From Tafel equation (4.3.3), current density is obtained on the active electrode boundary.
4. Current density serves for setting the boundary conditions for mass and species flux, as well as for setting the gradient for potential fields.
5. Solving Laplace equation for field distributions on top and bottom meshes.
6. Repeat until current density converges.

Boundary conditions for the two potential model are the as used in the `openFuelCell` code, with the addition of boundary conditions for potential fields. It was mentioned earlier that the mode is potentiostatic, so overall cell voltage is prescribed. That means that the top and bottom surfaces of a fuel cell have prescribed Dirichlet boundary conditions—anode boundary potential equals to 0, while fixed value on the cathode is $V$, the operating voltage of a fuel cell. On the outer boundaries, the fuel cell walls, zero gradient boundary conditions are prescribed, and on the adjacent surfaces of top and bottom mesh, Neumann boundary conditions are set.

Finally, the rest of the electrochemical parameters and constants for electrochemistry calculation ($\alpha$, experimental values for calculating exchange current density $i_0$, activation energy...) are based on experimental data from Leonide et al.[18]

## 4.4 Summary

In this chapter two potential model, an addition to the `openFuelCell` model, has been presented. It is an attempt for expanding the existing model with the ability to simulate potential distribution in fuel cells, which can be important when designing the geometry. Although some approximations were assumed, presented model can serve as a base for further research. In the following chapter results obtained with the two potential model will be presented.

# Chapter 5

# Model Validation and Results

## 5.1 Introduction

In the previous chapter the two potential model was introduced together with simplifications and modifications that were added to existing `openFuelCell` model with it.

In this chapter, results for several fuel cell configurations will be presented, along the comparison with simulations obtained with the existing model and results from previous studies. Furthermore, results will be put in physical context of SOFCs, and causes for discrepancies between the existing and the new model data will be explained.

## 5.2 Cases Set Up

Before the analysis of the results, different configurations of the used meshes will be described, along with the numerical schemes and boundary conditions.

### 5.2.1 Meshes

In the `openFuelCell` repository several cases with varying geometry or boundary conditions can be found. Four of them were re-purposed for the new model and the new mesh decomposition. They are all structured, three-dimensional, boundary-fitted meshes comprising of hexahedral cells.

The simplest one, *quickTest*, is a *co-flow* configuration that has sets of three channels, for

air and fuel each (Figure 4.3.3). It is a mesh with 49 920 cells, mostly used during model development and comparison. The three remaining meshes are larger, with 281 216 cells in total (not counting for the overlapping sub-meshes) and 13 channels for fluids on each side. They are divided in three configurations: *co-flow*, *counter flow*, and *cross flow* and it will be shown that different channel orientations (Figure 5.2.1) and fluid inlet orientations have a major impact on fuel cell performance.

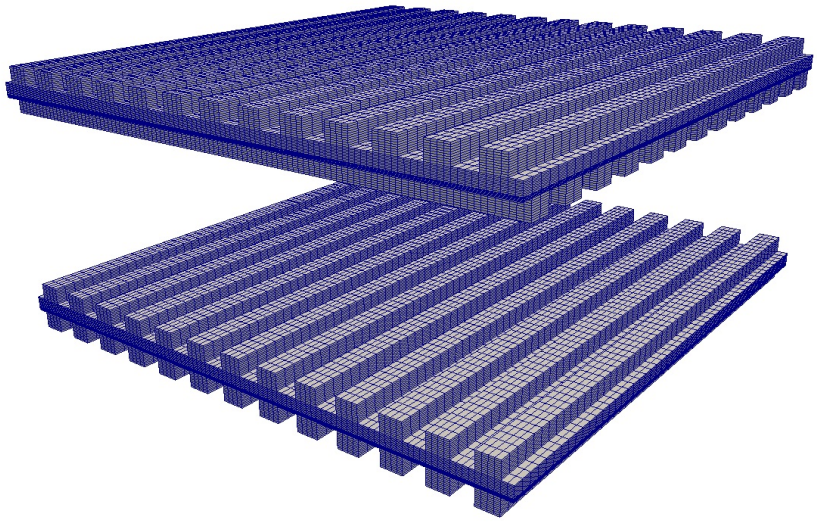

**Figure 5.2.1:** Orientation of channels in larger cases, suitable for co-, counter- and cross-flow.

### 5.2.2 Boundary Condition and Numerical Schemes

Since the two potential model is an addition to `openFuelCell` code, existing initial and boundary values were used here as well, and their values are presented below, with inlet and outlet orientations depending on the fuel cell configuration.

**Boundary and initial conditions**

- **Inlet**
  - *Velocity*: uniform `fixedValue` with values of 1 m/s and orientation that varies depending on configuration,
  - *Pressure*: `zeroGradient`,
  - *Density*: for `air` is `fixedValue 0.3516` and `fuel` is `fixedValue 0.0305`,

  - *Thermal conductivity*: for both `air` and `fuel` is set to `fixedValue 1e-15` to disallow outward diffusion,
  - *Species mass fractions*: for `air` oxygen and nitrogen mimic atmospheric conditions — `uniform fixedValue` equal to `0.233` and `0.767`, respecively. In `fuel`, values for hydrogen and water vapor are `uniformValue 0.782` for $H_2$ and `uniformValue 0.218` for water,
  - *Temperature*: temperatures are set to be `uniform` but depend on the case, as will be shown below.

- **Outlet**
  - *Pressure*: it is set equal to standard conditions with `fixedValue 101325` ,
  - *Remainder*: other fields are set to `zeroGradient` at the outlet of air and fuel channels.

- **Outer boundaries**
  - *Pressure*: it is set to `zeroGradient`, mimicking fuel cell walls that keep it pressurized,
  - *Temperature*: losses through walls are not taken into consideration and boundary conditions are set to `zeroGradient`,
  - *Remainder*: other fields are set to `zeroGradient`.

- **Electrode-electrolyte boundaries** (Explained more thoroughly in Section 4.3.3)
  - *Velocity*: velocity between `air/fuel` and `electrolyte` is set to `fixedValue 0` but during simulation sources/sinks change,
  - *Mass fractions*: boundary condition set to be `fixedGradient 0` but changes during simulation,
  - *Remainder*: Rest of the fields have `zeroGradient` conditions.

- **New decomposition** for potential fields

- *Bottom*: upper boundary has a `fixedGradient 0` boundary condition, while lower boundary is set to `fixedValue V`, where V is the value for voltage in our case; `zeroGradient` conditions for conductivity `sigma`,
- *Top*: upper boundary is `fixedValue 0`, while lower boundary is set to be `fixedGradient 0`. Conductivity has all `zeroGradient` conditions,

Table 5.2.1 below lists numerical schemes used in two potential model.

## 5.3 Results

Results presented below are obtained by running the `openFuelCell` package with the new two potential model included on three meshes for different configurations.

### 5.3.1 Heat and Mass Transfer Results

When designing fuel cells there are several significant parameters that should be optimized for maximum efficiency and best performance, with temperature and current density distributions being the most important ones. Inlet temperature of air and fuel was set to $T_{inlet} = 860\,\mathrm{K}$ the and since this is a potentiostatic mode, prescribed voltage was $V_{bottom} = 1.0\,\mathrm{V}$. Other parameter combinations for all mesh configurations were simulated as well (shown in Figure 5.3.1) and presented ones proved to be a good representation for field distributions at higher voltages and intermediate temperatures.

Three configurations provided similar results, with expected differences characteristic for their geometries. Temperature is just one of the parameters which is strongly affected by the flow configuration, as can be seen in Figure 5.3.2. It can be seen that there is a more even distribution for counter-flow, with cross-flow yielding greatest temperature gradients. Further, cross-flow exhibits highest temperature at the outlet corner. Although more uniform, counter-flow temperatures are slightly higher when compared with others, which is more clear in Figure 5.3.3. This temperature distribution due to flow orientation is in accordance with the results reported in studies[7][12]. Highest temperatures are observed in central regions, due to heat generation, while lower temperatures due to gases acting as coolants are near the inlets. Further, it can be seen that temperatures increase along channels because of

**Table 5.2.1:** Two potential model numerical schemes

| | |
|---|---|
| **Time schemes** | |
| default | steadyState |
| **Gradient schemes** | |
| default | Gauss linear |
| grad(p) | Gauss linear |
| **Divergence schemes** | |
| default | none |
| div(rhoCpPhi,T) | Gauss upwind |
| div(phi,U) | Gauss GammaV 0.2 |
| div(phi,y) | Gauss upwind |
| **Laplacian schemes** | |
| default | none |
| laplacian(k,T) | Gauss harmonic corrected |
| laplacian(k,U) | Gauss GammaV 0.2 |
| laplacian((rho \| A(U)),p) | Gauss linear corrected |
| laplacian(diff,y) | Gauss harmonic corrected |
| laplacian(gamma,y) | Gauss harmonic corrected |
| laplacian(sigma,potBottom) | Gauss harmonic corrected |
| **Interpolation schemes** | |
| default - cell | linear |
| default - regions | harmonic |
| interpolate(T) | harmonic |
| interpolate(k) | harmonic |
| interpolate(rho) | harmonic |
| **Surface normal gradient schemes** | |
| default | corrected |

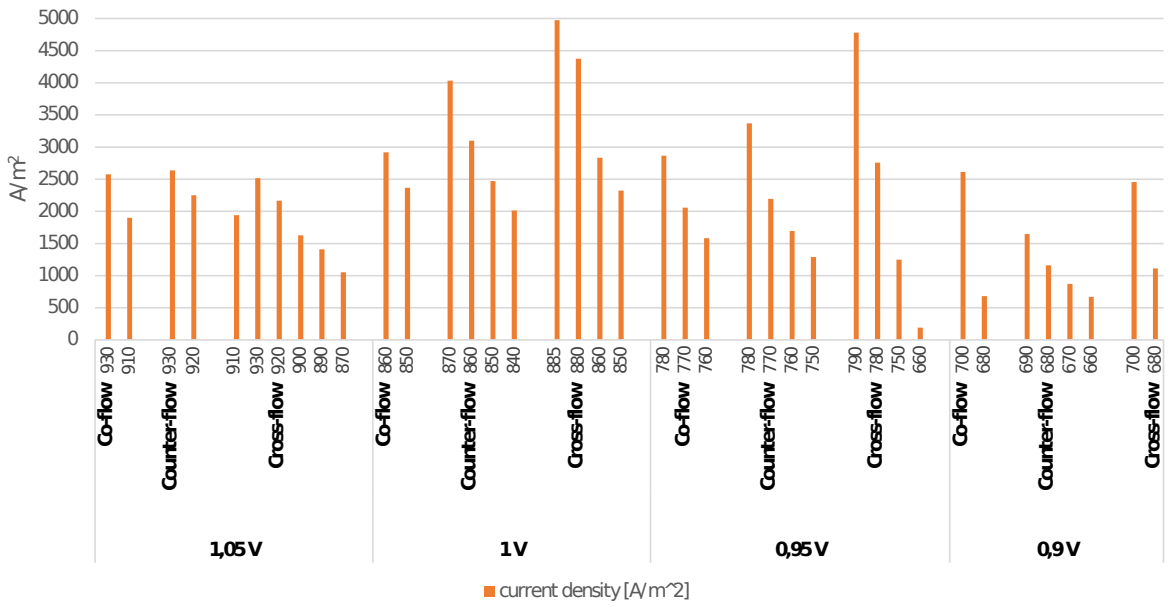


**Figure 5.3.1:** Variation of temperature and voltage for different cases configurations.

the exothermic reactions that are more intense where reactants are more abundant. More uniform distribution is crucial, since materials are sensitive to high gradients at high temperatures. Therefore it is beneficial that the spanwise gradients are rather small when compared to the streamwise differences.

Nernst potential, the theoretical maximum thermodynamic potential that can be obtained is temperature-dependent, but is even more is affected by reactant concentrations. It can be seen that performance degrades from gas inlets towards outlets, Figure 5.3.4, as fuel and oxygen are depleted and water is created. In case of cross-flow orientation, the corner nearest to inlets has the highest potential, due to abundance of reactants.

Knowing the local current density is of great interest when analyzing fuel cell geometry or designing a new one. Values on electrolyte surface can be seen in Figure 5.3.5. Local variations of current density associated with the presence of the channels and ribs can be observed and explained as the coupled effect of charge, heat, and mass transfer. Since the Butler-Volmer equation depends on temperature and indirectly on mass fractions, their joint effect influences current density distribution.

In Figure 5.3.6 local current density values for the electrolyte cross sections can be seen. They decrease with a steady slope from inlet towards outlet in streamwise direction (note that

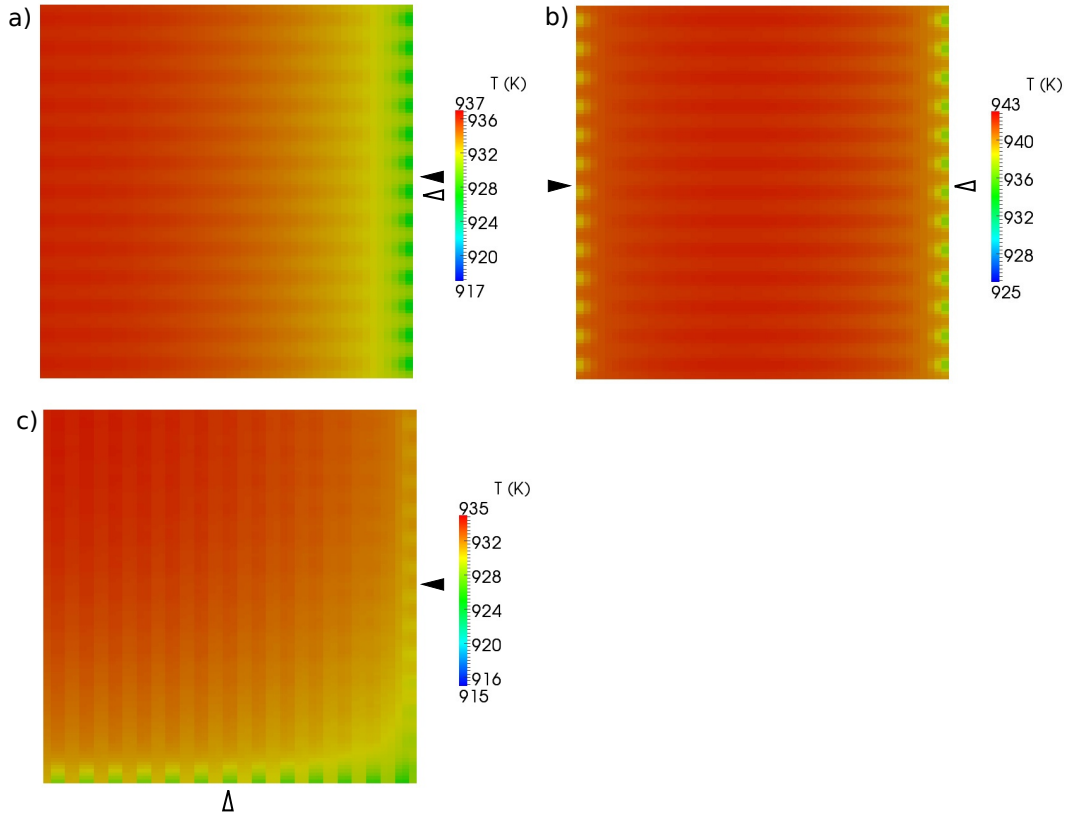


**Figure 5.3.2:** Temperature distributions on anode surface for a) co-flow, b) counter-flow and c) cross-Flow. Solid arrows show the direction of fuel, while hollow arrows show the direction of air flow.

for counter-flow fuel inlet is on the opposite side), with great influence of perpendicular channels (see checkered pattern in 5.3.5.b) in case of cross-flow, causing oscillations. The co-flow case has somewhat higher current density, which is in agreement with achieved higher temperatures. In spanwise cross section, significant oscillations can be seen for co- and counter-flow configurations as well, with cross-flow oscillations being slightly smaller.

Reactant mass fractions have a major impact on reaction kinetics. First, we can consider the channels and pressure in them. Clearly, pressure is highest at the inlets and decreases towards outlets. Figure 5.3.7 shows fuel pressure distribution on anode. The pressure mostly changes along the streamwise direction (co- and counter-flows), but in case of the cross-flow, changes in spanwise direction are also visible. They are present due to changes in the gas composition, mixture densities and temperature changes.

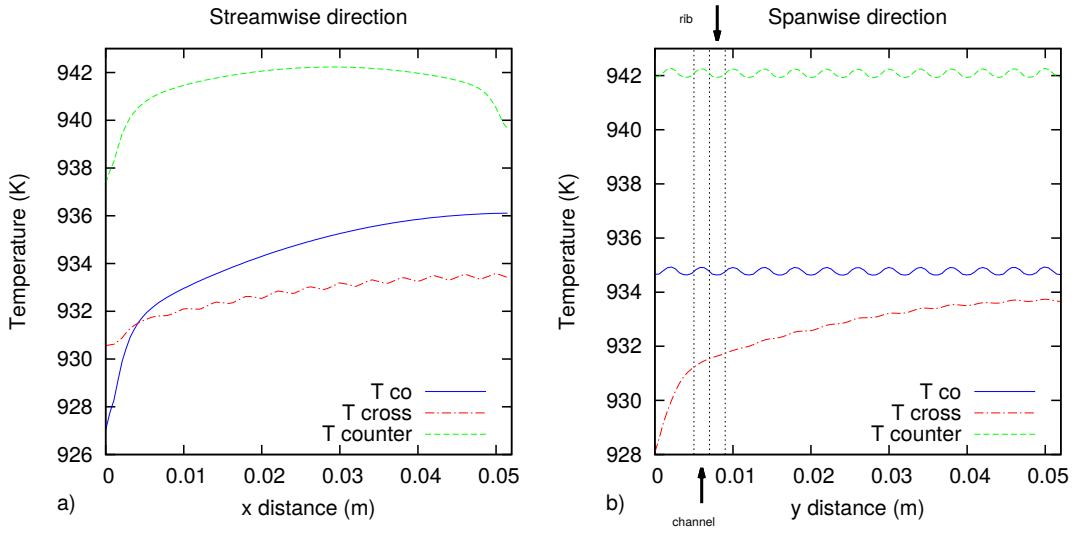


**Figure 5.3.3:** Temperature distributions across the cell

Mass fractions themselves indicate useful information about processes in fuel cell. As expected, Figure 5.3.8 show that mass fractions generally decrease going from inlet towards outlet. Cross sections offer more informations: Figure 5.3.10.a shows streamwise hydrogen mass fractions declining in a near-linear fashion, and Figure 5.3.10.b show spanwise oscillations due to channels. Spanwise oscillations are relatively small in comparison to the overall reduction from inlet to outlet, with counter-flow values slightly lower due to higher utilization and better performances (thus higher temperature as well). Hydrogen is depleted in reaction and its mass fraction decreases along the channel. In case of high current densities and fuel utilization, if geometry is not optimized mass fractions can drop to zero and lead to fuel cell starvation.

On the other side, oxygen levels also drop along the channels, and although overall decline is not as big as with the hydrogen, relative oscillations here are considerably bigger. Peaks in concentrations match the cathode volume above channels, where reaction rates are higher and oxygen can permeate more easily. Troughs correspond to the volume not directly adjacent to channels, yielding high oxygen concentration area. Hence, oscillations are caused by geometry of electrodes, in particular by their thickness. Anode is thicker and in it hydrogen can diffuse more easily and distribute more evenly, thus lowering the fluctuations (in Figure 5.3.15 thicknesses of top and bottom meshes can be compared). Thinner cathode does not allow enough oxygen to permeate to smooth the oscillations. However, thicker cathode

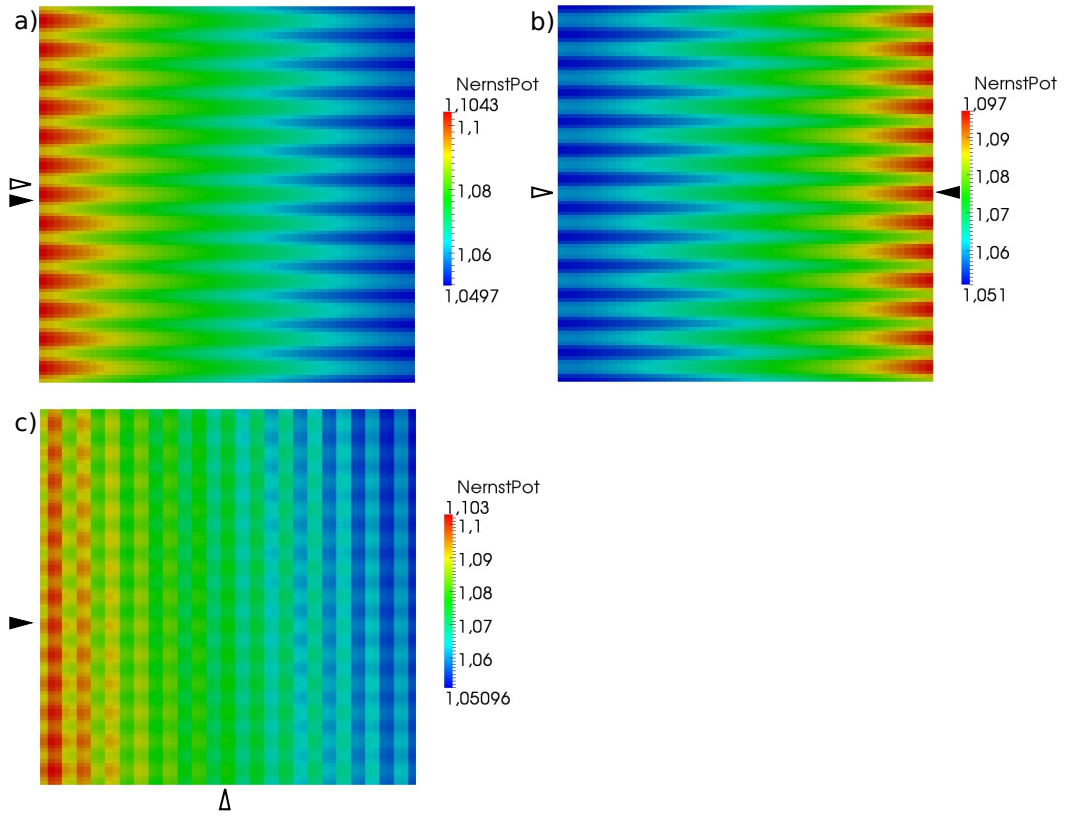


**Figure 5.3.4:** Nernst potential on electrolyte surface for a) co-flow, b) counter-flow and c) cross-flow.Solid arrows show the direction of fuel, while hollow arrows show the direction of air flow.

in this anode-supported system can lead to overall efficiency decline, overall deterioration of mass transport and higher thermal stresses[12].

Combined plot of current density and mass fractions in counter-flow configuration is shown in Figure 5.3.12. In the spanwise direction, the impact of previously described oxygen distribution can be seen: hydrogen mass fractions are nearly linear, but oxygen mass fractions vary. This variation (mass transfer limitation) causes lowering and oscillation of the current density, and subsequently temperature. Another reason for the oscillations are the heat transfer effects—heat sources above the channels (where reactions are more fervent) are more intense when compared to the volume of the ribs. This can be seen in Figure 5.3.3.b, with higher temperatures under channels and lower under ribs.

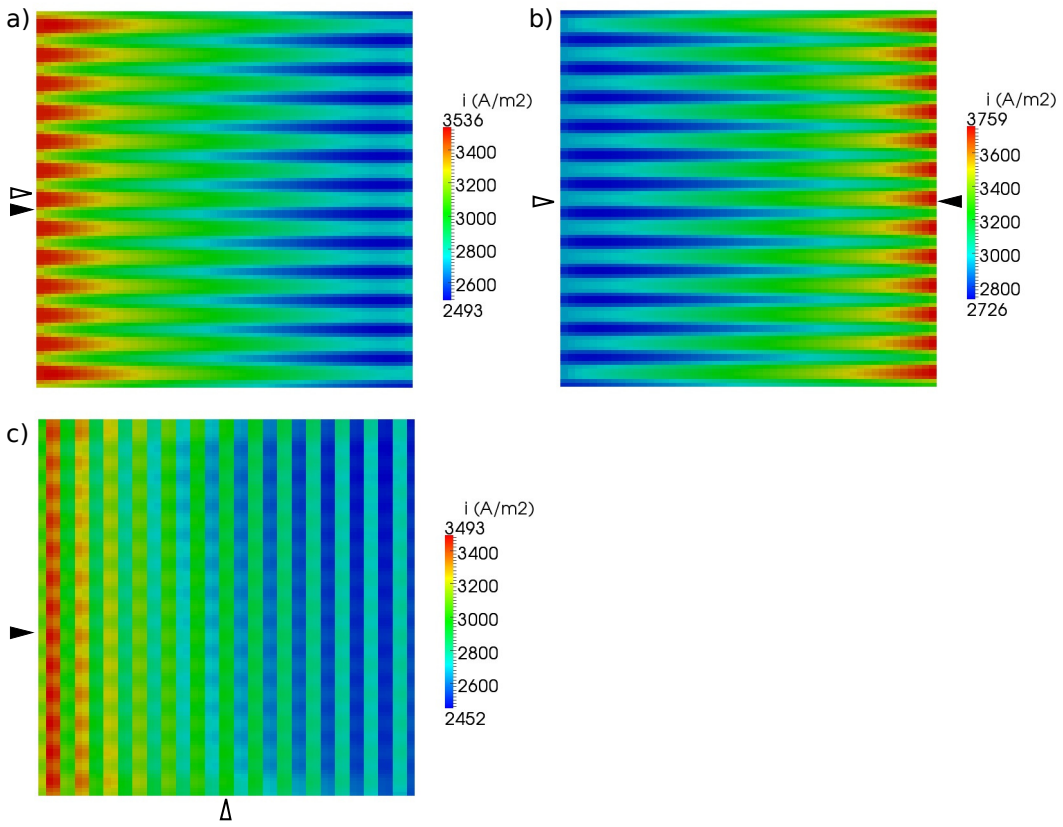


**Figure 5.3.5:** Current density on electrolyte surface for a) co-flow, b) counter-flow and c) cross-flow

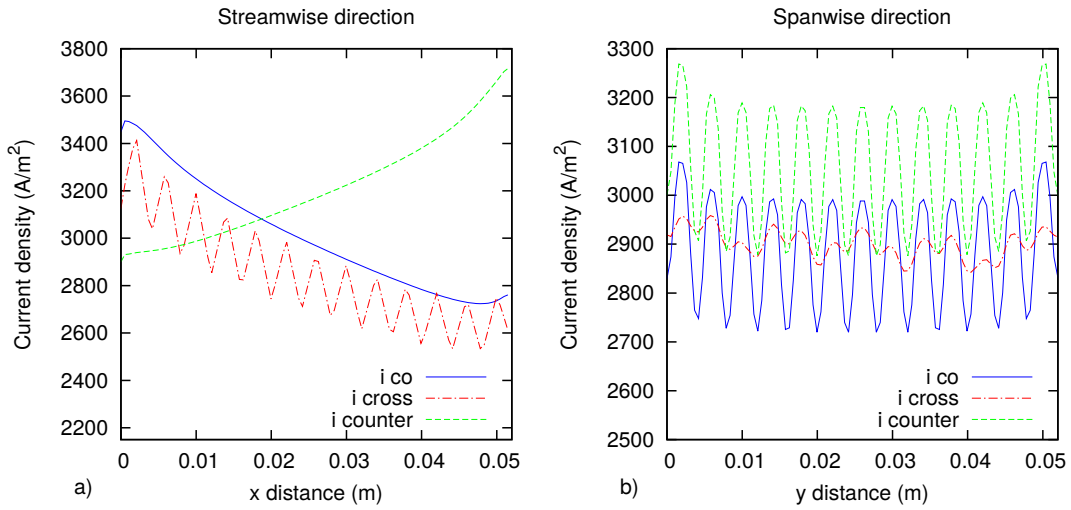


**Figure 5.3.6:** Current density plots across electrolyte in streamwise and spanwise direction for co-flow counter-flow and cross-flow.

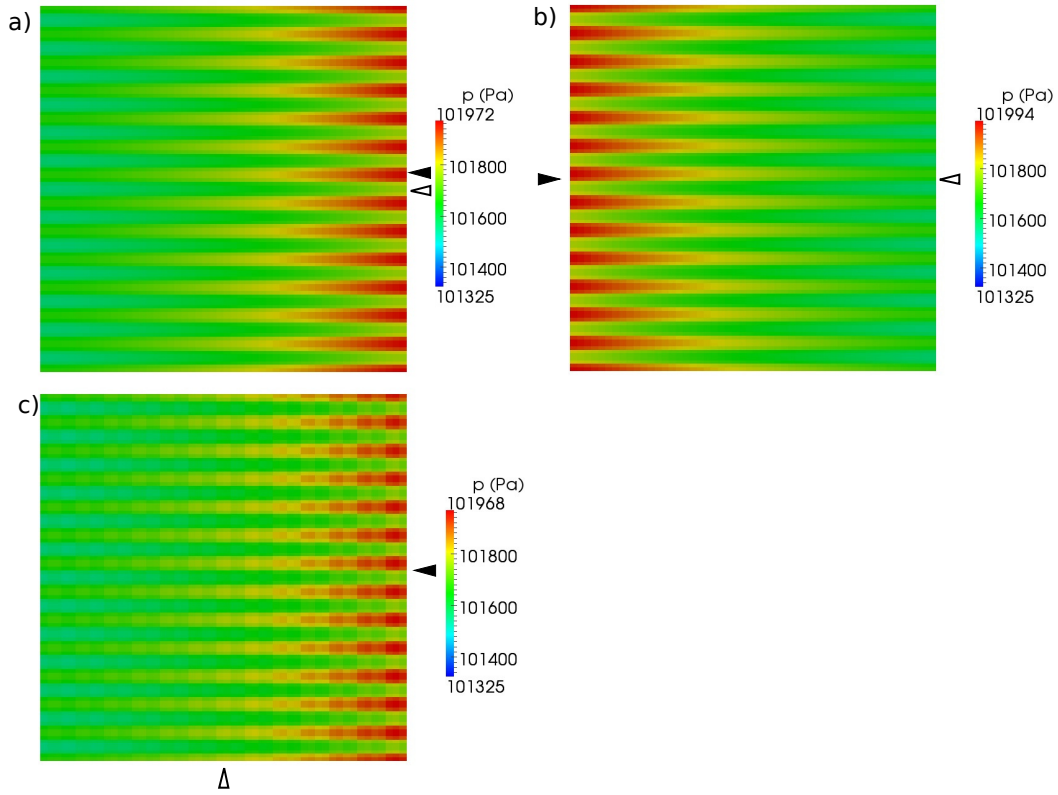


**Figure 5.3.7:** Fuel mesh pressures for a) co-flow, b) counter-flow and c) cross-flow. Solid arrows show the direction of fuel, while hollow arrows show the direction of air flow.

### 5.3.2 Potentials

Potential fields were solved on two region meshes, *top* and *bottom*. Conductivity distribution is a function of temperature, and potential depends on it. Because of different materials and their properties for anode and cathode (top and bottom respectively), different formulas were used (see Section 4.3.3, Figure 4.3.4). The bottom conductivity is inversely proportional to temperatures, and has the highest values where temperatures are the lowest. Opposite is valid for the top mesh, where conductivity is directly proportional to temperature.

Potential fields on these two "child meshes" are shown in Figures 5.3.13 and 5.3.14. It can be seen that changes in potential fields are caused by reactions occurring more intensely under the channels, with moderate influence of `zeroGradient` boundary conditions on outer boundaries. Extremes in potential fields are of opposite sign (direction) for bottom and top mesh. On bottom mesh potential rises above nominal value (in present cases 1 V) and on top it drops below 0 V which is set on the boundary. This is due to the implemented model

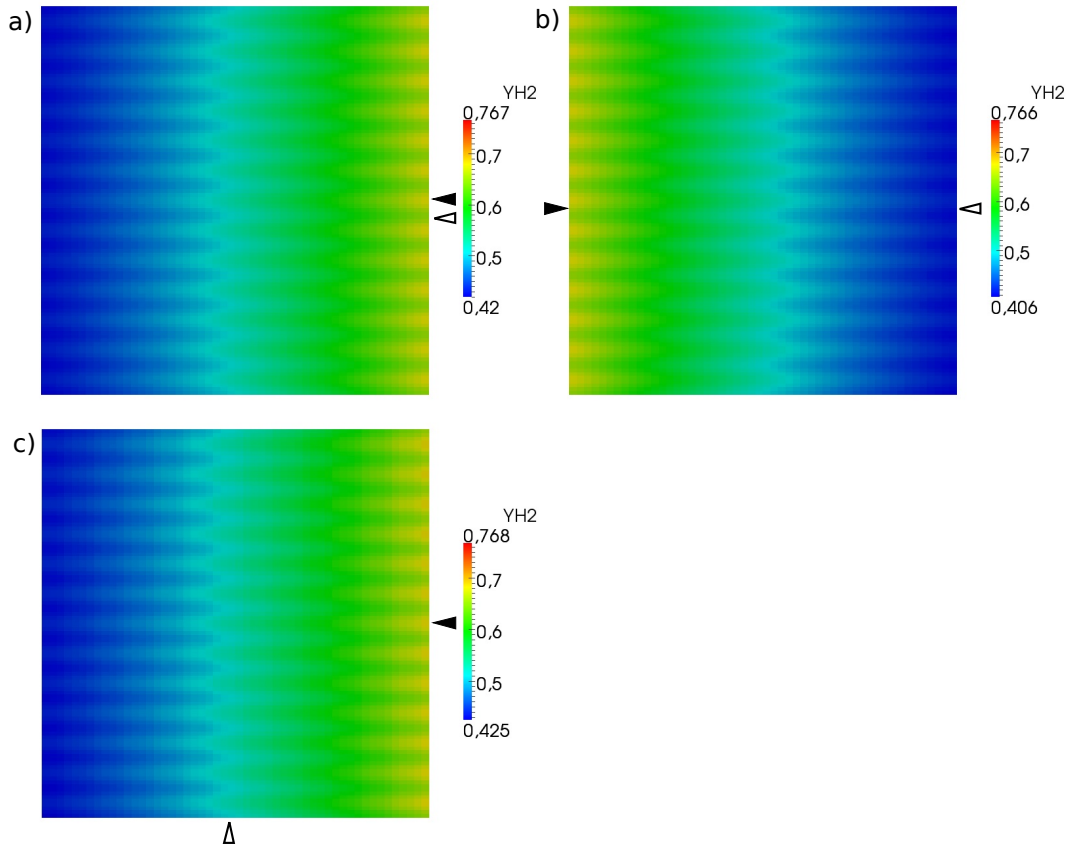


**Figure 5.3.8:** Hydrogen mass fractions on fuel mesh for all three configurations. Solid arrows show the direction of fuel, while hollow arrows show the direction of air flow.

with potentials calculated based on the "Kirchoff-Ohm equation" and the greater the values of local current densities are, bigger the potential drop between adjacent points on meshes is.

Figure 5.3.15 shows cross sections of top and bottom meshes with potential distributions. It can be seen that solving the Laplace equation results in smooth transitions from prescribed fixed boundary values to fixed gradients due to calculated current densities. In regions above and below channels, where reactions are more vivid and current densities are high, potential gradients are higher. This also corresponds with volume between non-conducting channels, so iso-potential surfaces are more dense here. This is important when analyzing existing or designing new geometries, since bad channel layout can, except for mass transfer problems, cause undesirable potential gradients, which in turn lead to high current densities in ribs and accompanying heat sources because of Joule heating. In the presented model these heat sources were not modeled, but nonetheless potential distributions can serve as a guide for

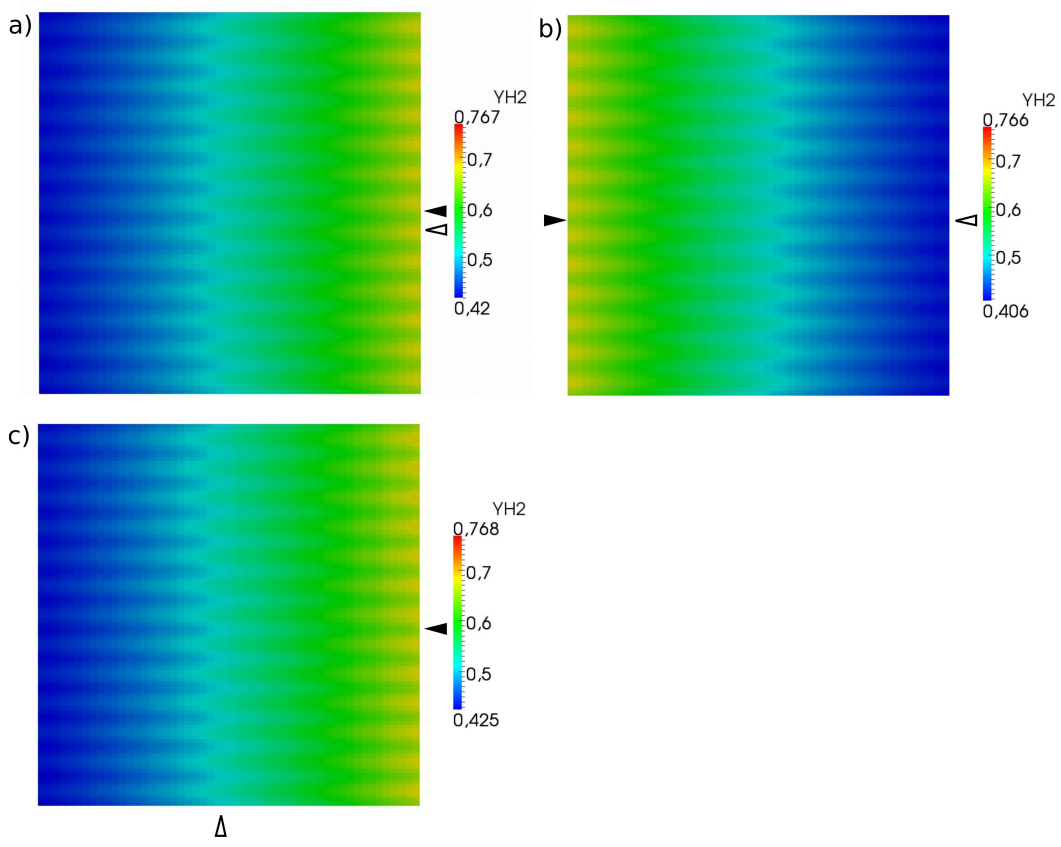


**Figure 5.3.9:** Oxygen mass fractions on fuel mesh for all three configurations. Solid arrows show the direction of fuel, while hollow arrows show the direction of air flow.

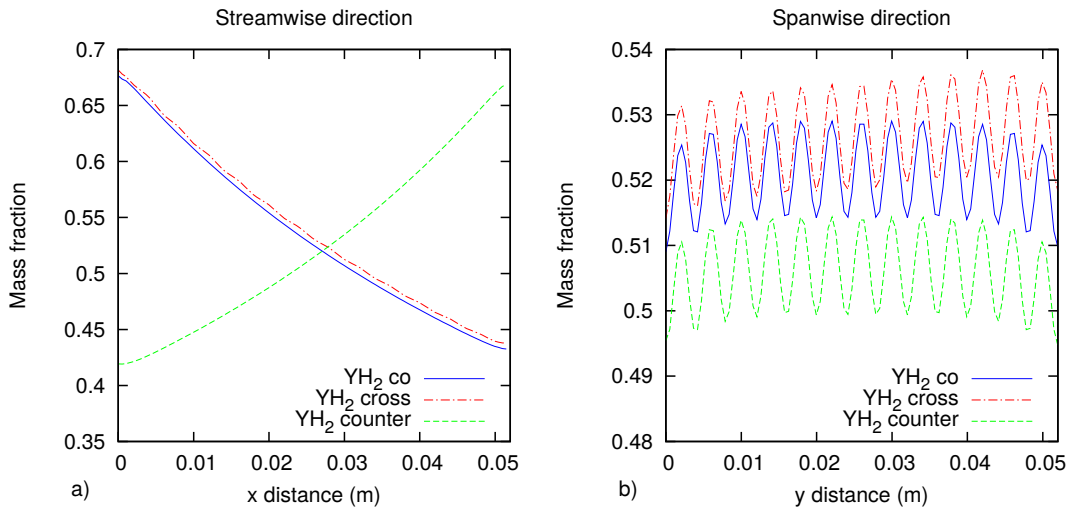


**Figure 5.3.10:** Hydrogen mass fractions across fuel mesh.

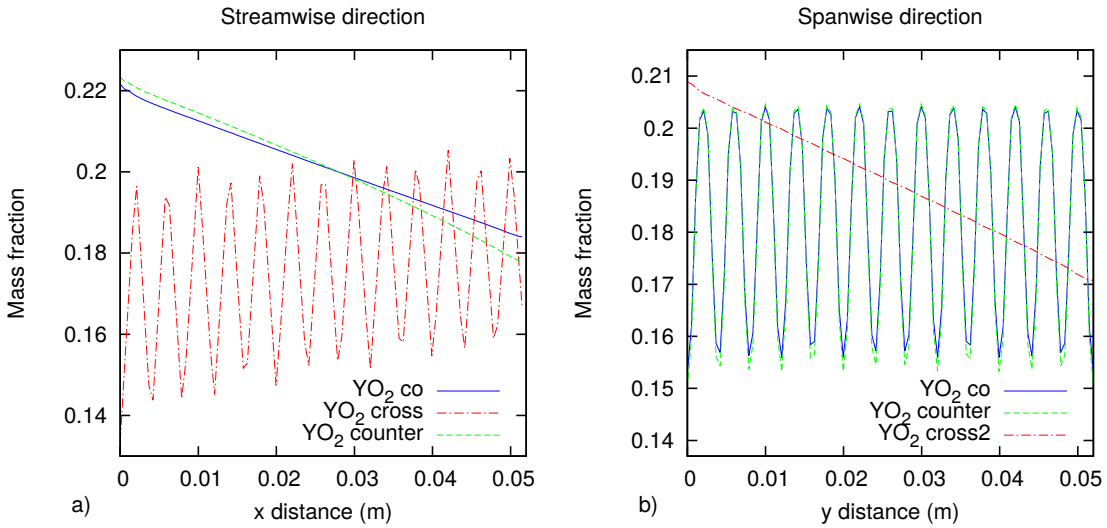


**Figure 5.3.11:** Oxygen mass fractions across fuel mesh.

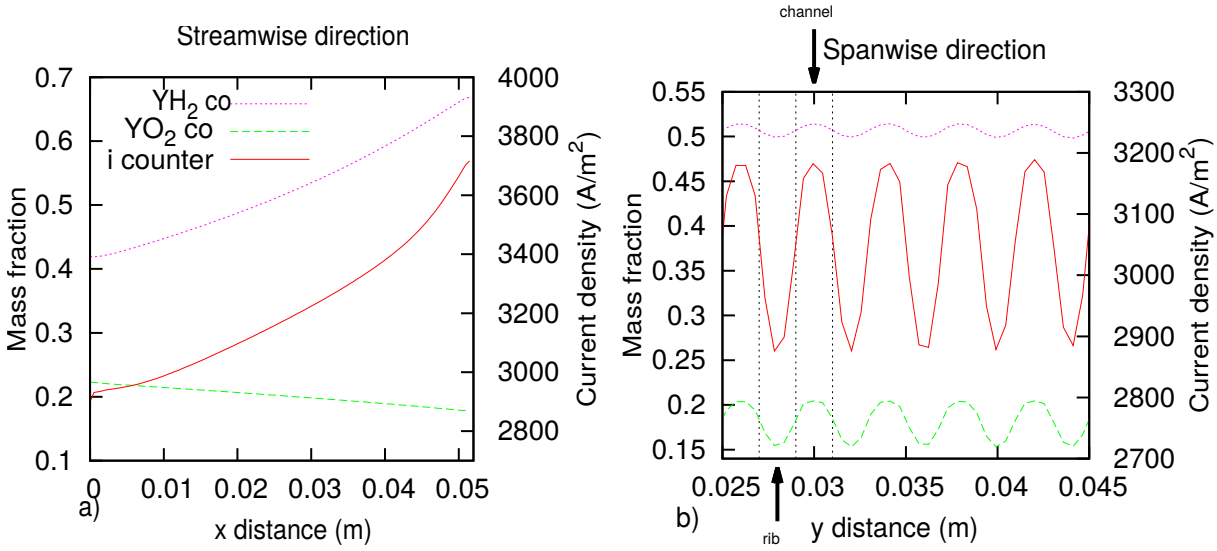


**Figure 5.3.12:** Combined current density and mass fractions across counter-flow mesh

geometry quality assessment.

Experimental data for SOFC potential fields are scarce, and existing models for SOFC do not include potential distributions in whole cell, making direct comparison difficult. Data provided by Meng and Wang[19], although being for PEM fuel cells, can serve for a rough comparison, since the two potential model for SOFCs at present has several assumptions. In Figure 5.3.16 a section of proton exchange membrane fuel cell can be seen. Electronic potential field distribution is presented on anode and cathode solids that relate to top and

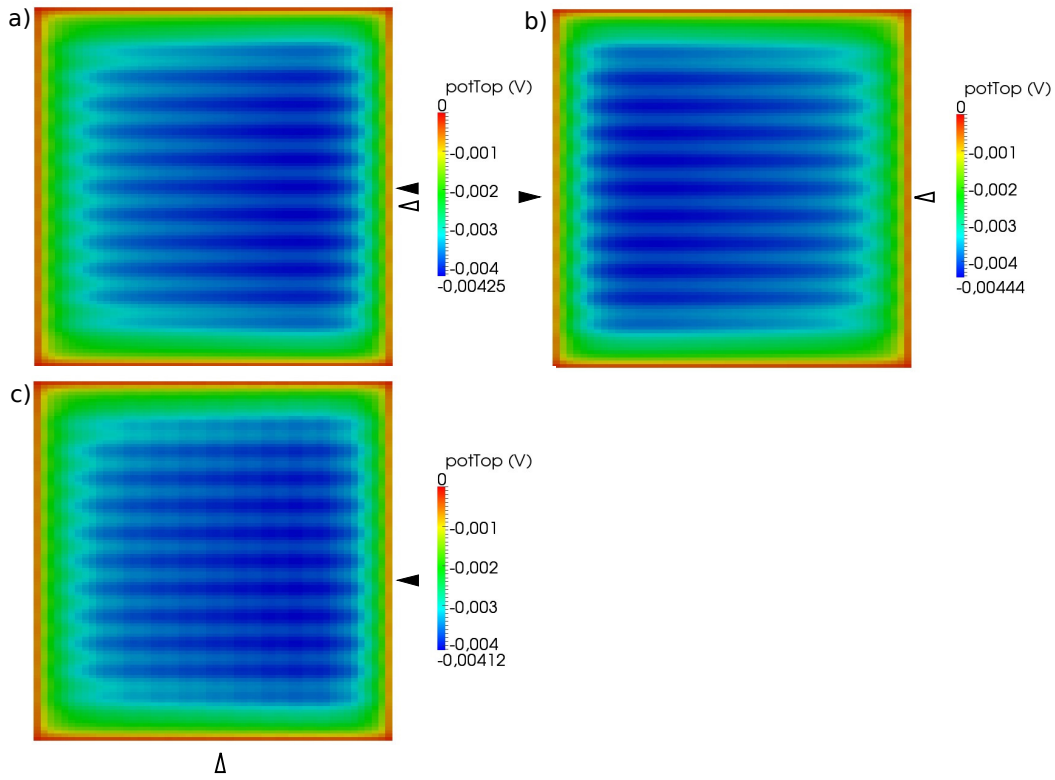


**Figure 5.3.13:** Potential distribution on top mesh, bottom view, for a) co-flow, b) counter-flow and c) cross-flow

bottom regions in two potential model. When compared with Figure 5.3.15, it can be seen that distributions are analogous, albeit with different magnitudes. Orientations of potential rise and decline through the solid are the same, but changes for the PEMFC model are bigger by an order of magnitude. This is probably because of disparate formulas for the conductivity calculation, although some of it might be due to assumption in the two potential model that neglects effect of electroyte and interconnect conductances.

## 5.4 Validation

While two potential model was being developed, several assumptions were made, most significant among them being the use of Tafel equation and presuming a passive cathode (see Section 4.3.1). Simplifying the model this way led to difficulties with validation: current models for solid oxide fuel cells do not have *both* of these assumptions, and the present two potential

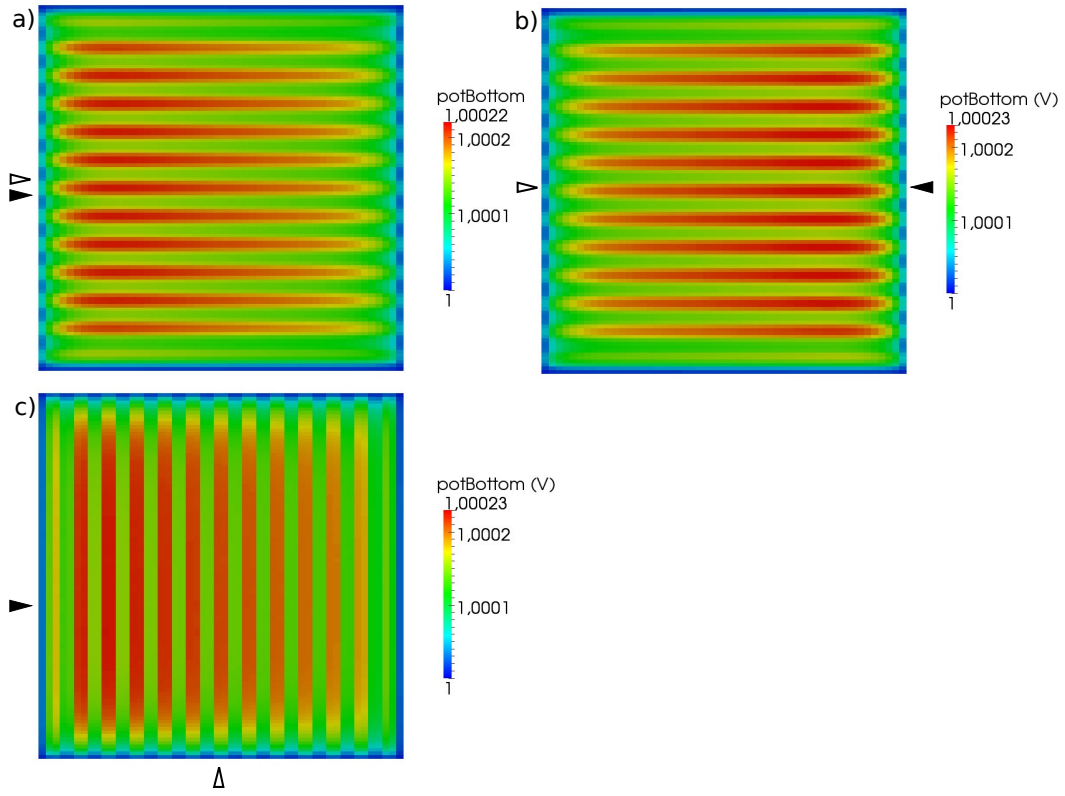


**Figure 5.3.14:** Potential distribution on bottom mesh, top view, for a) co-flow, b) counter-flow and c) cross-flow

model is not directly comparable with them.

Furthermore, when running simulations with ranges of input parameters such as inlet temperature and boundary potential, the model has sometimes shown some instability and diverged under lower potentials and high temperatures. Figure 5.4.1 shows maximum inlet temperatures for used potentials. Simulations for work-points with high potentials and high temperatures (that correspond to real SOFCs at ideal working conditions) converged successfully, but when decreasing the potential, maximum temperatures that simulations converged dropped below range that SOFCs can operate in. However, for high-temperature, high-potential ranges, $i - V$ curve derived from results provides characteristic shape, Figure 5.4.2. This suggests that the model behaves in accordance with predictions in presence of high voltages—simulating high activation overpotential region. Linear region represents increasing losses due to higher ohmic losses (calculating potential fields). Unfortunately, at low voltages and high current densities characteristic mass transfer losses could not have been

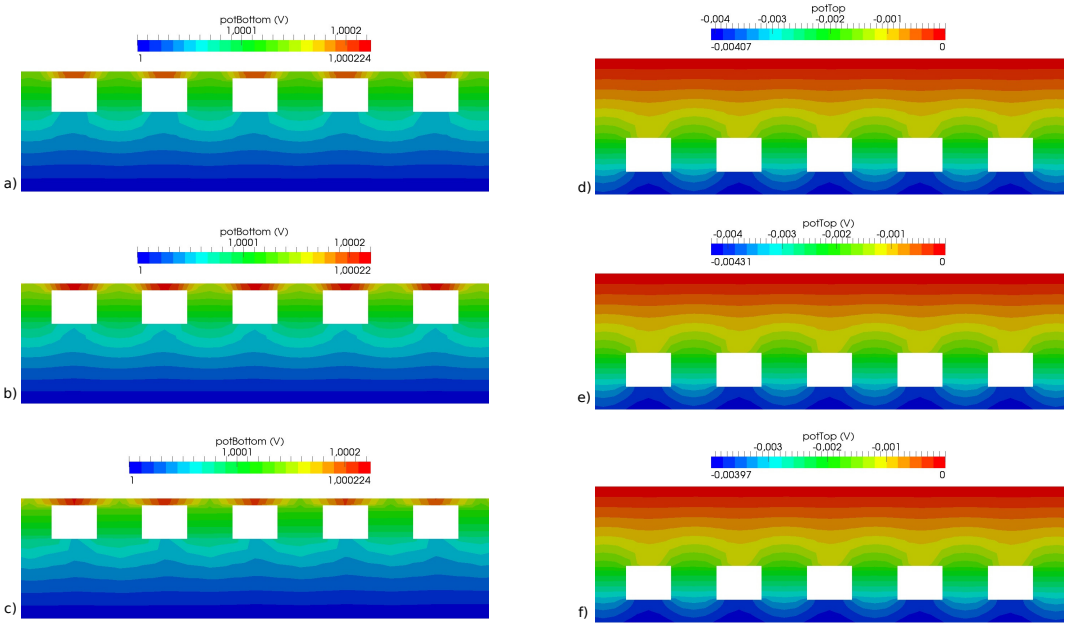


**Figure 5.3.15:** Potential distributions across top (right) and bottom (left) mesh, for a), d) co-flow; b), d) counter-flow; c), e) cross-flow. Figures are clipped do not show side boundaries.

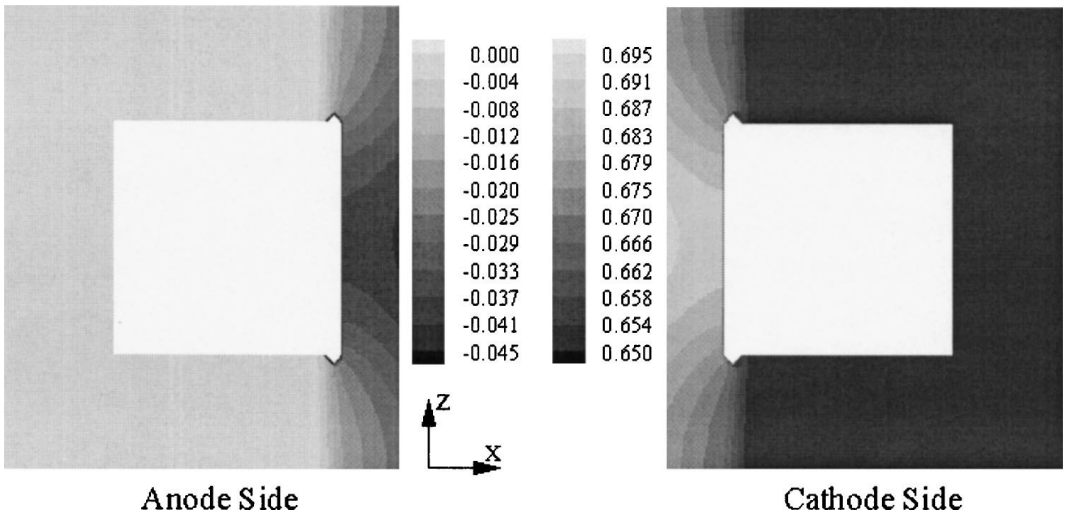


**Figure 5.3.16:** Potential distributions on anode and cathode of a PEMFC mesh[19]

simulated, because when lowering voltages at constant temperatures, model started diverging (presented in Figure 5.4.1). Lowering temperatures even further, to achieve convergences as low voltages as well, would decrease working parameters below ones stated for SOFC.

In order to obtain the results that could be used for the two potential model validation, regular `openFuelCell` model was modified to match the two potential model (denoted 2pot):

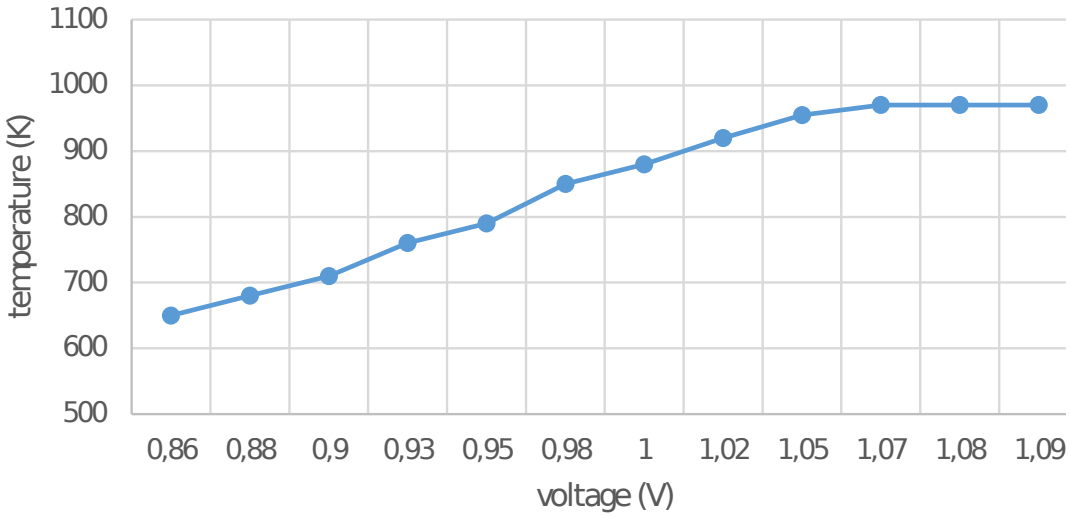


**Figure 5.4.1:** Upper boundary for inlet temperatures due to model limitations

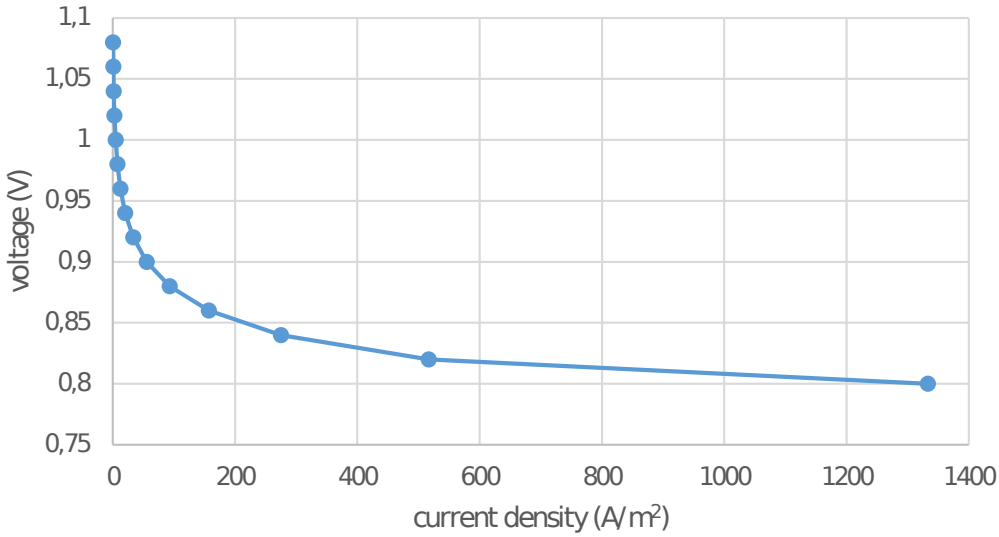


**Figure 5.4.2:** i-V curve for the two potential model

cathode has been made passive, and simple kinetics with Tafel equation were implemented. Third model used for comparison was regular `openFuelCell` model. Figure 5.4.3 shows resulting current densities for several voltage and temperature values. Modifying the `openFuelCell` code (denoted oFCm) caused instability with respect to inlet temperatures. With limitations set to both oFCm and 2pot models, appropriate comparison proved hard to acieve. However, all models displayed plausible and physically correct distributions similar to ones

in Section 5.3.1, but for similar output currents displayed in Figure 5.4.3, input temperatures had to vary significantly. It can be seen that the two potential model had to be run generally at lower temperatures, which is in accordance with declining maximum temperatures in Figure 5.4.1.

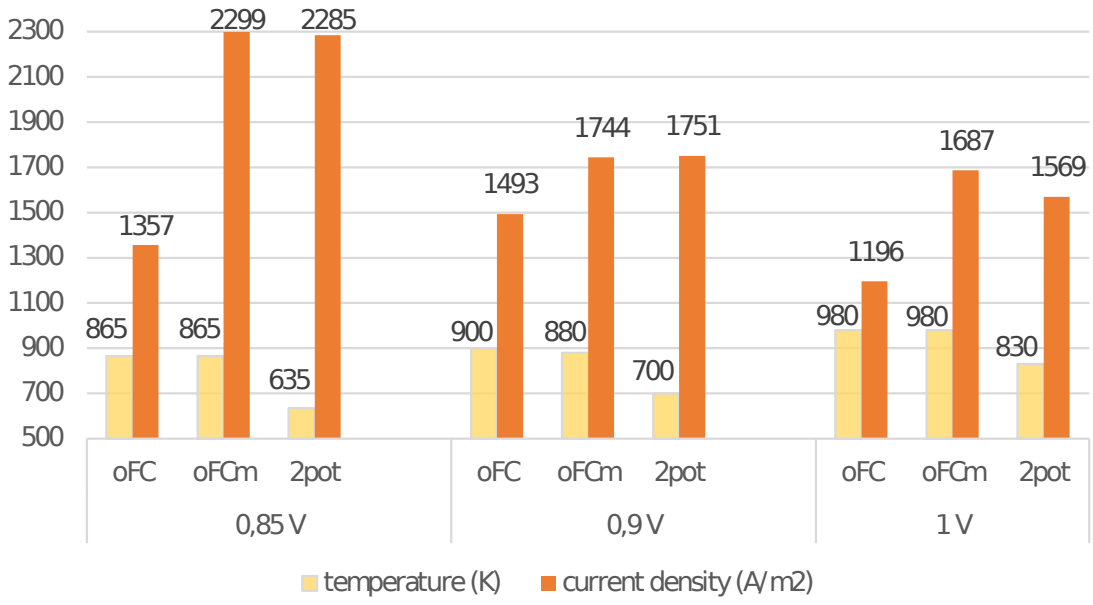


**Figure 5.4.3:** Comparison of three models: `openFuelCell` (oFC), modified `openFuelCell` (oFCm) and two potential model (2pot). Inlet temperature and voltage are input parameters, with current density as result

Overall, resulting current densities varied too much to draw any concise conclusion as to whether and in which conditions the new two potential model is valid.

## 5.5 Closure

In this chapter results obtained with the newly-developed two potential model were presented. Despite the assumed simplifications, it was shown that results for mass and heat transfer are analogous to results from previous studies,[7][6][12][11] and that results can be described by the same physical phenomena occuring in fuel cells. Furthermore, potential distributions match those reported by Meng and Wang[19], with magnitudes of potential field changes lower, probably due to different calculation parameters such as conductivity.

Although being similar and showing the same gradients and shapes as the existing models, absolute values generated by the two potential model vary significantly and cannot be considered as accurate. Currently, it is unclear whether the cause is in model assumptions or there errors in the code, with former being more likely since results showed a similarity with existing data. It has been proposed that model should be modified for simulation of low-temperature SOFCs or repurposed for simulating high-temperature PEMFCs. First of these propositions goes along the current model instabilities at high temperatures, and both of them require further modifications of the model.

Presented model, although introduces some approximations, nonetheless takes into account some of the phenomena that was ignored by previous studies and provides an option to activate detailed simulation of potential field. Further analysis and comparison is still needed, to fully evaluate this models applicability. The proposed change of modeled fuel cell type is probable, since after this study doubts in validity of presented approach with Tafel equation and passive cathode for SOFCs are raised. However, the two potential model can still be used for examining potential fields for new geometries and assessment of possible heat sources, along with the previously available insight in mass and heat transfer phenomena.

Additional improvements for model are still needed, and in this stage the two potential model could serve as basis for further model developments.

# Bibliography


[1] U. D. o. E. National Energy Technology Laboratory, *Fuel Cell Handbook*. University Press of the Pacific, 7th edition ed., 2005.

[2] R. O'Hayre, S.-W. Cha, W. Colella, and F. B. Prinz, *Fuel Cell Fundamentals*. John Wiley & Sons, Inc., Hoboken, New Jersey, third ed., jun 2016.

[3] J. Larminie and A. Dicks, *Fuel Cell Systems Explained (Second Edition)*. Wiley, 2003.

[4] B. S. Prakash, S. S. Kumar, and S. Aruna, "Properties and development of ni/ysz as an anode material in solid oxide fuel cell: A review," *Renewable and Sustainable Energy Reviews*, vol. 36, pp. 149 – 179, 2014.

[5] D. H. Jeon, "A comprehensive {CFD} model of anode-supported solid oxide fuel cells," *Electrochimica Acta*, vol. 54, no. 10, pp. 2727 – 2736, 2009.

[6] J. P. A.D. Le, S.B. Beale, "Validation of a solid oxide fuel cell model on the international energy agency benchmark case with hydrogen fuel," vol. 15, pp. 27–41, 2015.

[7] S. B. Beale, H.-W. Choi, J. G. Pharoah, H. K. Roth, H. Jasak, and D. H. Jeon, "Open-source computational model of a solid oxide fuel cell," *Computer Physics Communications*, vol. 200, pp. 15 – 26, 2016.

[8] B. Sunden, *Transport Phenomena In Fuel Cells (Developments in Heat Transfer)*. WIT Press / Computational Mechanics, 2005.

[9] S. Beale, Y. Lin, S. Zhubrin, and W. Dong, "Computer methods for performance prediction in fuel cells," *Journal of Power Sources*, vol. 118, no. 12, pp. 79 – 85, 2003. Scientific Advances in Fuel Cell Systems.

[10] S. Patankar, *Numerical Heat Transfer and Fluid Flow*. Hemisphere Series on Computational Methods in Mechanics and Thermal Science, Taylor and Francis, 1 ed., 1980.

[11] S. Beale, A. D. Le, H. Roth, J. Pharoah, H.-W. Choi, L. D. Haart, and D. Froning, "Numerical and experimental analysis of a solid oxide fuel cell stack," The Electrochemical Society, 2011.

[12] D. H. Jeon, S. B. Beale, H.-W. Choi, J. G. Pharoah, and H. Roth, "Computational study of heat and mass transfer issues in solid oxide fuel cells," 2010.

[13] H. H. Girault, *Analytical and Physical Electrochemistry*. Fundamental Sciences, EFPL Press, 1 ed., 2004.

[14] Y. Lin and S. Beale, "Performance predictions in solid oxide fuel cells," *Applied Mathematical Modelling*, vol. 30, no. 11, pp. 1485 – 1496, 2006. Selected papers from the Third International Conference on {CFD} in the Minerals and Process Industries3rd International Conference on {CFDSelected} papers from the Third International Conference on {CFD} in the Minerals and Process Industries.

[15] S. Beale, "Calculation procedure for mass transfer in fuel cells," *Journal of Power Sources*, vol. 128, no. 2, pp. 185 – 192, 2004.

[16] C.-Y. Wang*, "Fundamental models for fuel cell engineering," *Chemical Reviews*, vol. 104, no. 10, pp. 4727–4766, 2004. PMID: 15669167.

[17] S. Campanari and P. Iora, "Definition and sensitivity analysis of a finite volume {SOFC} model for a tubular cell geometry," *Journal of Power Sources*, vol. 132, no. 12, pp. 113 – 126, 2004.

[18] A. Leonide, Y. Apel, and E. Ivers-Tiffee, "SOFC modeling and parameter identification by means of impedance spectroscopy," in *ECS Transactions*, The Electrochemical Society, 2009.

[19] H. Meng and C.-Y. Wang, "Electron transport in PEFCs," *Journal of The Electrochemical Society*, vol. 151, no. 3, p. A358, 2004.